

DESIGN OF A PLANAR KU BAND RECEIVE ANTENNA ARRAY FOR MOBILE
PLATFORMS

by

Mustafa Murat BİLGİÇ

Submitted to the Institute of Graduate Studies in
Science and Engineering in partial fulfillment of
the requirements for the degree of
Philosophy of Doctorate
in
Electrical and Electronics Engineering

Yeditepe University

2014

DESIGN OF A PLANAR KU BAND RECEIVE ANTENNA ARRAY FOR MOBILE
PLATFORMS

APPROVED BY:

Assoc. Prof. Dr. Korkut Yeğin
(Supervisor)



Prof. Dr. Uğur Çilingiroğlu



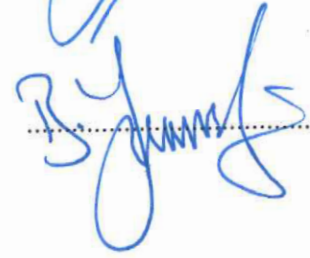
Prof. Dr. Yunus Emre Erdemli



Prof. Dr. Filiz Güneş



Dr. Bülent Yağcı



DATE OF APPROVAL: / /

ACKNOWLEDGEMENTS

It has been a long and tiring work which without the support of friend and loved ones, would not be possible to finish.

First of all I would like to thank my supervisor for he has been a great advisor and also acted as an older brother giving me strength to struggle during hard times.

Thanks to my mother, Vildan BİLGİÇ and my father, Oruç BİLGİÇ for their never ending support both morally and materially, in believing that one day they would see this work come to such nice ending. The day I finished this thesis, I saw the happiness in their eyes which I wouldn't change anything in return with.

Thanks to my friends and colleagues Deniz GÜRHAN, Bora TAR, Anıl ÖZDEMİRLİ and Hüseyin BÜYÜKEŞMELİ for the time they spent drinking, coffee and cigarettes, through long talks about the undetermined future. Thanks for all the joy, too.

Finally I would like to thank the love my life, Gülay EROL. Having you by my side, holding my hand is all I need to overcome the struggles of life. It is time make our own music and walk this fascinating adventure together.

ABSTRACT

DESIGN OF A PLANAR Ku BAND RECEIVE ANTENNA ARRAY FOR MOBILE PLATFORMS

A wideband, planar and low profile antenna array is proposed and designed for Ku band direct broadcast from satellite reception for mobile systems. Contrary to earlier designs, the array antenna covers entire downlink Ku-band frequencies (10.8 - 12.75 GHz) for simultaneous reception from multiple transponders. In this thesis, we first propose figure-of-merits (FOMs) to classify antennas in terms of their performances. Among possible antenna configurations, we show that aperture coupled antennas exhibit superior performance when FOM based comparisons are made. Using this single antenna element, we form small arrays first, then large arrays. Besides single antenna element, feed network design also requires a number of challenges to meet low-loss, wideband and phasing requirements. The most straightforward design of feed network is the use of low-loss microstrip lines with power dividers/combiners. However, at Ku band these microstrip lines become too lossy so that array antenna becomes almost useless. A combination of microstrip feed network and waveguide feed network, therefore, is ideal. Then, the main question is how one can form the subarrays and their accompanying waveguide feed network. This thesis answers that question by formulating the subarray and array feed network loss as an optimization problem with constraints on the size and the weight of the array. With all these improvements in the antenna element and the feed network design, the array antenna exhibits 16.5% bandwidth and has 28.4 - 31.3 dBi gain for both vertical and horizontal polarizations. Overall height of the planar antenna with waveguide feed network is under 25 mm. The antenna is built and tested for reception quality. The carrier-to-noise ratio of 9.5 dB is observed for the target transponder (42° E) at 11.9 GHz using IF loop-out of the receiver.

ÖZET

HAREKETLİ PLATFORMLAR İÇİN DÜZLEMSEL Ku BANDI ALICI DİZİ ANTENİ TASARIMI

Mobil sistemler için, Ku bandında uydu vericisinden doğrudan yayın alışı yapabilen genişbantlı, düzlemsel ve düşük profilli anten dizisinin tasarımı ve gerçekleşmesi sunulmuştur. Önceki tasarımlardan farklı olarak, bu anten dizisi çoklu vericilerden Ku bandındaki tüm frekansların (10.8 - 12.75 GHz) uydu indirme bandındaki anlık alışı kapsamaktadır. Bu tezde, öncelikle antenleri performansları bakımından sınıflandırabilmek adına başarımlar ölçütlerini sunulmaktadır. Olası anten yapılandırmaları arasında başarımlar ölçütlerine göre bir kıyaslama gerçekleştirildiğinde, açıklık kuplajlı antenlerin diğerlerinden üstün performansa sahip olduklarını gösterilmiştir. Bu birim anten elemanını kullanarak önce alt dizileri daha sonra da ana dizileri oluşturuldu. Birim anten elemanının yanısıra besleme ağı tasarımı da düşük kayıplı, genişbantlı ve faz farklı olma şartlarına uyabilmek için birtakım zorlukları aşarak gerçekleştirildi. Besleme ağının doğrudan tasarımı, güç bölücüleri/birleştiricileri içeren düşük kayıplı mikroşerit hatlarının kullanımıyla mevcuttur. Ne var ki, Ku bandında bu mikroşerit hatlar fazla kayıplı olup anten dizisini neredeyse faydasız hale getirmektedir. Mikroşerit besleme ağı ile dalga kılavuzu besleme ağının bir kombinasyonu ise ideal biçimde çalışmaktadır. O takdirde asıl soru, altdiziler ve onlara eşlik eden dalga kılavuzu besleme ağının nasıl oluşturulacağıdır. Bu tez, sözkonusu soruyu, altdizi ve dizi besleme ağı kayıplarını dizinin büyüklük ve ağırlığı kısıtlarında bir optimizasyon problemi olarak ele almak suretiyle yanıtlamaktadır. Birim anten ve besleme ağı tasarımlarındaki tüm bu geliştirmelerle, anten dizisi %16.5'lük bant genişliği sunmakta ve hem dikey hem de yatay polarizasyonlarda 28.4 - 31.3 dBi kazanç sağlamaktadır. Dalga kılavuzu besleme ağına sahip düzlemsel antenin toplam yüksekliği 25 milimetrenin altındadır. Anten, alıcı kalitesi gözetilerek inşa edilmiş ve test edilmiştir. Hedef verici için (42° E), 11.9 GHz'de alıcının arkasında bulunan IF çevrimi kullanılarak elde edilen 9.5 dB'lik taşıyıcı-gürültü oranı uygun olarak tespit edilmiştir.

TABLE OF CONTENTS

| | |
|--|------|
| ACKNOWLEDGEMENTS..... | iii |
| ABSTRACT..... | iv |
| ÖZET | v |
| TABLE OF CONTENTS..... | vi |
| LIST OF FIGURES | viii |
| LIST OF TABLES..... | xiv |
| LIST OF SYMBOLS / ABBREVIATIONS..... | xv |
| 1. INTRODUCTION | 1 |
| 2. SYSTEM LEVEL REQUIREMENTS FOR MOBILE SATELITE TV | |
| ANTENNA | 4 |
| 3. STATIONARY SATELLITE TV DISH BASED ANTENN..... | 8 |
| 4. WIDEBAND, HIGH GAIN ANTENNA ELEMENT DESIGN | 13 |
| 4.1. GAIN-BANDWIDTH PRODUCT OF RECTANGULAR PATCH | 14 |
| ANTENNA | |
| 4.2. APERTURE COUPLED MICROSTRIP PATCH ANTENNA | 18 |
| 4.3. PARAMETRIC STUDY OF THE APERTURE COUPLED STACKED | |
| MICROSTRIP PATCH ANTENNA | 22 |
| 4.4. DESIGN OF Ku BAND ANTENNA | 28 |
| 4.5. FOM DEFINITIONS AND COMPARATIVE STUDY WITH PREVIOUS | |
| ANTENNA DESIGNS | 31 |
| 4.6. DESIGN OF X/Ku BAND ANTENNA ELEMENT..... | 32 |
| 4.7. PRACTICAL EXAMPLES OF SUB-ARRAYS SUITABLE FOR | |
| SATELLITE COMMUNICATION SYSTEMS BUILT UP ON PROPOSED | |
| STRUCTURES..... | 37 |
| 4.7.1. Ku band sub-array antenna..... | 37 |
| 4.7.2. X/Ku band sub array antenna..... | 44 |
| 5. SIMULATION AND EXPERIMENTAL RESULTS..... | 48 |
| 5.1. ARRAY SYNTHESIS | 48 |
| 5.2. HYBRID MICROSTRIP AND WAVEGUIDE FEED NETWORK | 51 |

| | |
|--|----|
| 5.3. DESIGN OF A 4 BY 8 (32 ELEMENT) SUBARRAY | 59 |
| 5.4. DESIGN OF 8-TO-1 WAVEGUIDE POWER COMBINER | 63 |
| 5.5. DESIGN EXAMPLE OF A 64 ELEMENT BROADSIDE ANTENNA ARRAY WITH HYBRID FEED NETWORK..... | 66 |
| 6. COMPLETE ARRAY REALIZATION AND FIELD TESTS..... | 75 |
| 7. CONCLUSION..... | 80 |
| REFERENCES | 81 |

LIST OF FIGURES

| | |
|--|----|
| Figure 2.1. System configuration of the array antenna | 6 |
| Figure 3.1. Standard parabolic dish | 8 |
| Figure 3.2. Gain of the dish antennas | 9 |
| Figure 3.3. Gain pattern for 80 cm dish antenna..... | 9 |
| Figure 3.4. Gain pattern for 60 cm dish antenna..... | 10 |
| Figure 3.5. Gain pattern for 40 cm dish antenna..... | 10 |
| Figure 3.6. Mobilsat antenna (Reference Antenna)..... | 11 |
| Figure 3.7. Mobilsat dish antenna gain..... | 11 |
| Figure 3.8. Mobilsat gain pattern (elevation pattern) | 12 |
| Figure 3.9. Mobilsat gain pattern (azimuth pattern) | 12 |
| Figure 4.1. GBWP vs. k_0h for different dielectric materials..... | 17 |
| Figure 4.2. GBWP vs. k_0h for different W/L ratios | 17 |
| Figure 4.3. GBWP vs. k_0h comparison between aperture coupled (non-resonant slot) microstrip antenna and pin-feed microstrip antenna | 18 |
| Figure 4.4. Aperture coupled antenna and possible aperture shapes | 20 |

| | |
|---|----|
| Figure 4.5. Equivalent circuit representation of aperture coupled antenna. | 21 |
| Figure 4.6. Simulated and Calculated Input Reflection Coefficients of Aperture Coupled Antennas (Fig. 2.) and Equivalent Circuit Model (Fig. 3.), respectively..... | 22 |
| Figure 4.7. Effects on gain and impedance for parametric changes in L_1 | 23 |
| Figure 4.8. Effects on gain and impedance for parametric changes in W_1 | 24 |
| Figure 4.9. Effects on gain and impedance for parametric changes in h_1 and h_2 | 25 |
| Figure 4.10. Effects on gain and impedance for parametric changes in L_{pp} | 26 |
| Figure 4.11. Effects on gain and impedance for parametric changes in L_{rp} | 27 |
| Figure 4.12. Effects on gain and impedance for parametric changes in L_{stub} | 28 |
| Figure 4.13. Aperture coupled stacked microstrip patch antenna..... | 29 |
| Figure 4.14. Antenna prototype: top (patch) side and bottom (feed line) side. | 29 |
| Figure 4.15. Simulated and measured, Gain and Input Reflection Coefficient vs. Frequency graphs of Aperture coupled antenna | 30 |
| Figure 4.16. Simulated and measured, normalized gain patterns at 11.5 GHz..... | 30 |
| Figure 4.17. Single element antenna..... | 34 |
| Figure 4.18. Normalized gain patterns for different offset values at 11 GHz | 36 |
| Figure 4.19. Gain of the broadside and beam tilted antenna structures..... | 36 |

| | |
|--|----|
| Figure 4.20. $ \Gamma $ of the antenna | 37 |
| Figure 4.21. Aperture coupled microstrip patch antenna..... | 38 |
| Figure 4.22. Single element input reflection coefficient and gain at 0° , 10° , 20° , 30° , and 40° | 40 |
| Figure 4.23. Single element antenna gain pattern at 12 GHz. | 40 |
| Figure 4.24. 2x4 Eight-element antenna array, a) 3D view (slot plane removed), b) looking from top (slot plane removed), c) looking from bottom (slots are shown in red) | 41 |
| Figure 4.25. Single and eight-element antenna gain at $\theta = 20^\circ$ and input reflection coefficient of array. | 41 |
| Figure 4.26. 3D gain pattern at 12 GHz.3D gain pattern at 12 GHz | 41 |
| Figure 4.27. Array antenna prototype, a) top (patch) side, b) bottom (feed line) side ... | 42 |
| Figure 4.28. Measured antenna array gain at $\theta = 20^\circ$ and its return loss..... | 43 |
| Figure 4.29. Measured array gain pattern at 10.8, 11.8 and 12.3 GHz..... | 43 |
| Figure 4.30. 16-element fixed beam array with feed network..... | 45 |
| Figure 4.31. Fabricated 4x4 array, a) top view, b) bottom view..... | 46 |
| Figure 4.32. Gain of 4x4 array..... | 46 |
| Figure 4.33. Input impedance match of proposed array | 47 |

| | |
|--|----|
| Figure 4.34. Normalized gain pattern @ 11.5 GHz..... | 47 |
| Figure 5.1. Two dimensional array..... | 48 |
| Figure 5.2. Formation of 256 element (8x32) antenna array..... | 50 |
| Figure 5.3. Array Factor elevation pattern of synthesized array..... | 50 |
| Figure 5.4. Microstrip-to-waveguide transition..... | 55 |
| Figure 5.5. Simulated transmission loss and impedance match of microstrip to waveguide transition..... | 55 |
| Figure 5.6. Layout of the feed network..... | 56 |
| Figure 5.7. Subarray configuration for a) vertical polarization, b) horizontal polarization..... | 60 |
| Figure 5.8. Prototypes of subarrays..... | 60 |
| Figure 5.9. Input reflection coefficient of 32 element subarray, a) vertical polarization, b) horizontal polarization. | 61 |
| Figure 5.10. Radiation pattern of 32 element subarray at 11.9 GHz. a) vertical polarization, b) horizontal polarization. | 61 |
| Figure 5.11. 8-to-1 Power combiner..... | 63 |
| Figure 5.12. Waveguide bends and junctions. a) Bend b) T-Junction..... | 64 |
| Figure 5.13. Simulated input reflection coefficient of 8-to-1 power combiner..... | 65 |

| | |
|--|----|
| Figure 5.14. Simulated transmission coefficients of 8-to-1 power combiner..... | 65 |
| Figure 5.15. Realized power combiner..... | 66 |
| Figure 5.16. 32 element subarray with microstrip feed network..... | 66 |
| Figure 5.17. Subarray gain and input match..... | 67 |
| Figure 5.18. Normalized gain patterns of subarray a) azimuth b) elevation..... | 68 |
| Figure 5.19. Waveguide combiner..... | 69 |
| Figure 5.20. Simulation of surface currents for waveguide combiner..... | 69 |
| Figure 5.21. Microstrip to waveguide transition..... | 70 |
| Figure 5.22. Waveguide combiner prototype..... | 70 |
| Figure 5.23. Wilkinson power divider on the inputs of waveguide combiner..... | 71 |
| Figure 5.24. Measured transition and waveguide loss..... | 71 |
| Figure 5.25. Prototype of the array (L= 176 mm, W= 86 mm). | 72 |
| Figure 5.26. Array gain and input match..... | 72 |
| Figure 5.27. Measured gain patterns of the full array..... | 73 |
| Figure 5.28. CNR measurement using DBS receiver and spectrum analyzer..... | 74 |
| Figure 5.29. CNR measurement using DBS receiver and spectrum analyzer..... | 74 |

| | |
|---|----|
| Figure 6.1. Prototype of vertical polarization 256 element array | 76 |
| Figure 6.2. S_{11} of array antenna. | 76 |
| Figure 6.3. Gain of array antenna ($\theta=20^\circ$ cut). | 77 |
| Figure 6.4. Radiation pattern of vertical polarized full array in azimuth plane..... | 77 |
| Figure 6.5. Radiation pattern of vertically polarized full array in θ -plane | 78 |
| Figure 6.6. Radiation pattern of vertically polarized full array in θ -plane | 78 |
| Figure 6.7. Spectrum analyzer measurement of DBS signal. | 79 |

LIST OF TABLES

| | | |
|------------|--|----|
| Table 2.1. | Target specifications for Mobile Satellite TV antenna..... | 4 |
| Table 4.1. | Comparison of Antenna Parameters | 22 |
| Table 4.2. | Comparison of Antenna Structures | 32 |
| Table 4.3. | L_{off} (mm) vs. Beam Tilt and Gain | 35 |
| Table 5.1. | Electrical properties Nelco NX9300 | 52 |
| Table 5.2. | Summary of losses..... | 56 |

LIST OF SYMBOLS / ABBREVIATIONS

| | |
|------------------|--|
| ACMSA | Aperture coupled microstrip antenna |
| AF | Array factor |
| BW | Bandwidth |
| CNR | Carrier-to-noise ratio |
| D | Directivity |
| dB | Decibel |
| dB _i | Decibel isotropic |
| DBS | Direct broadcast from satellite |
| dBW | Decibel watt |
| EIRP | Effective isotropically radiated power |
| FBW | Fractional Bandwidth |
| FOM | Figure of merit |
| G | Gain |
| GBWP | Gain bandwidth product |
| h | Height |
| HPBW | Half power beam width |
| IF | Intermediate Frequency |
| L | Length |
| MOM | Method of moments |
| MSA | Microstrip antenna |
| Q | Quality factor |
| SAR | Synthetic aperture radar |
| SCMSA | Slot coupled microstrip antenna |
| S _{ij} | ijth scattering parameters |
| SMD | Surface mount device |
| SNR | Signal-to-noise ratio |
| TEM | Transverse electromagnetic |
| TM _{ij} | Transvers magnetic field, ijth mode |
| TV | Television |

| | |
|----------|-----------------------------|
| VSWR | Voltage standing wave ratio |
| W | Width |
| Γ | Reflection coefficient |

1. INTRODUCTION

Information and entertainment systems for reception of direct broadcast from satellite (DBS) on mobile environments have been a great challenge for the automotive industry. Over the last two decades there has been great interest for developing low-cost, high performance systems working on mobile platforms. Such systems in automobiles now demand compact mobile antennas for reception of direct broadcast from satellite (DBS) from different service providers simultaneously.

Antenna being the most crucial part of the reception system must satisfy several challenging demands such as low profile, high gain, broadband, and low cost. Although reflector based antennas are ideal for stationary reception systems, their relatively large size and height preclude their use in automobiles and minibuses. In addition, satellite tracking under fast moving vehicle applications together with dynamically changing road conditions makes the antenna design complicated. The antenna system must be capable for uninterrupted reception in variable geographic terrains in which elevation angles change vastly. Research made on middle sized vehicles have pointed out that such vehicles are capable of making turns with 60 degree/s speed and 100 degree/s² acceleration [1].

Due to cost constraint; most designs utilize mechanical scanning in azimuth and electronic scanning in elevation. Electronic scanning over broad elevation range using phase shifters coupled with low-noise amplifiers is also not preferred due to added electronics for phase shifter control circuitry. Instead, fixed beam at some elevation angle with electronic scanning around that elevation angle due to changing road conditions is preferred due to less phase shifters and reduced antenna complexity. At the heart of these configurations, low-loss antenna array play a critical role to satisfy gain-over-temperature requirement. Loss in the antenna array is mostly dominated by the feedline loss which can be prohibitively large at Ku band frequencies.

A slotted waveguide antenna array with relatively large beam tilt capability was designed for Japanese DBS system in [2]. However, relatively small bandwidth (11.7 - 12 GHz) and moderate gain (~ 26.5 dBi) makes the design unsuitable for multiple service providers.

For the same DBS system, microstrip antenna arrays were also proposed [3, 4]. Aperture coupled transmit and receive antenna array for mobile satellite communication systems was detailed in [5], but the antenna size and height were relatively large for automobile rooftop use. Active phased array with a beam squint around main beam (similar to sequential lobing) was suggested as an alternative to monopulse tracking of satellites in [6], but the results were presented at 12 GHz only and the bandwidth of the system was not mentioned. Microstrip antenna array for uplink Ku band was presented in [7] using simulations. Degenerate mode microstrip patch antenna was used in [1] for dual circular polarization in a relatively small bandwidth (12.2 - 12.7 GHz). In addition, the design required 496 elements to obtain 31.5 dBi gain. A series fed slot coupled antenna array was designed in [8] over a small portion of the downlink band (11.8 - 12.2 GHz). A hybrid microstrip and waveguide feed network was proposed for Ku band DBS systems with 4% bandwidth in [9]. Most of these designs were targeted for a specific satellite service provider operating over 400 or 500 MHz of the downlink band (10.8 - 12.75 GHz). When multiple service providers operating at different parts of the downlink band are targeted, the antenna design and its accompanying feed network must be broadband to cover the entire downlink band. Antenna gain and beam tilt must also be satisfied over the band of interest.

The goal of this study is to present a planar antenna array that covers entire downlink frequencies. We are particularly interested in Turkish DBS system (42° E) which operates over 10.8 - 12.75 GHz frequency band. Broadband antenna element design with 16.5% bandwidth may not be difficult to achieve, but designing a low-loss compatible feed network together with the antenna array is rather intricate. We propose nonresonant aperture coupled stacked antenna elements with corporate feed network to form subarrays. The subarrays, which are relatively distant to each other, are combined in a waveguide to reduce feed network loss. We developed a novel microstrip to waveguide transition to fulfill the bandwidth and low loss requirements. The designed antenna has only 25 mm in height and achieves gain in excess of 29.4 dBi at 42° fixed elevation tilt.

The thesis is arranged as follows: the main specification and size of the antenna are presented in Chapter 2. The characteristics of some parabolic reflectors and the reference quasi-parabolic antenna are detailed in Chapter 3. We discuss the gain bandwidth product

of patch antennas and propose a broadband, high gain aperture coupled stacked microstrip patch antenna in Chapter 4. In Chapter 5, step by step design of a large array and its feed network, considering the losses are examined in detail. It is finally shown that the full array and its field results in Chapter 6.

2. SYSTEM LEVEL REQUIREMENTS FOR MOBILE SATELITE TV ANTENNA

Most of the existing commercial products were based on reflector type antennas which possess excellent bandwidth, gain, noise figure and half power beam width (HPBW) characteristics. These aspects also make these antennas ideal candidate for control and tracking of satellites while the vehicle is on the move. However, their bulky size and high profile cause aerodynamic problems on vehicles, also these structures are not suitable for smaller vehicles. A low profile structure such as microstrip antenna arrays with reduced size would be advantageous. Based on the previous studies and commercial products target system specifications are formed and summarized in Table 2.1.

Table 2.1. Target specifications for Mobile Satellite TV antenna

| Specification | Value |
|---|--|
| Frequency | 10.8 - 12.8 GHz |
| Polarization | Dual Linear (V and H) |
| Antenna G/T (EIRP >54 dBW) | > 5.5 dB/°K at 45° elevation |
| Antenna Gain | 29 dBi (per polarization) |
| Spatial Coverage | 35° - 75° elevation 0° - 360° azimuth |
| Antenna height (w/ max mechanical tilt) | < 70 mm |
| System diameter | < 75 cm |
| Weight (w/o electromechanical components) | < 3 kg |

Low profile system constraint can be met with waveguide slot elements or microstrip patch antenna elements. The bandwidth of the system is much greater than many DBS systems currently used. Such large bandwidth with waveguide slot arrays require special waveguide structures such as ridged or dielectric loaded waveguides which significantly increase production cost of the system. Microstrip antenna elements, on the other hand, are more

attractive due to their light weight, low profile and low production costs. However, broadband antenna design with its feed network requires a careful study.

Satellite scanning is envisioned with one-dimensional electronic beam scanning in elevation and mechanical tracking in azimuth. Full electronic scanning in both planes is not preferred due to large number of phase shifters required, which significantly impact system cost.

Geostationary satellites for TV broadcasting are mostly spaced with 6° or more for azimuth tracking. Thus, the antenna half power beamwidth in azimuth is usually designed for 5° or less but not lesser than 1.5° as tracking becomes challenging in a moving vehicle. Minimum 7 dB of carrier-to-noise ratio (CNR) is assumed for satellite lock (tracking and reception) over a 32 MHz IF (intermediate frequency) bandwidth which is the maximum bandwidth for TurkSat.

It is possible to achieve antenna gain with max 3° of azimuth HPBW in a planar microstrip antenna array with appropriate number of elements. However, maintaining target antenna gain at low elevation angles becomes difficult with broadside antenna elements. TM_{20} mode type radiation pattern may be more suitable, but achieving target bandwidth with such patch is extremely difficult. Besides, the antenna size would be much larger compared to TM_{01} mode broadside looking patch. A compromise would be using panels or subarrays of antenna each mounted on a platform that can be mechanically tilted to certain elevation angle without significantly increasing the height profile of the antenna. Although this brings additional cost and control to the system, this idea has been used in earlier works [4 - 5], [7 - 9], and is very common to many satellite communication systems. Added complexity of the system overweighs the benefits of fulfilling electrical specifications. In the following design, we suggest the use of two panels, built from microstrip patch antennas, for each polarization to minimize the added complexity of this implementation. Mechanical tilt is capable of providing up to 22° of array tilt. This enables the antenna to cover lower elevation angles easily, and at the same time, relax scan range in elevation axis. The system configuration of the proposed design is illustrated in Figure 2.1.

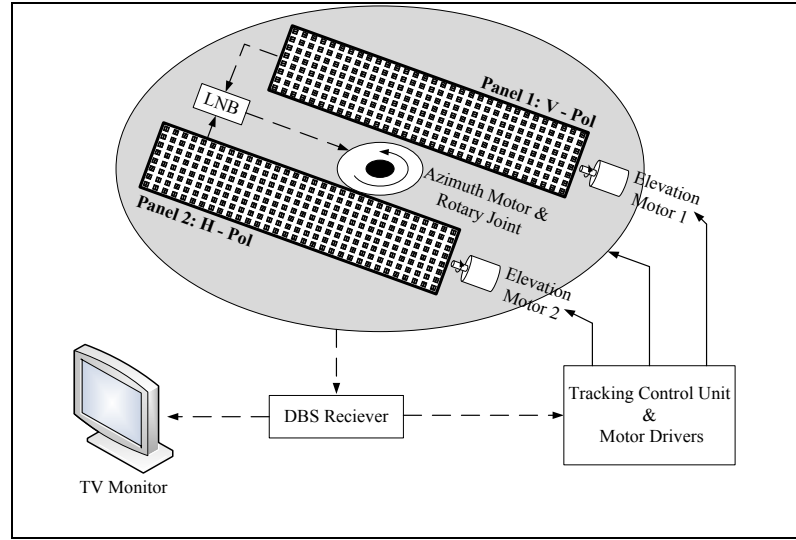


Figure 2.1. System configuration of the array antenna.

The directivity of TM_{01} mode broadside patch is roughly:

$$D_p = \frac{4\pi}{\Omega_A} \approx \frac{4\pi}{\pi} = 4 \text{ (6 dBi)} \quad (2.1)$$

where, Ω_A represents beam solid area. For K elements, array directivity D_A becomes:

$$D_A \approx K D_p \quad (2.2)$$

If elevation scanning of $\pm 15^\circ$ is assumed, $HPBW_\theta$ in elevation can be taken as 30° . $HPBW_\phi$ can be set to 3° for azimuth tracking. Then, the directivity of the array is roughly [10]:

$$D_A \approx \frac{40000}{HPBW_\theta HPBW_\phi} \approx 444 \text{ (26.47 dBi)} \quad (2.3)$$

Furthermore, if 55% total efficiency (due to feed network loss, mismatch loss) is assumed, the gain of the array should be 807 (29 dBi). Number of broadside patch elements required for this gain is 202. To preserve symmetry and to account of other losses (e.g. radom,

mutual coupling among array elements), we estimate 256 elements per polarization.

To meet bandwidth requirements of the array antenna, the element antenna should possess even broader bandwidth than the array. Although feed network loss indirectly improves impedance match of the array, inter element coupling reduces single antenna bandwidth. Nonresonant slot coupled stacked patch antenna was shown to exhibit very good bandwidth and gain characteristics at this frequency band [11].

The following section presents some of the most common reflector type antennas and a quasi-parabolic reflector designed by NETA Technologies, which is a commercial product used for mobile DBS systems. This “Reference Antenna” and the specifications given in Table 2.1 shape our antenna design.

3. STATIONARY SATELLITE TV DISH BASED ANTENNAS

Three dish antennas with different parabola dimensions are analyzed in this chapter. The dish diameters are chosen as 80 cm, 60 cm and 40 cm. These are the most widely used dish types for Ku band DBS reception systems. It is necessary to analyze these antennas so that subsequent comparative studies can be performed with the proposed antenna.

Figure 3.1 shows the structure of a standard dish antenna. The gain and the patterns of the 80 cm, 60 cm and 40 cm parabolic reflectors are shown in Figure 3.2 through Figure 3.5.

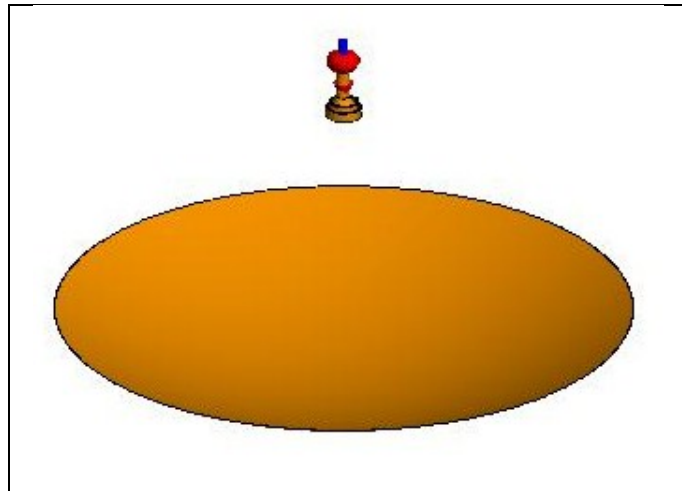


Figure 3.1. Standard parabolic dish.

The gain and radiation patterns of the 80 cm and 60 cm dish antennas are very difficult to replicate with a planar antenna. Actually, given the transverse dimension constraints, it is not possible to create a planar antenna even in theory unless super directive antenna elements with proper phasing are used. On the other hand, the 40 cm dish antenna can be our reference, since it is possible to replicate similar characteristics in a planar array. Most of the commercial systems utilize this size dish antenna. A commercial product used by NETA Electronics A.Ş., is shown in Figure 3.6 where a quasi-parabolic dish antenna which has nearly the properties of the 40 cm dish antenna is used. The antenna has an offset feed in order to set its beam direction. This antenna is taken as the reference structure for comparison.

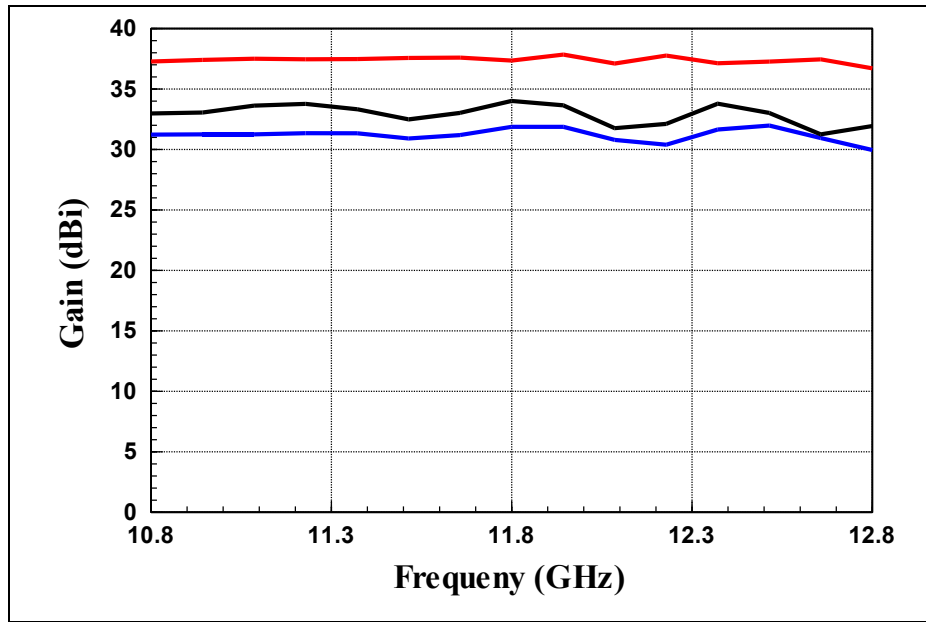


Figure 3.2. Gain of the dish antennas. (— 80 cm, — 60 cm, — 40 cm)

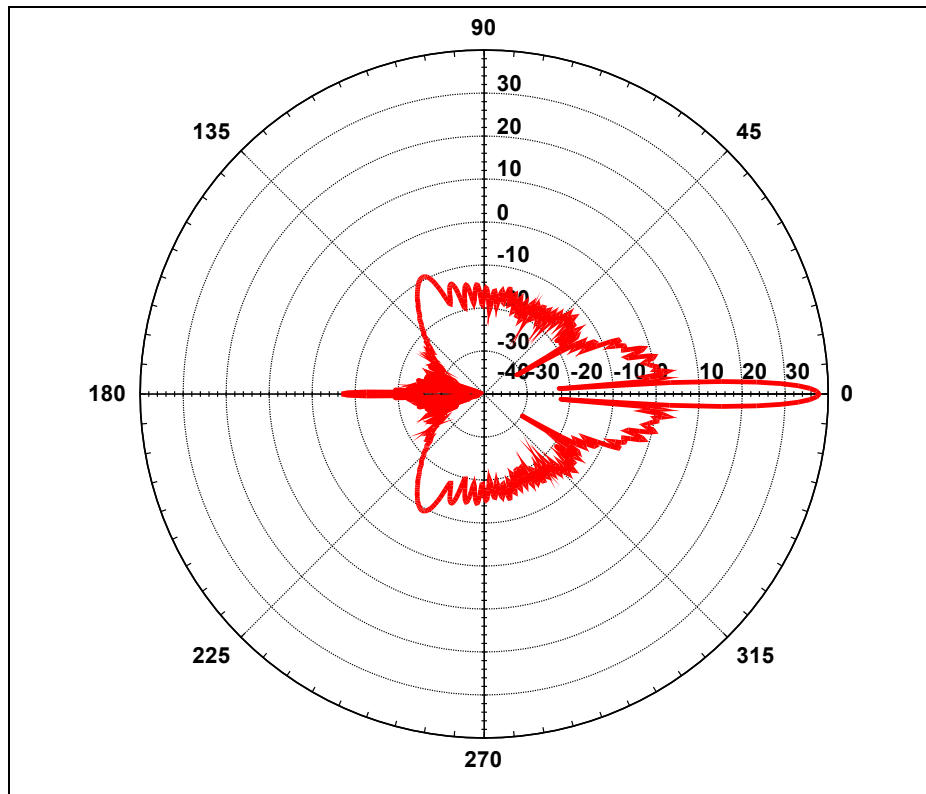


Figure 3.3. Gain pattern for 80 cm dish antenna.

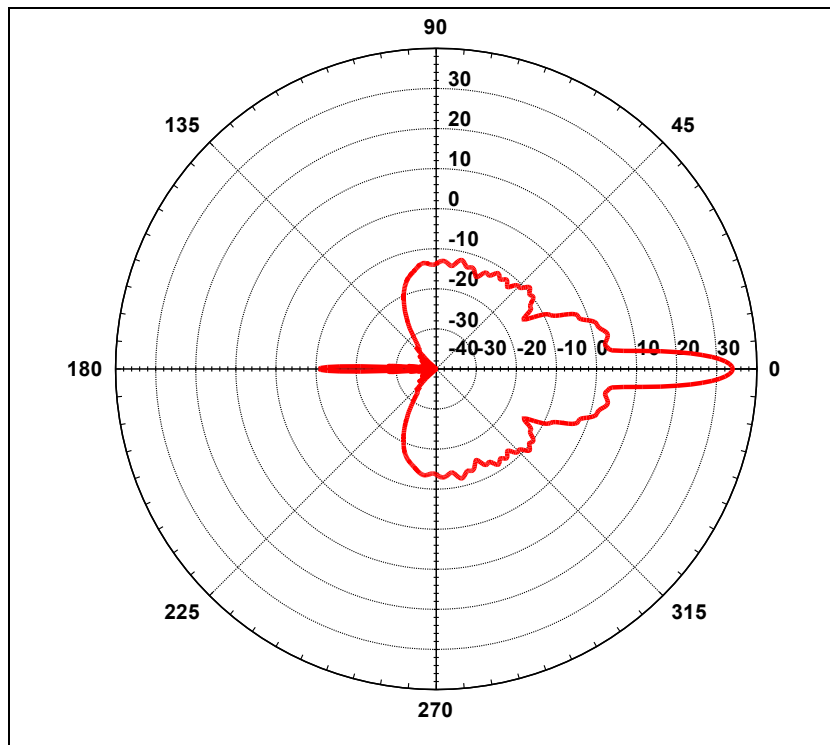


Figure 3.4. Gain pattern for 60 cm dish antenna.

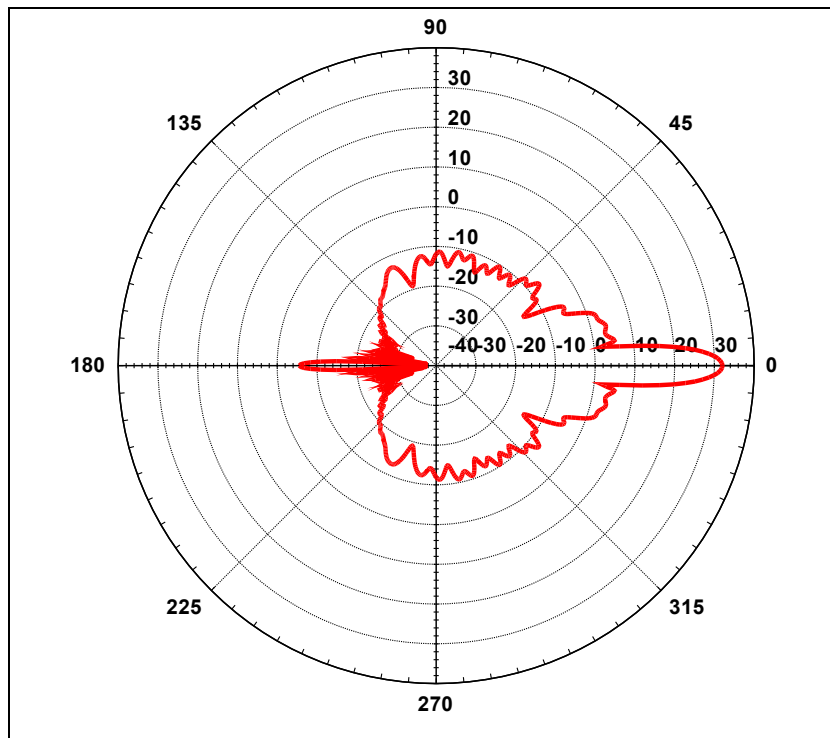


Figure 3.5 Gain pattern for 40 cm dish antenna.

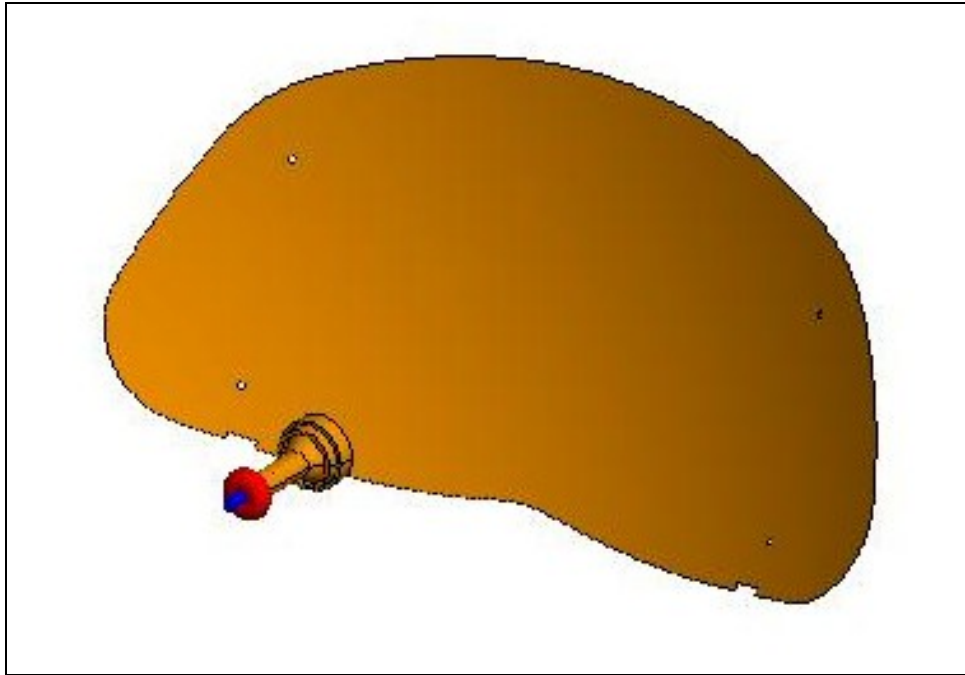


Figure 3.6. Mobilsat antenna (Reference Antenna).

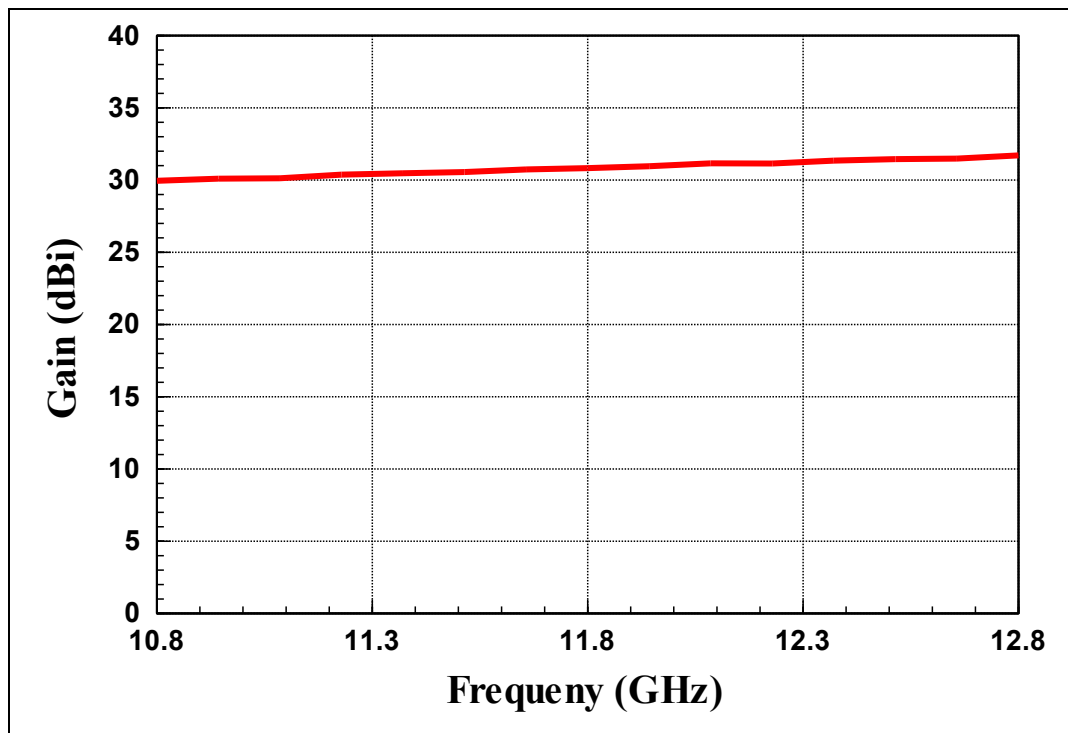


Figure 3.7. Mobilsat dish antenna gain.

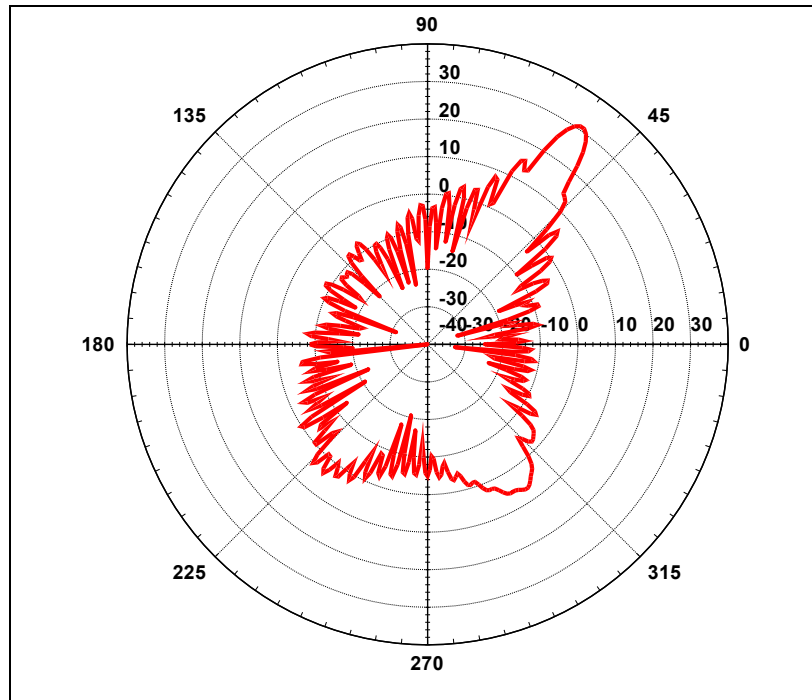


Figure 3.8. Mobilsat gain pattern (elevation plane).

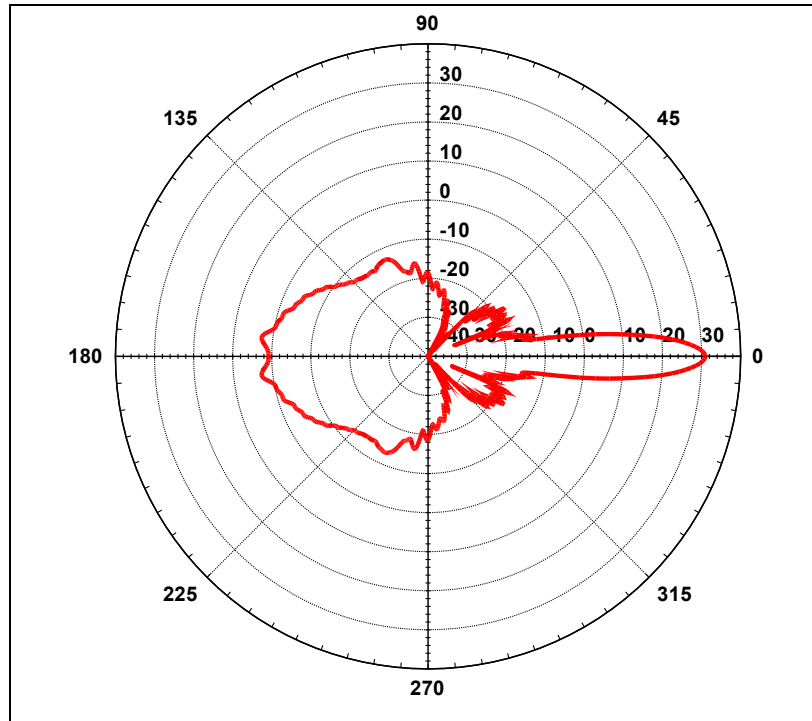


Figure 3.9. Mobilsat gain pattern (azimuth plane).

4. WIDEBAND, HIGH GAIN ANTENNA ELEMENT DESIGN

High gain and wideband planar antennas are vital to meet system specifications in many wireless systems. Once target bandwidth is achieved in the design, antenna gain becomes the next goal because gain directly impacts signal-to-noise ratio (SNR) of the system. Often, minimum gain in the target bandwidth is specified to fulfill SNR requirement. However, gain and bandwidth are usually complementary metrics such that improvement in one results degradation in the other. Thus, one must optimize the design for gain-bandwidth product (GBWP) rather than bandwidth only. An upper bound on gain-bandwidth product can be placed for electrically small antennas [12, 13], but this is rather difficult for multiple resonant or wideband antennas.

One of the most common planar antenna configurations is the aperture coupled microstrip antenna (ACMSA) configuration [14]. Slot coupling is also suitable for high frequency applications where structural dimensions are in millimeter or sub millimeter range. Most of these applications require high directive gain; thus, utilize phased arrays where high gain and wideband antenna elements are required. To increase the bandwidth of an ACMSA, parasitic elements in the form of stacked patches or coplanar parasitic elements were proposed [15, 16]. Unlike coplanar parasitic elements, stacked patches do not increase the aperture area of the antenna, hence does not require increased inter-element spacing that may cause grating lobes. Either a nonresonant slot is coupled to stacked resonant patches or a resonant slot radiates with resonant stacked elements. Stacked patches coupled with a resonant slot exhibited fractional bandwidth (FBW) in excess of 50% with gain in excess of 5 dBi [17, 18]. For nonresonant slot coupling, various slot shapes ranging from rectangular slots to dog-bone shape slots have been proposed [14, 15, 16, 17, 18, 19 and 20]. Hourglass shape nonresonant slot was identified as the best configuration in terms of fractional bandwidth [15]. However, none of these studies considered GBWP, and which configuration produces best gain-bandwidth performance is yet unknown. Also, it is still unclear whether resonant slot or nonresonant slot has better performance.

In any antenna design, bandwidth, gain, and HPBW are the most essential design characteristics along with other features such as cross polarization ratio, front-to-back

ratio, in-band gain ripple, electrical height, and physical dimensions. Although it is difficult to define a common figure-of-merit (FOM) to combine all these metrics into one, we defined several FOMs based on GBWP. We compare performances of various nonresonant and resonant slot coupled stacked patches to identify the best configuration in terms of these FOMs. We are particularly interested in Ku band applications for mobile satellite TV reception and satellite communications. We derive a wideband equivalent circuit representation of ACMSA to study the impact of design parameters on bandwidth. Based on this study, we propose a high gain, wideband antenna structure operating at Ku band with highest FOM compared to earlier works, followed by a parametric study on the antenna.

Specific contributions of this section are: i) GBWP analysis of microstrip and aperture coupled antennas, ii) comparison of resonant versus nonresonant slot coupled antennas in terms of gain and bandwidth, iii) determination of nonresonant slot shape that provides best performance, iv) design of a nonresonant slot coupled antenna and with high FOM. GBWP for single mode rectangular patch antenna will be driven. Aperture coupled antennas and their equivalent circuit representations are presented in sub-section 4.2. A parametric study of the structure is presented in section 4.3 Ku band antenna element design is detailed in sub-section 4.4. FOM definitions and comparison table are given in sub-section 4.5. Section 4.6 will introduce a wideband antenna with high aspect ratio with tilted beam. The final section provides example subarray designs using these two element antennas.

4.1. GAIN-BANDWIDTH PRODUCT OF RECTANGULAR PATCH ANTENNA

The bandwidth for a rectangular patch antenna with length L , width W and substrate height h is given as:

$$BW = \frac{VSWR - 1}{Q\sqrt{VSWR}} \quad (4.1)$$

where, Q represents the quality factor of the patch. Fractional bandwidth rather than absolute bandwidth is regarded as the bandwidth, thus, BW can also be expressed as:

$$BW = \frac{f_U - f_L}{f_C} \quad (4.2)$$

where, f_U , f_L , and f_C represent upper, lower and center frequency of the impedance match frequency band.

For $VSWR < 2$, BW becomes:

$$BW = \frac{1}{Q\sqrt{2}} \quad (4.3)$$

For electrically thin substrates ($h/\lambda \ll 1$), BW can be estimated as [25]:

$$BW = \frac{16}{6\pi\sqrt{2}} \frac{c_1 p}{e_r} \frac{k_0 h}{\epsilon_r} \frac{W}{L} \quad (4.4)$$

where, e_r is the efficiency, $k_0 = 2\pi/\lambda_0$ (free space wavenumber), ϵ_r is the permittivity of the substrate, c_1 and p are functions used in the approximation [26]. For $W/L < 2$, p becomes almost 1, and c_1 becomes 0.4 for air–dielectric and nearly 1 for high permittivity substrates. It is clear from (4.4) that the electrical height of the antenna is directly proportional to the bandwidth. For a given substrate height, the bandwidth is relatively wider at higher frequencies.

The gain of the patch antenna is approximated as [28]:

$$G = \frac{4(k_0 W)^2}{\pi\eta_0} e_r R_r \quad (4.5)$$

where, R_r represents radiation resistance. R_r given in [27] was not very accurate as stated by its authors so a more accurate representation given in [29] can be used. R_r in [29] is approximated to its leading terms and is proportional to:

$$R_r \propto \frac{1}{(k_0 h)^2 \left(k_0 \frac{W}{2} \right)^2 \left[-1 + \frac{14}{\left(k_0 \frac{W}{2} \right)^2} \right]} \quad (4.6)$$

The gain of the antenna is inversely proportional to $(k_0 h)^2$. Hence, neglecting the constants and assuming p equals to 1, $GBWP$ for rectangular patch is proportional to:

$$GBWP \propto \frac{1}{k_0 h} \frac{W}{L} \frac{1}{\left[-1 + \frac{14}{\left(k_0 \frac{W}{2} \right)^2} \right]} \quad (4.7)$$

Therefore, increasing $k_0 h$ for bandwidth improvement deteriorates attainable gain and limits $GBWP$. High aspect ratio (W/L) also improves $GBWP$ if higher order modes are not excited. It is interesting to see that substrate permittivity and antenna efficiency are not the factors of $GBWP$. Low permittivity substrates are good for bandwidth improvement but relatively worse for antenna gain. Aperture coupled antennas mostly follow the same trend those of rectangular antennas, however, approximate relations are quite difficult to obtain.

Although these approximate formulas have been widely accepted, they are only valid for electrically thin substrates. We performed 3D simulations on rectangular patch antenna with pin feed and defined $GBWP$ as:

$$GBWP = \frac{\int_{f_L}^{f_U} G(f) df}{f_U - f_L} \left(\frac{f_U - f_L}{f_C} \right) \quad (4.8)$$

where, $f_L = f_i \leq f_i \leq f_N = f_U$, $i=1,2,\dots,N$ and $G(f)$ represents gain (linear not decibel) as a function of frequency. Rectangular patch antenna is optimized for best $GBWP$ for different $k_0 h$'s and substrates of different relative permittivity ϵ_r . The results are shown in figure 4.1. Unlike approximate formulas, simulations show that $GBWP$ has a maximum at certain $k_0 h$ and it is maximum for air-dielectric substrate. We also ran similar analysis for different

patch aspect ratios for air-dielectric patch only. Again, it appears that there exists an optimum electrical height where *GBWP* is optimal. All simulations were run around Ku-band downlink frequency band (10.8-12.75 GHz).

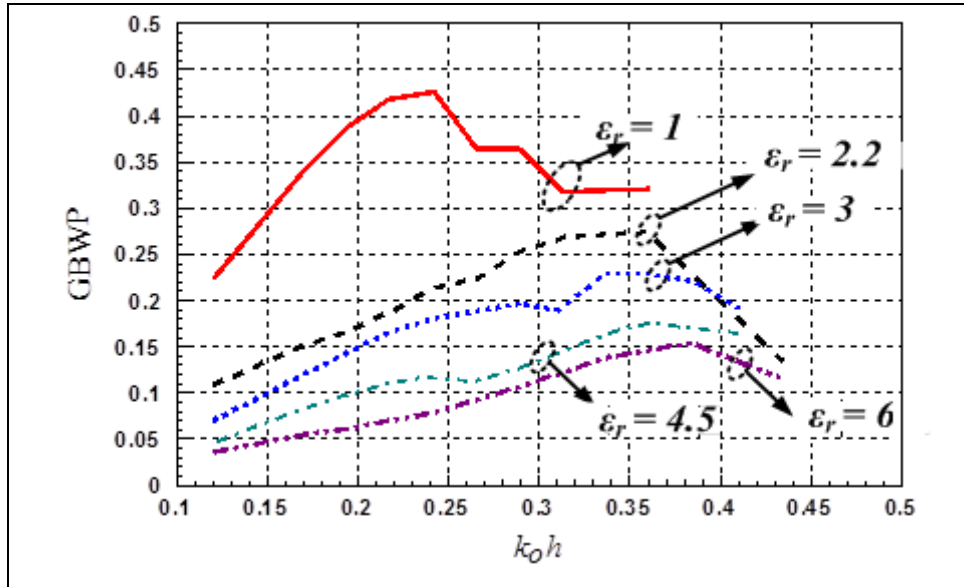


Figure 4.1. GBWP vs. k_0h for different dielectric materials.

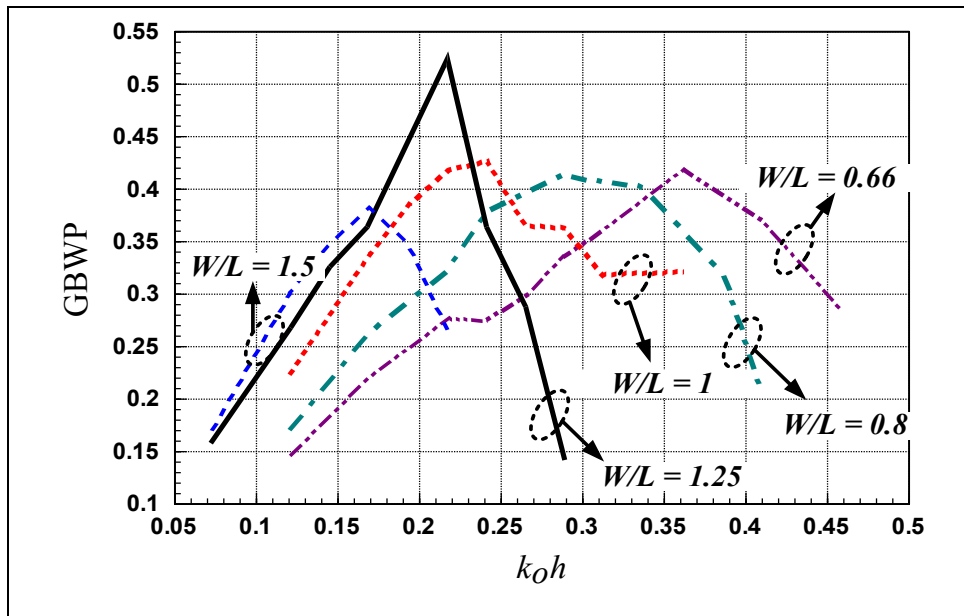


Figure 4.2. GBWP vs. k_0h for different W/L ratios.

We have also compared GBWP performance of pin-feed rectangular patch antenna to that of nonresonant rectangular slot coupled patch antenna and the results are displayed in Figure 4.3. We observed that slot-coupled geometry produces much better GBWP performance as the inductance of pin feed severely limits BW of rectangular patch antenna.

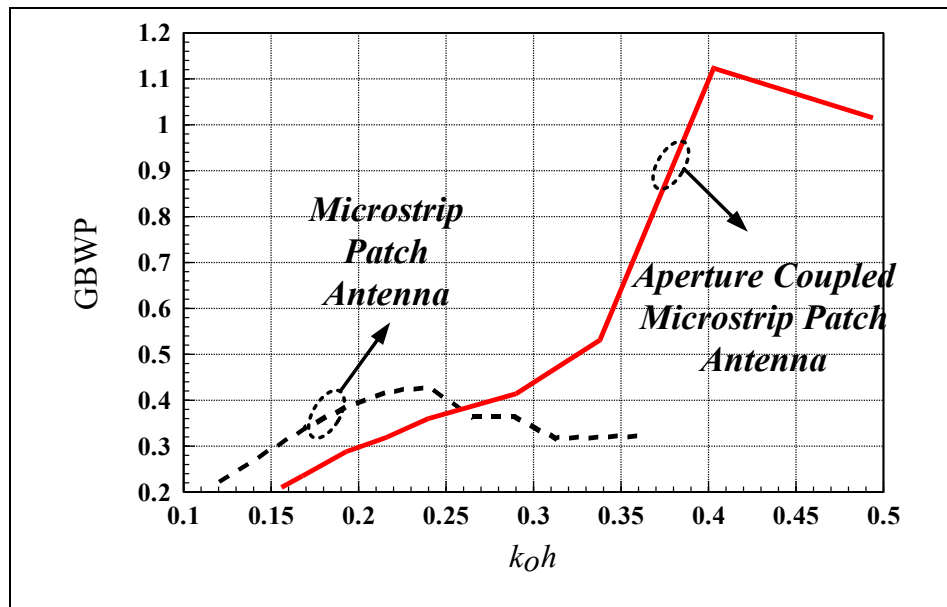


Figure 4.3. GBWP vs. k_0h comparison between aperture coupled (non-resonant slot) microstrip antenna and pin-feed microstrip antenna (antenna substrate is air and ϵ_r for feed substrate of aperture coupled antenna is 2.2)

4.2. APERTURE COUPLED MICROSTRIP PATCH ANTENNA

A typical aperture coupled antenna configuration with possible aperture shapes is illustrated in Figure 4.4. The feed line substrate is Nelco NX9300 ($\epsilon_r = 3$, $\tan\delta = 0.0023$) with 0.5 mm thickness. Radiating and parasitic patches are placed above the slot plane, suspended in air, at h_1 and h_2 , respectively. The feed line is tuned to 50 ohms and open circuited stub is used to give the desired impedance match. The heights of the suspended patches are 1 mm for the radiating patch and 3 mm for the parasitic patch (measured from the slot plane). As it is evident from the configuration, there are too many structural parameters involved in antenna performance evaluation. Equivalent circuit representation of this structure is shown in Figure 4.5. Coupling between the patches and patch-to-

ground are expressed in terms of jX_{M1} and jX_{M2} . These two impedances are particularly important to achieve wideband corroboration of circuit model with simulation results of a 3D electromagnetic solver. The input impedance of the circuit is derived as:

$$Z_{in} = Z_o \frac{Z'_{in} + jZ_o \tan(\beta_{eff} L_{eff})}{Z_o + jZ'_{in} \tan(\beta_{eff} L_{eff})} \quad (4.9)$$

where, β_{eff} is calculated for effective dielectric constant of material and Z'_{in} is given by:

$$Z'_{in} = Z''_{in} + jZ_o \tan(\beta_{eff} L_{stub}) \quad (4.10)$$

and Z''_{in} is:

$$\zeta_1 = Z_{ap} Z_{rp} (n_1^2 Z_{M1} + Z_{pp}) \quad (4.11)$$

$$\zeta_2 = (n_1 n_2)^2 Z_{ap} Z_{rp} (Z_{M1} + Z_{rp}) \quad (4.12)$$

$$\zeta_3 = n_2^2 Z_{ap} Z_{pp} Z_{M2} \quad (4.13)$$

$$\zeta_4 = n_3^2 Z_{rp} (n_1^2 Z_{M1} + Z_{pp}) \quad (4.14)$$

$$\zeta_5 = (n_1 n_2 n_3)^2 (Z_{M1} + Z_{rp}) (Z_{M2} + Z_{ap}) \quad (4.15)$$

$$\zeta_6 = (n_2 n_3)^2 Z_{pp} (Z_{M2} + Z_{ap}) \quad (4.16)$$

$$Z''_{in} = \frac{\zeta_1 + \zeta_2 + \zeta_3}{\zeta_4 + \zeta_5 + \zeta_6} \quad (4.17)$$

Z_{ap} , Z_{rp} , Z_{pp} , Z_{M1} , Z_{M2} , n_1 , n_2 and n_3 were calculated using relations in [25, 26, 27, 28, 29, 30]. Antenna structures are modeled and simulated using FEKO, a commercial electromagnetic field solver based on Method of Moments. For nonresonant slot coupling, rectangular, H-shaped and hourglass slot dimensions are optimized for bandwidth performance.

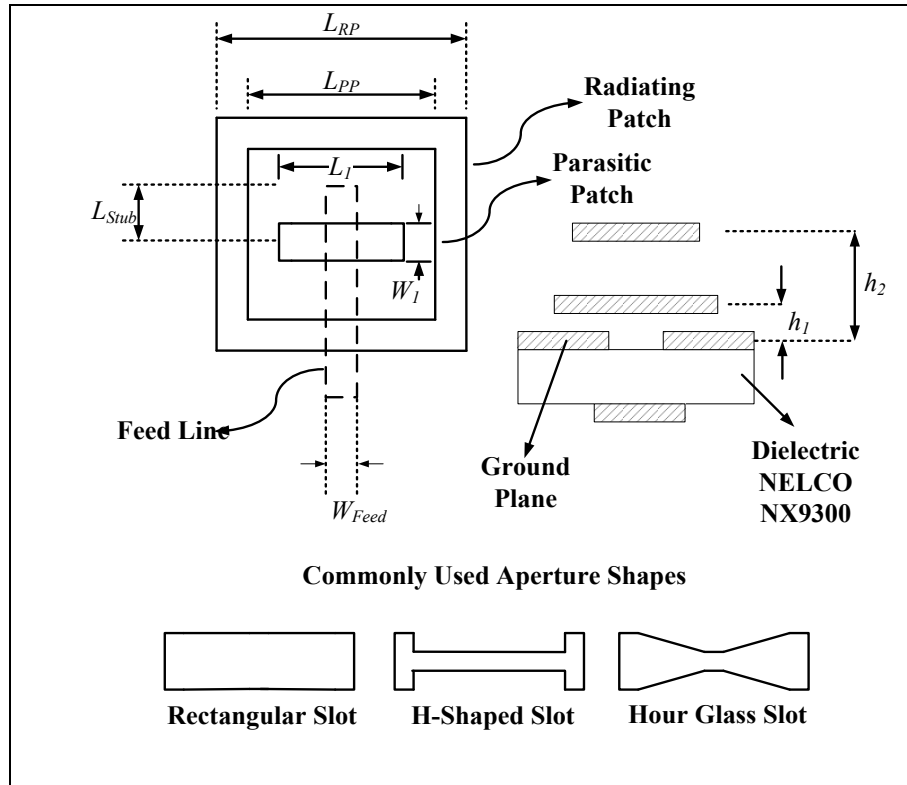


Figure 4.4. Aperture coupled antenna and possible aperture shapes.

Input reflection coefficient for all non-resonant slot coupled antennas and equivalent circuit model for rectangular slot coupled antenna are shown in Figure 4.6. We observe that there is small difference between non-resonant slots for bandwidth ($VSWR < 2$). Equivalent circuit model has fairly close performance to that of rectangular slot. Thus, broadband circuit model of rectangular slot coupled antenna has been verified. Perturbation analysis on structural dimensions reveals that parasitic patch dimensions, slot length and patch heights are more influential on bandwidth whereas, slot width, radiating patch dimensions are less important.

To compare the antenna performances, we defined FOM_I as $GBWP$ without considering the electrical height and half-power beamwidth ($HPBW$) of the antenna. We also studied resonant slot coupled patch antenna, pin-feed microstrip antenna (MSA) and resonant slot with two stacked patches (3 resonators), all optimized for performance. The results are shown in Table 4.1.

We observe that all non-resonant slot coupled antennas have very similar performance, but hour-glass is slightly better than the others. Resonant slot with two stacked patches achieves almost 54% BW.

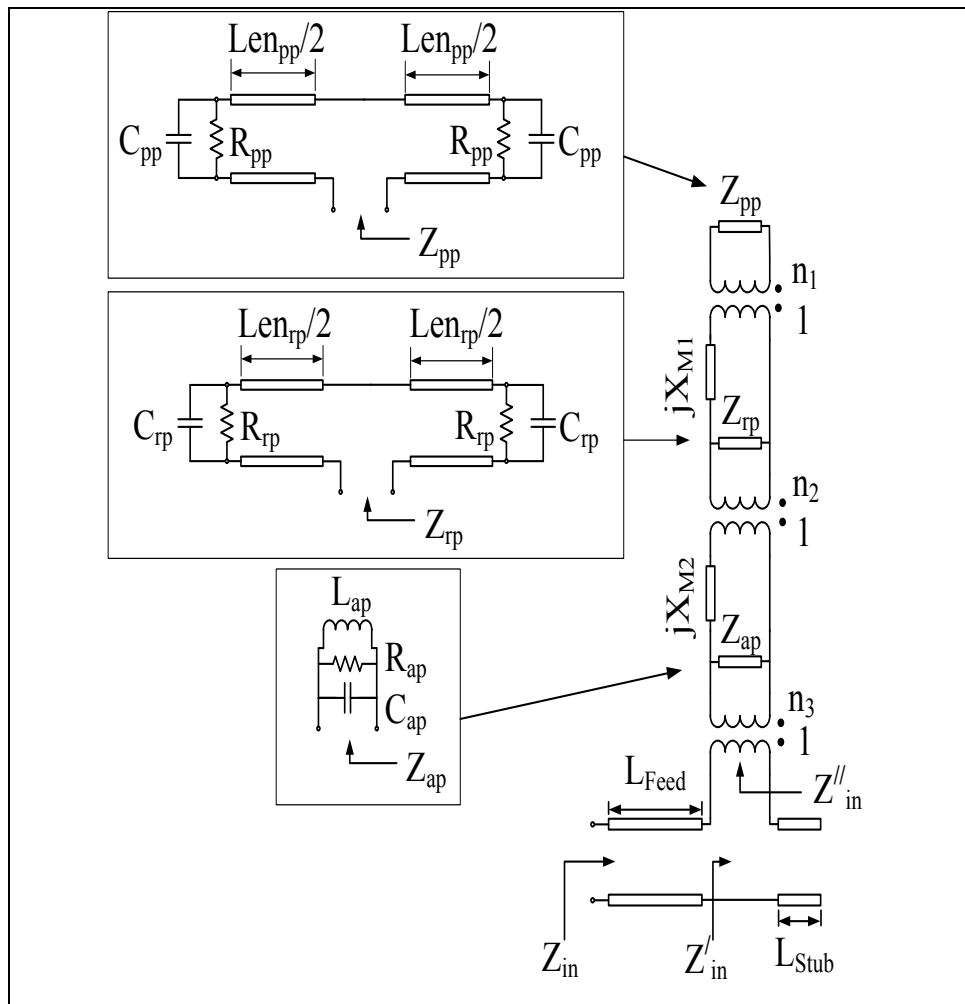


Figure 4.5 Equivalent circuit representation of aperture coupled antenna.

Table 4.1 Comparison of Antenna Parameters

| Antenna | Gain (dBi) | BW | k_{oh} | FOM_1 |
|------------------|-------------|-------|----------|---------|
| H-Shaped Slot | 7.87 – 9.06 | 0.275 | 0.837 | 2.088 |
| Hour Glass Slot | 7.88 – 9.07 | 0.283 | 0.837 | 2.150 |
| Rectangular Slot | 7.89 – 9.04 | 0.275 | 0.837 | 2.083 |
| Resonant Slot | 3.51 – 9.19 | 0.350 | 0.736 | 2.142 |
| 3 Resonators | 5.14 – 8.88 | 0.539 | 0.431 | 1.314 |
| Pin-feed MSA | 9.2 – 9.3 | 0.047 | 0.277 | 0.401 |

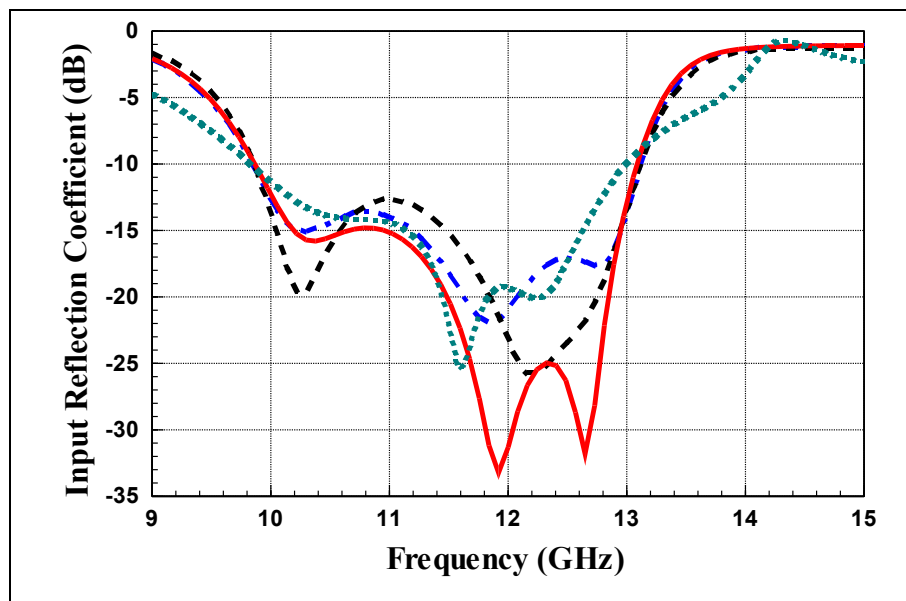


Figure 4.6. Simulated and calculated input reflection coefficients of aperture coupled antennas (Fig. 2.) and equivalent circuit model (Fig. 3.), respectively.

(— SCMSA with rectangular slot, - - - SCMSA with H-shaped slot, - · - SCMSA with hour glass shaped slot, ······ Equivalent circuit model SCMSA with rectangular slot).

4.3 PARAMETRIC STUDY OF THE APERTURE COUPLED STACKED MICROSTRIP PATCH ANTENNA

This section is given in order to understand how the gain and impedances of an aperture coupled stacked microstrip patch antenna affected by the change of parameters. The parameter investigated will be change while keeping the other parameters constant. This study will give an insight on the antennas behavior. The parameters to be investigated are given in Figure 4.4. The effects of material parameters will not be included in this work but detailed investigations can be found in [15].

The antenna will be analyzed in three sections: Aperture dimensions, radiating and parasitic patch dimensions and heights, feed line dimensions. Analysis of an antenna with an hour glass aperture via theoretical analysis methods is complicated due to its structure. Hence the parametric study will be carried out using a MOM based commercial full wave electromagnetic solver FEKO.

The slot show in figure 4.4 has mainly two parameters the length L_1 and the width W_1 . Effects on impedance and gain for variations in these parameters are shown in figure 4.7 and figure 4.8.

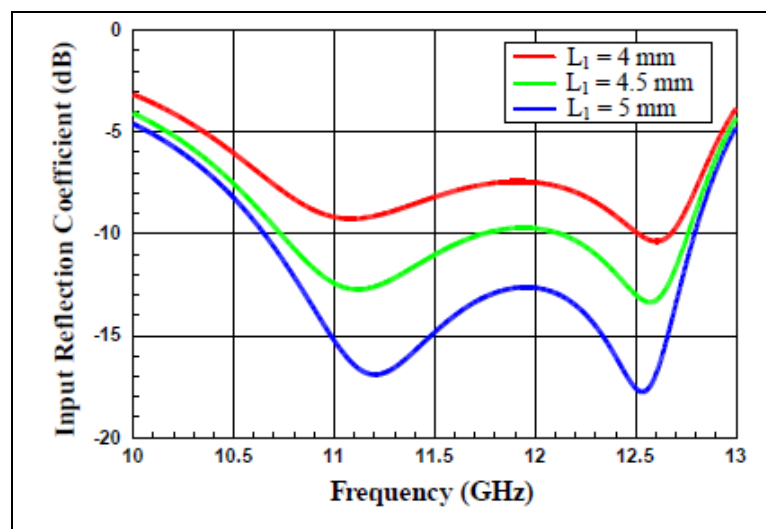


Figure 4.7. Effects on gain and impedance for parametric changes in L_1 .

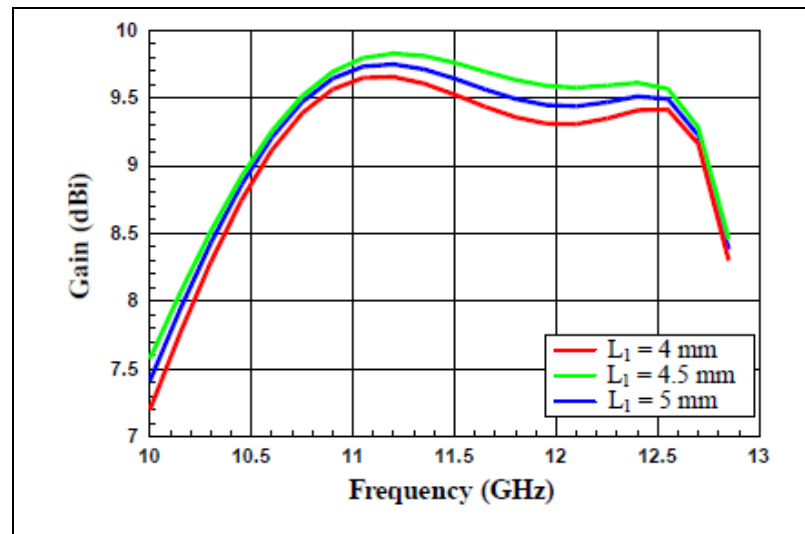


Figure 4.7. Effects on gain and impedance for parametric changes in L_1 . (continued...)

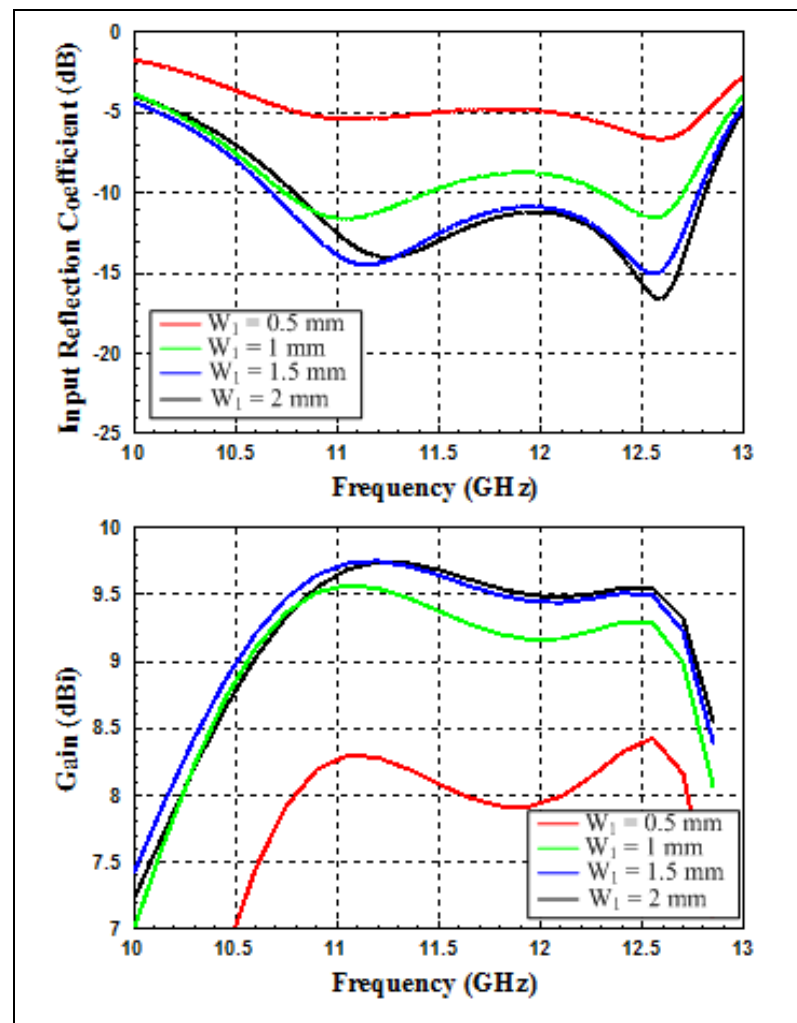


Figure 4.8. Effects on gain and impedance for parametric changes in W_1 .

Due to its nonresonant dimensions the resonance of the slot is far away from the operation band. The wide band width is achieved from the double resonance characteristic of the stacked patches. Figure 4.9 through Figure 4.12 shows the effects of patch dimensions and heights on the double resonance characteristic. Figure 4.9 shows how different heights can change the resonance conditions. Optimal values for h_1 and h_2 can be found near 1 mm and 3 mm, respectively. Figure 4.10 and Figure 4.11 shows how patch dimensions L_{pp} and L_{rp} effect the double resonance characteristic. For parasitic and radiating patches, values 9.2 mm and 11 mm, respectively, are nearly optimal dimensions. Figure 4.12 shows how different stub lengths affect the impedance match. It can be seen that after a good optimization of all the parameters a final tuning on stub length can give us an optimal design. The stub length, beside its better matching ability has a very important property. A careful look at Figure 4.12, it can be seen that the flatness in gain with respect to frequency can be minimized with an optimal stub length.

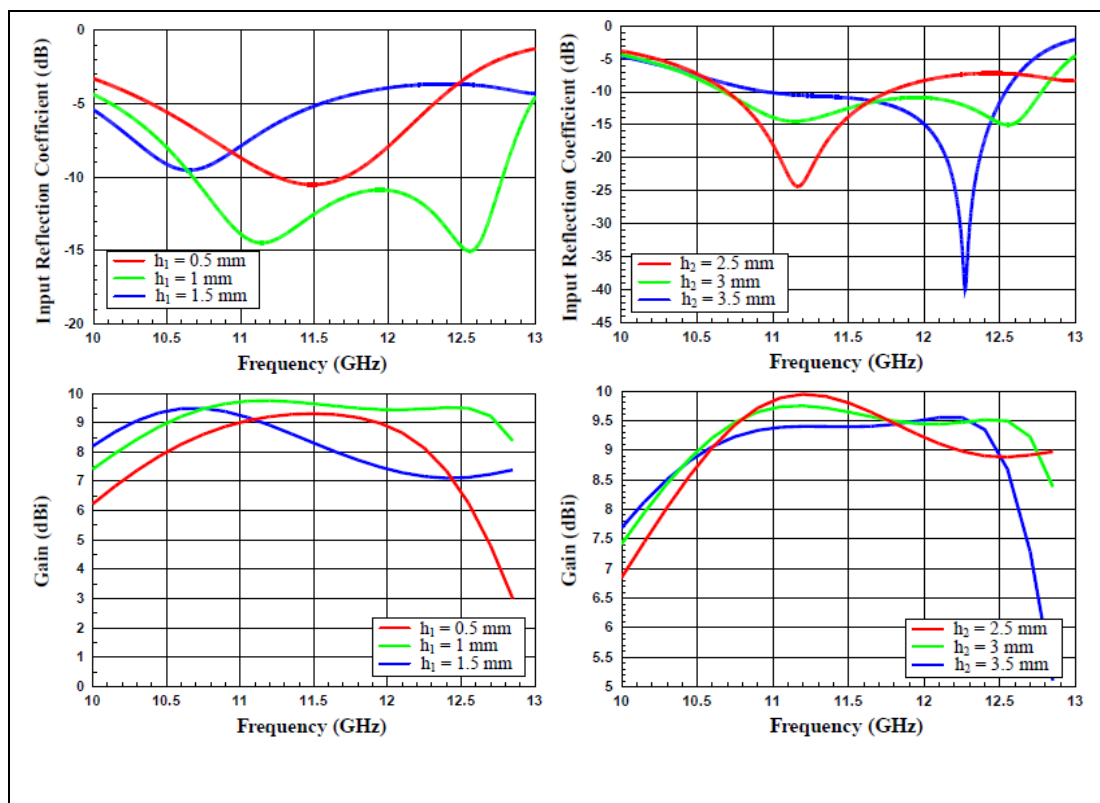


Figure 4.9. Effects on gain and impedance for parametric changes in h_1 and h_2 .

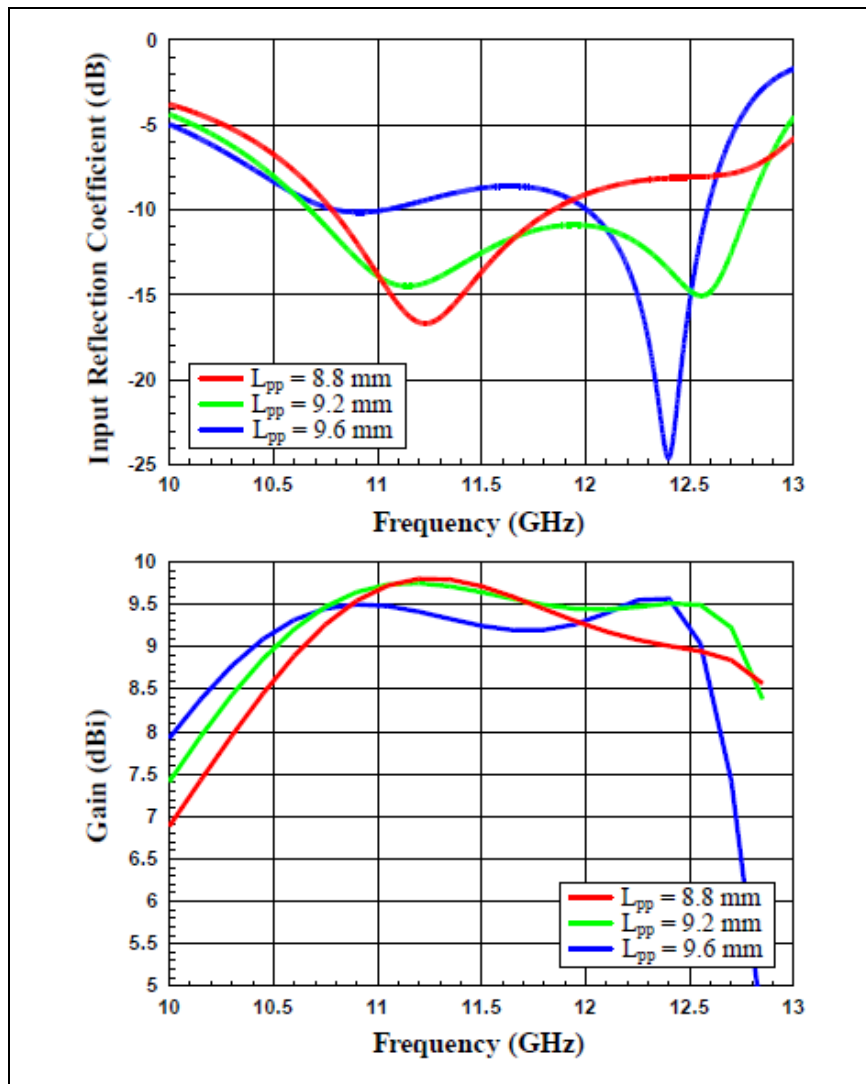


Figure 4.10. Effects on gain and impedance for parametric changes in L_{pp} .

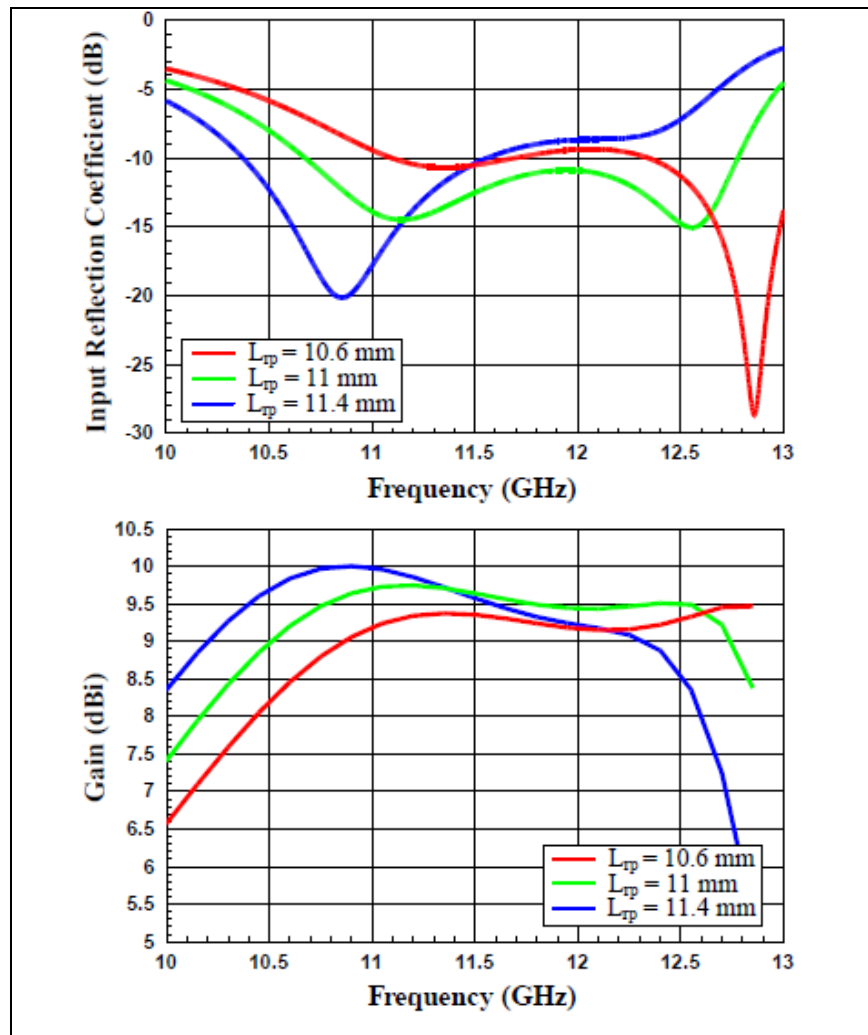


Figure 4.11. Effects on gain and impedance for parametric changes in L_{rp} .

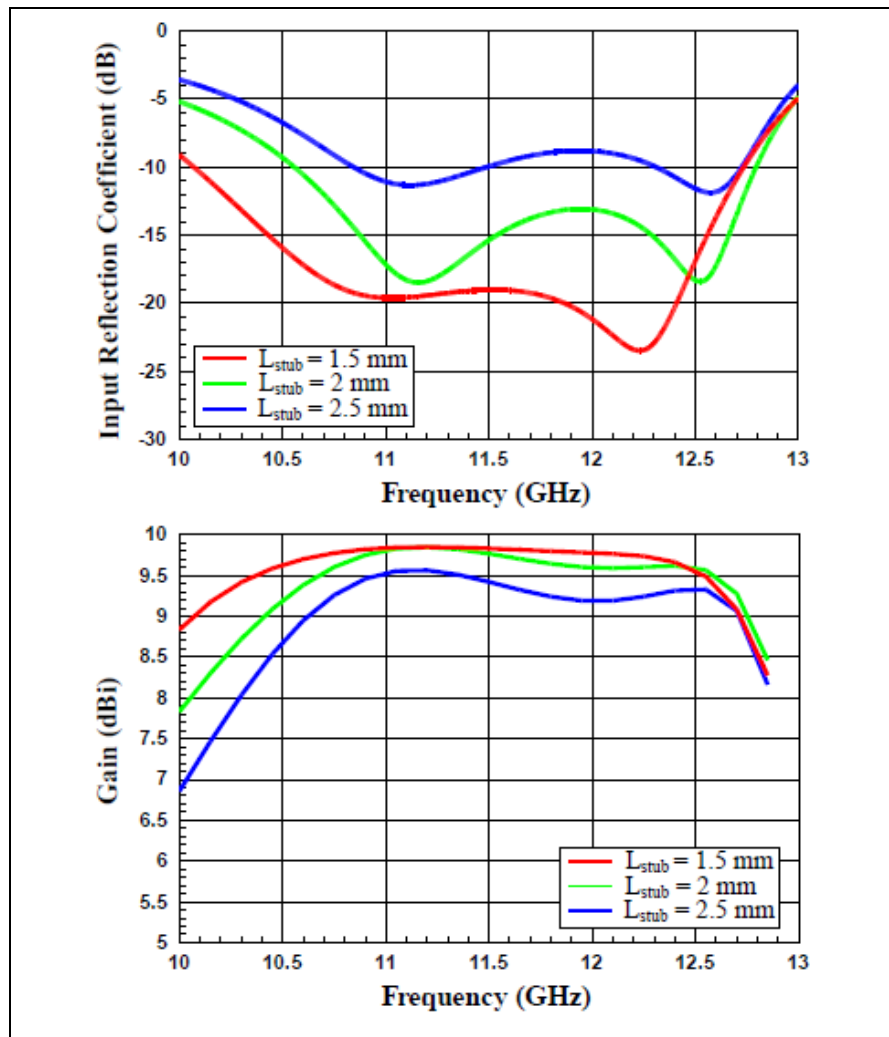


Figure 4.12. Effects on gain and impedance for parametric changes in L_{stub} .

4.4. DESIGN OF Ku BAND ANTENNA

Figure 4.13 shows the designed antenna using an hour glass slot. The antenna was optimized to give the best results possible, followed by this optimization the realized antenna is shown in Figure 4.14. Target band is Ku Band downlink frequencies. Radiating and parasitic patches were formed on flexible PCB's with $75 \mu\text{m}$ thickness and placed over the slots using Rohacell HF 31 foam ($\epsilon_r = 1.046$, $\tan\delta = 0.0017$). Measurements were carried out in an anechoic chamber using R&S ZVA40 Network Analyzer, and measurement results are displayed in figure 4.15. Impedance match bandwidth is defined as $|S_{11}| < -9.5$ dB (VSWR < 2).

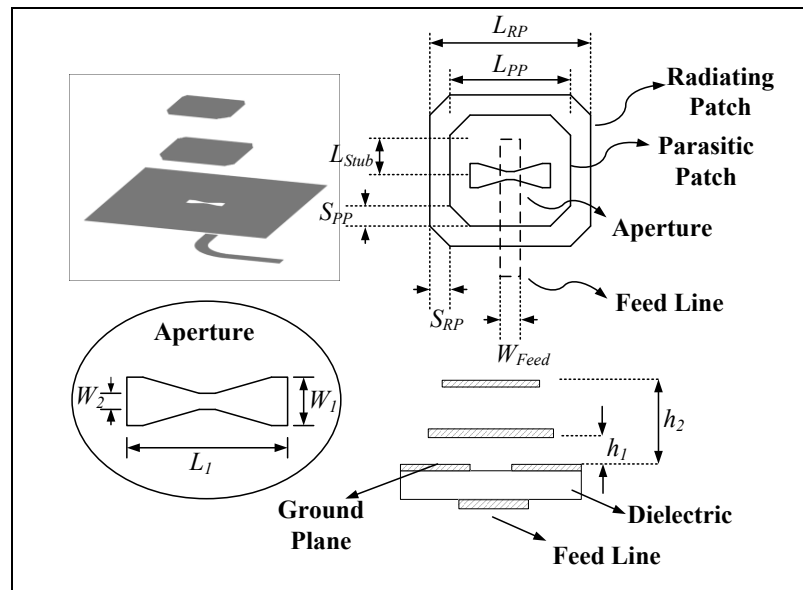


Figure 4.13. Aperture coupled stacked microstrip patch antenna.

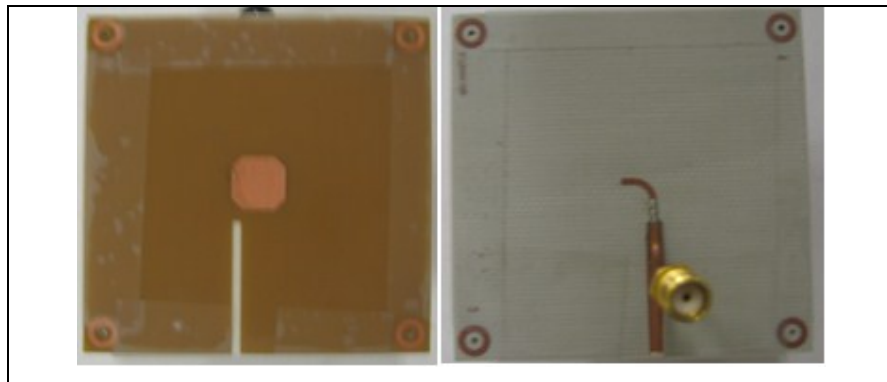


Figure 4.14. Antenna prototype: top (patch) side and bottom (feed line) side.

Simulations show that the antenna has 25% FBW with maximum broadside gain of 9.67 dBi at 11.24 GHz. Measured antenna has 29% FBW and maximum broadside gain of 9.5 dBi. In band gain ripple is less than 0.5 dB, which is also desirable in phased array antenna applications. Broadside gain is greater than 9.3 dBi in 10.8 – 12.75 GHz frequency band. Vertical polarization principal plane ($\phi = 0^\circ$) radiation pattern at 11.9 GHz, center frequency of Ku band downlink, is shown in figure 4.16. The HPBW is almost 80° . Due to its wide beamwidth, the antenna can be utilized in electronically beam-tilted phased array antennas. Measurements corroborate well with simulation results in terms of gain, impedance bandwidth, radiation patterns, and HPBW.

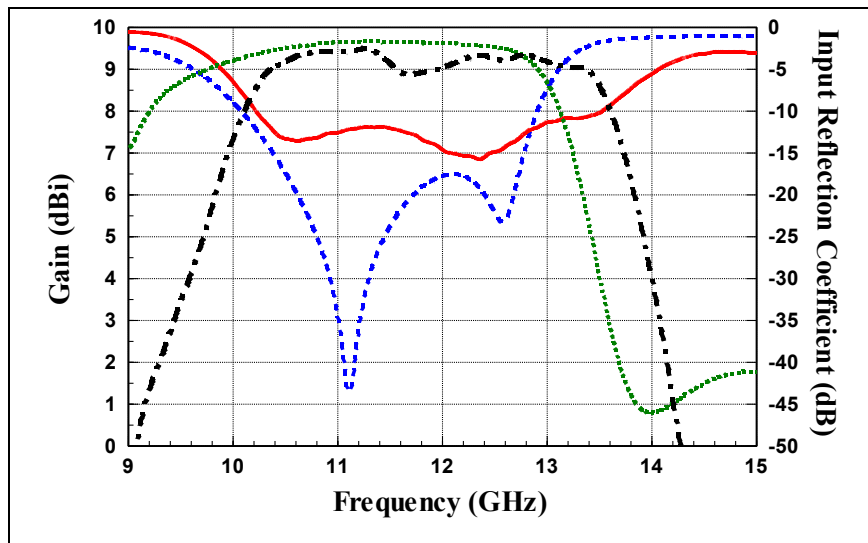


Figure 4.15. Simulated and measured, gain and input reflection coefficient vs. frequency graphs of aperture coupled antenna (Fig. 5.).

(— Measured Input Reflection Coefficient, - · - Measured Gain, Simulated Gain, - - - Simulated Input Reflection Coefficient.)

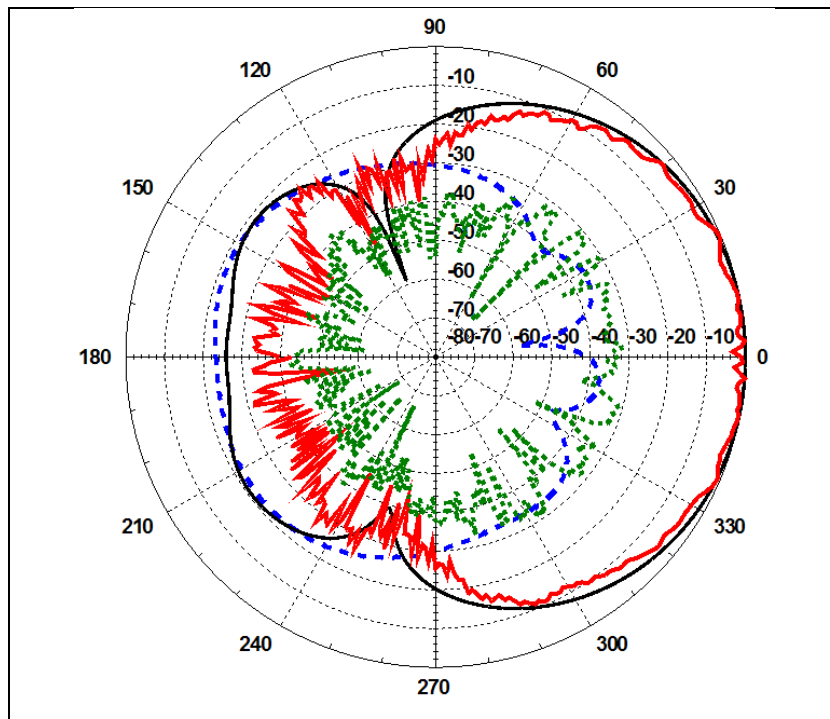


Figure 4.16 Simulated and measured, normalized gain patterns at 11.5 GHz.

(— Measured Co-Pol pattern, — Simulated Co-Pol pattern, Measured X-pol pattern, - - - Simulated X-pol pattern.)

4.5. FOM DEFINITIONS AND COMPARATIVE STUDY WITH PREVIOUS ANTENNA DESIGNS

In a typical system design minimum in-band gain is more critical than average gain to satisfy minimum target SNR . Hence, we modified FOM_1 in terms of minimum gain and electrical height of the antenna as:

$$FOM_2 = G_{\min} BW \frac{1}{k_0 h} \quad (4.18)$$

where, G_{\min} represents the minimum gain throughout the band and $k_0 h$ represents electrical height ($2\pi h/\lambda$) at f_C . Finally, we define a third FOM to include $HPBW$ as:

$$FOM_3 = G_{\min} \left(\frac{HPBW}{\pi} \right) BW \frac{1}{k_0 h} \quad (4.19)$$

where $HPBW$ is normalized to π .

It is clear that this work is very close to [8] in FOM_1 where electrical height is not taken into account. Present work is better than all other antennas in FOM_2 and FOM_3 . We believe FOM_2 and FOM_3 are critical in array applications as the height of the antenna can be further increased with suspended or inverted substrate etched structures to enhance gain at the expense of increased antenna profile.

It is observed that the antenna has the highest FOM among all antennas reported in the literature in terms of gain, bandwidth, and electrical height. Other metrics such as $HPBW$ and cross-polarization level can be added into the FOM's, but they were not provided explicitly in the reference works. We believe that the proposed antenna element can be used in demanding array applications where element gain, bandwidth, in band gain variation, and scan angle are among critical design specifications.

Table 4.2. Comparison of Antenna Structures

| Antenna | Gain (dBi) | BW (%) | HPB W/π | k_0h | FOM_1 | FOM_2 | FOM_3 |
|-----------|---------------|-----------|----------------|--------|--------------|--------------|--------------|
| This Work | 9 – 9.5 | 0.290 | 0.438 | 0.868 | 2.389 | 2.118 | 0.929 |
| [17] | 5 – 7 | 0.525 | 0.431 | 1.452 | 2.424 | 1.142 | 0.493 |
| [19] | 7 – 8.9 | 0.391 | 0.444 | 1.925 | 2.388 | 0.642 | 0.285 |
| [20] | 8.2 – 9.1 | 0.155 | 0.437 | 0.607 | 1.211 | 1.806 | 0.790 |
| [21] | 9 – 9.3 | 0.110 | 0.433 | 0.617 | 0.905 | 1.413 | 0.612 |
| [21] | 12 – 13.9 | 0.110 | N/A | 3.539 | 2.221 | 0.492 | N/A |
| [22] | 8 – 13.5 | 0.235 | 0.138 | 4.451 | 3.485 | 0.333 | 0.046 |
| [23] | 9.2 – 9.7 | 0.190 | 0.435 | 1.007 | 1.601 | 1.313 | 0.571 |
| [24] | 8.5 - 9.17 | 0.355 | 0.435 | 1.171 | 2.777 | 1.836 | 0.799 |
| [1] | 6.2 – 6.7 | 0.040 | 0.351 | 0.544 | 0.187 | 0.344 | 0.120 |

4.6. DESIGN OF X/Ku BAND ANTENNA ELEMENT

X/Ku band is an important part of the frequency spectrum for missile guidance systems, sense and warn radars, maritime civil navigation radars, and synthetic aperture radars (SAR's). In these applications, small and light weight antennas are essential to meet system requirements. Thus, low profile, high gain and wideband antenna arrays are often desired. Especially for airborne radar use, microstrip antennas have become the primary choice for designers despite their narrow band limitation.

Broadband microstrip fed dielectric resonator antenna for X-band applications has been designed with 50% fractional bandwidth in [31]. However, the gain of the antenna, though not reported, is expected to be low. Square ring type aperture coupled wideband antenna with good gain was shown in [32], but the antenna size was relatively large and the design required 11 layers of stack-up. Most aperture coupled antennas used for X-band SAR applications have bandwidths ranging from 10% to 20% with moderate to low gains [33-34]. Wideband stacked patch antenna consisting of 21 layers was reported in [36] for wide scan angle in 4 - 12 GHz frequency band. Other types of wideband arrays also have been

reported, but most of them have limited gain [37].

Thus, different antennas for each band or multi-band antennas are required to meet bandwidth and gain requirements simultaneously. A high gain single element antenna which covers most portions of X and Ku bands is definitely a need for multimode radar applications.

The frequency band from 9 GHz to 12 GHz is widely utilized in many applications of these multimode radars. In conventional radar, a typical range resolution of 30 cm requires at least 500 MHz bandwidth, which in turn, necessitates an antenna array operating from 8.75 to 12.25 GHz (approximately 41% fractional bandwidth). Array gain, depending on system requirements vary differently, but broadside gain in excess of 15 dBi is highly desired. We studied center-fed and offset slot fed aperture coupled patch antennas for bandwidth and gain. Offset slot coupled TM_{01} mode patch was studied for bandwidth improvement [38] and beam symmetry [39]. But our goal is to have a single antenna that is broadband and has high gain (≥ 10 dBi) which can operate over X and Ku bands. We also show that offset slot fed aperture coupled antenna can provide beam tilt up to 30° , and still maintain high gain and wideband impedance match. Instead of electronic scanning, mechanical steering at the range axis is assumed. Although it is more difficult to design a tilted array than broadside array, we designed 16 element (4x4) antenna array with fixed beam tilt at 20° , and performed measurements to validate the design. The advantages of fixed beam tilted array over broadside array are also mentioned.

Bandwidth ($VSWR = 2$) of a rectangular patch antenna with length L , width W , and substrate height h can be approximated in Equation 4.4. For $W/L < 2$, p becomes almost 1, and c_l becomes 0.4 for air-dielectric and nearly 1 for high permittivity substrates. Although the approximation is valid for electrically thin substrates ($h/\lambda \ll 1$), it is clear that the electrical height ($k_0 h$) and aspect ratio (W/L) are directly proportional to the bandwidth. Similar analogy can be established for aperture coupled antennas such that high aspect ratio would improve bandwidth if higher order modes are not invoked.

Proposed offset aperture coupled stacked patch antenna geometry is shown in Figure 4.17. Aspect ratios of the driven and parasitic elements are 2.1 and 2.62, respectively. Thus, not

only parasitic patch but also high aspect ratios are used in an attempt to obtain wideband and high gain performance. Hour-glass shape aperture is used to couple the microstrip feedline to stacked patch antenna. Aspect ratios, patch heights, and aperture dimensions were optimized for gain and impedance match. Simulations were performed using CST Microwave Studio. Nelder-Mead simplex algorithm inside CST optimization toolbox was used in the optimization.

When there is no offset in slot position, the antenna has maximum gain at broadside, and when there is offset, beam tilt is observed depending on the offset amount (L_{off}). Peak gains and tilt angles at three different frequencies are displayed in table 4.3.

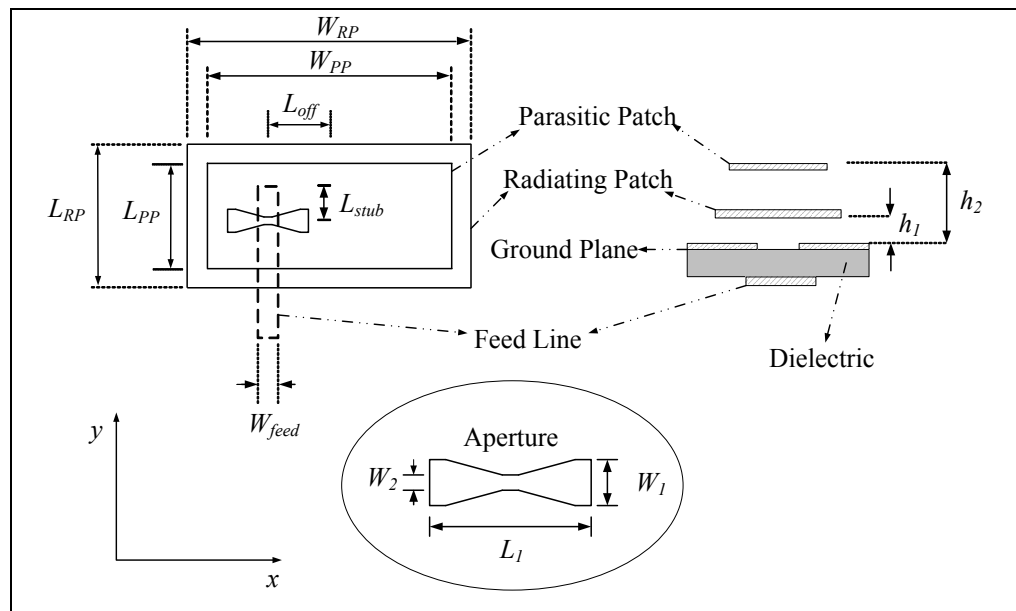


Figure 4.17. Single element antenna ($L_{off}=0$, $L_{RP}=11.9$, $L_{PP}=9.3$, $W_{RP}=25$, $W_{PP}=24.4$, $W_1=1.12$, $W_2=0.5$, $L_I=7.4$, $h_1=1$, $h_2=2$, all in mm).

Table 4.3. $L_{off}(mm)$ vs. Beam Tilt and Gain

| L_{off} | 10 GHz | | 11 GHz | | 12 GHz | |
|-----------|------------|----------|------------|----------|------------|----------|
| | Gain (dBi) | Tilt (°) | Gain (dBi) | Tilt (°) | Gain (dBi) | Tilt (°) |
| 3 | 11.5 | 15 | 9.9 | 28 | 10 | 28 |
| 4 | 11.5 | 21 | 9.8 | 29 | 10.2 | 29 |
| 5 | 11.4 | 25 | 9.8 | 30 | 10.2 | 30 |
| 6 | 11.4 | 27 | 9.9 | 31 | 10.3 | 30 |
| 7 | 11.4 | 28 | 9.9 | 31 | 10.4 | 30 |
| 8 | 11.3 | 29 | 9.9 | 31 | 10.4 | 31 |
| 9 | 11.3 | 31 | 10 | 31 | 10.4 | 31 |
| 10 | 11.2 | 32 | 10.1 | 32 | 10.3 | 32 |

Although beam tilt differs over the frequency range, maximum deviation is less than the half power beamwidth (HPBW) of the antenna. For three different offset feeds, radiation patterns of the single antenna at 11 GHz are shown in Figure 4.18. HPBW's are nearly preserved for these offsets. When offset amount is increased, the pattern resembles to TM_{20} mode pattern due to phase inversion of the current on the driven patch.

Gains of single element antenna with no offset (broadside) at $\theta = 0^\circ$ and at $\theta = 20^\circ$ as frequency changes are shown in Figure 4.19. The gain of the antenna with 5mm offset feed at $\theta = 20^\circ$ is also shown in Figure 4.19. Broadside looking antenna (no offset) has degradation in gain at $\theta = 20^\circ$, whereas offset fed antenna has better gain up to 11 GHz. For beam tilted antenna, the dimensions were tweaked for impedance match. Input reflection coefficients (Γ) for both antennas are shown in figure 4.20. Broadside antenna has gain greater than 10 dBi from 9.2 to 12.9 GHz and impedance match ($|\Gamma| < -9.5$ dB) from 8.7 to 12.25 GHz. Beam tilted antenna with 5 mm offset has gain over 9.5 dBi throughout 8.8 - 12.2 GHz and impedance match from 8.7 GHz to 12.5 GHz. Both antennas are good candidates for target applications.

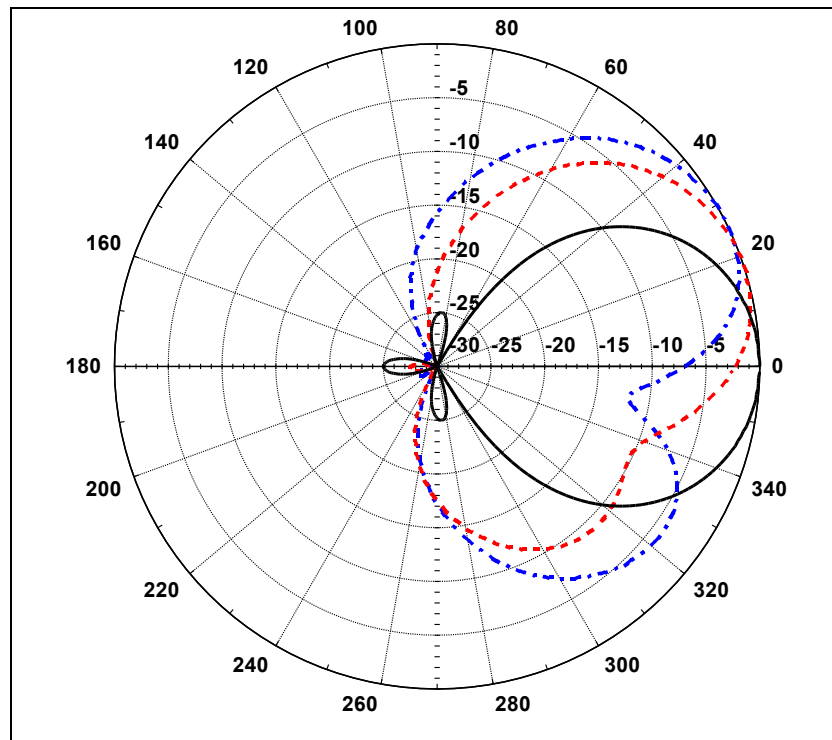


Figure 4.18. Normalized gain patterns for different offset values at 11 GHz

(— $L_{off} = 0$ mm. - - - $L_{off} = 3$ mm. - · - $L_{off} = 8$ mm).

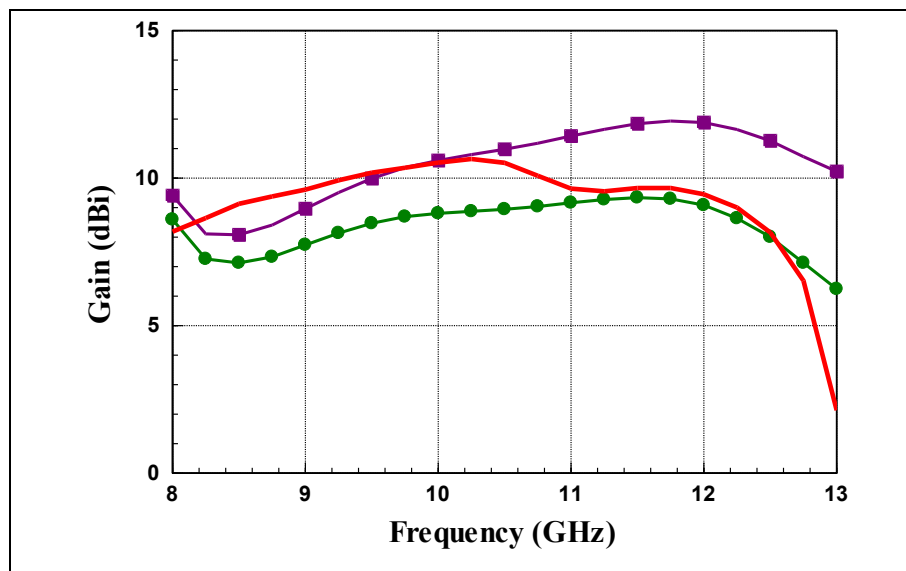


Figure 4.19. Gain of the broadside and beam tilted antenna structures

(— Gain of single element antenna with 5mm offset at $\theta = 20^\circ$, —■—■—■— Gain of single element antenna with no offset at $\theta = 0^\circ$, —●—●—●— Gain of single element antenna with no offset at $\theta = 20^\circ$).

An antenna element with beam tilt is particularly important for array applications where gain loss of broadside looking antenna element at desired tilt angle becomes considerable. For instance, in this particular antenna if the tilt angle is 20° then the broadside antenna has almost 3dB less gain than its peak gain at 0° . If 40° tilt is desired, then element antenna has 10 dB less gain than its broadside gain. Thus, although the antenna is wideband and has high gain, it is only suitable for a narrow sector scanning radar applications.

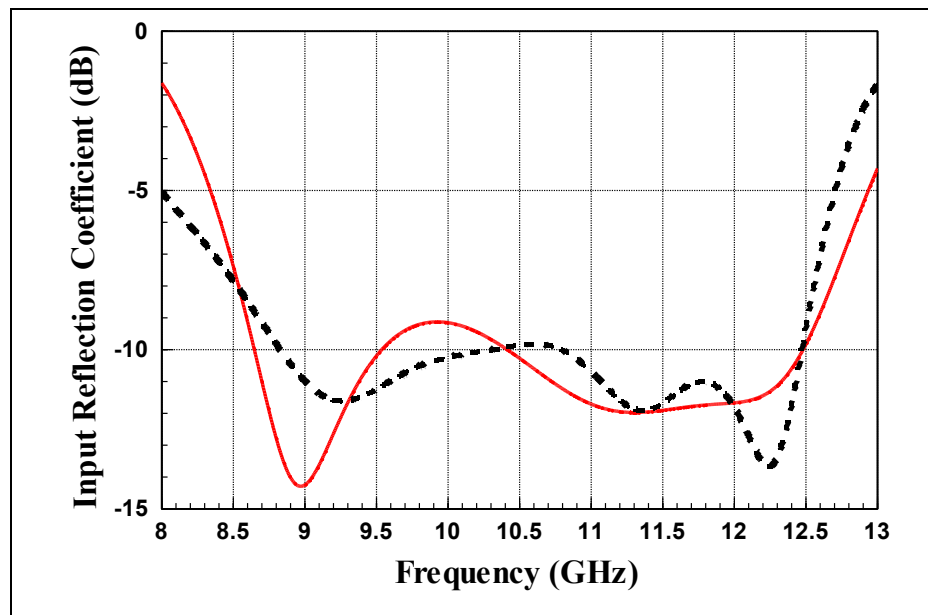


Figure 4.20. Input reflection coefficient of the antenna.

(— No offset, - - - 5mm offset).

4.7. PRACTICAL EXAMPLES OF SUB-ARRAY SUITABLE FOR SATELLITE COMMUNICATION SYSTEMS BUILT UP ON PROPOSED STRUCTURES

Based on the designs made in the previous sections, an antenna array with fixed beam tilt examples are given in the following sub-sections.

4.7.1. Ku band sub-array antenna

This section introduces an example design of 8 element antenna array. Before concluding on the design of an array containing large amounts of elements the array performance of

must be analyzed and verified that it is suitable for the design. The antenna element given in Section 4.4 was modified to have a radial stub at the slot feeding and the patches have been optimized to have sharp corners instead of clipped ones. The element antenna dimension and layout are shown in Figure 4.21.

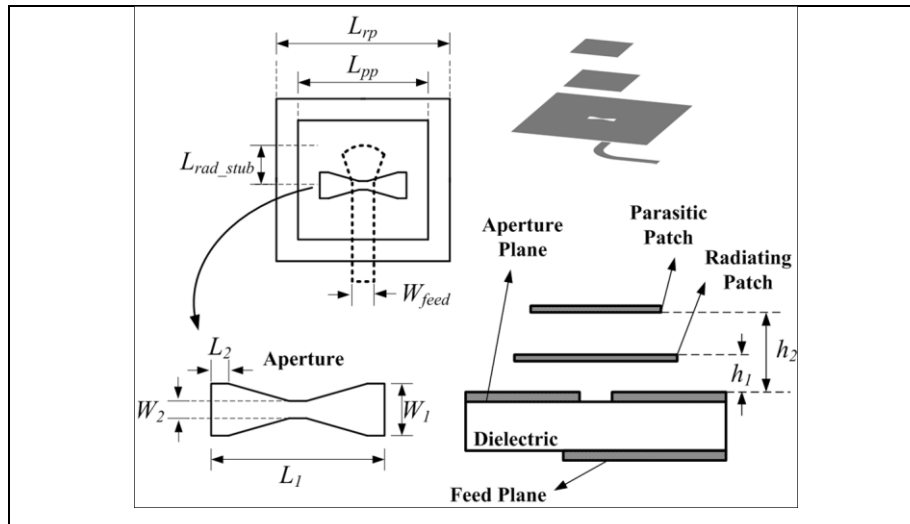


Figure 4.21. Aperture coupled microstrip patch antenna.

($L_{rp} = 10.8$ mm, $L_{pp} = 9.3$ mm, $L_{rad_stub} = 1.8$ mm, $W_{feed} = 1$ mm, $W_1 = 1.5$ mm, $W_2 = 0.5$ mm, $L_1 = 4.7$ mm, $L_2 = 0.75$ mm, $L_3 = 0.5$ mm, $h_1 = 1$ mm, $h_2 = 3$ mm).

The antenna structure is modeled and simulated using FEKO. Broadside gain and off-bore sight gain at 10° , 20° , 30° and 40° are shown in Figure 4.22. Input reflection coefficient (50 Ohm port impedance) is also shown in Figure 4.22 (right axis). Impedance match bandwidth is defined as $|S_{11}| < -9.5$ dB (VSWR < 2) and the antenna has bandwidth greater than 2.6 GHz in the 10.2 to 12.8 GHz. Simulations also show that maximum broadside gain of 8.67 dBi occurs at 11.24 GHz. Broadside gain is greater than 8.3 dBi in 10.8 – 12.75 GHz frequency band. Vertical polarization principal plane ($\varphi = 0^\circ$) radiation pattern at 12 GHz is shown in Figure 4.23. The HPBW is almost 80° . Due to its wide beamwidth, the antenna can be utilized in fixed beam-tilt and/or phased arrays, where loss due to beam tilt is around 1 dB up to $\theta = 20^\circ$.

Antenna element presented above is used in a 2×4 array with fixed beam tilt to 20° . This beam tilt is chosen to support potential mechanical tilt to lower angles. The goal is to show that antenna element can be integrated into an array design without losing its important

features such as gain, bandwidth and HPBW. Simple array theory would predict an increase of 9 dB in peak gain with this array configuration. Assuming 1 dB loss due to beam tilt, one would expect peak gain at 20° to be around 17.3 dBi excluding feed network loss.

Although the antenna element is wideband, feed network must also be wideband to result in broad band operation. Corporate feed networks have broadband characteristics by their nature, but they take up considerable space for large arrays and the antenna will suffer from low efficiency due to copper and dielectric losses. Despite these disadvantages, corporate feed network with 90° inter element phase difference is used to reach the required beam tilt and wideband operation. Inter element spacing along $\phi = 0^\circ$ and $\phi = 90^\circ$ are chosen as 0.82λ and 0.73λ , respectively where free space wavelength λ is calculated at 11.9 GHz, center frequency of downlink band (will be explained briefly in section 5.). Tapered impedance line transformers are designed using AWR, Microwave Office and incorporated into antenna design in FEKO. For array antenna simulations, infinite ground plane and dielectric substrate are assumed to reduce computation time. Designed antenna array is shown in Figure 4.24. Unlike simulations of single element, array simulations are performed using infinite ground (slot plane) and dielectric layer. Its gain at $\theta = 20^\circ$ and input reflection coefficient are shown in Figure 4.25. Maximum simulated gain of 16.7 dBi is reached around band center as desired. Simulated array gain is slightly higher than its expected value due to simulation model discrepancies (infinite versus finite dielectric and ground). Throughout the entire Ku downlink band, the array antenna has minimum 16 dBi gain and fairly small in-band gain variation (0.35 dB). Its HPBW is 38° in elevation and 17.5° in azimuth which are fully consistent with array theory. Worst case impedance match is -8 dB, which is not as good as the single element performance, but acceptable given the wideband nature of the feed network. Impedance match could have been improved by using Wilkinson balanced combiners, but that would have required SMD components on the feed network which was avoided due to cost and manufacturing reasons. 3D gain pattern of the array antenna at 12 GHz is displayed in Figure 4.26.

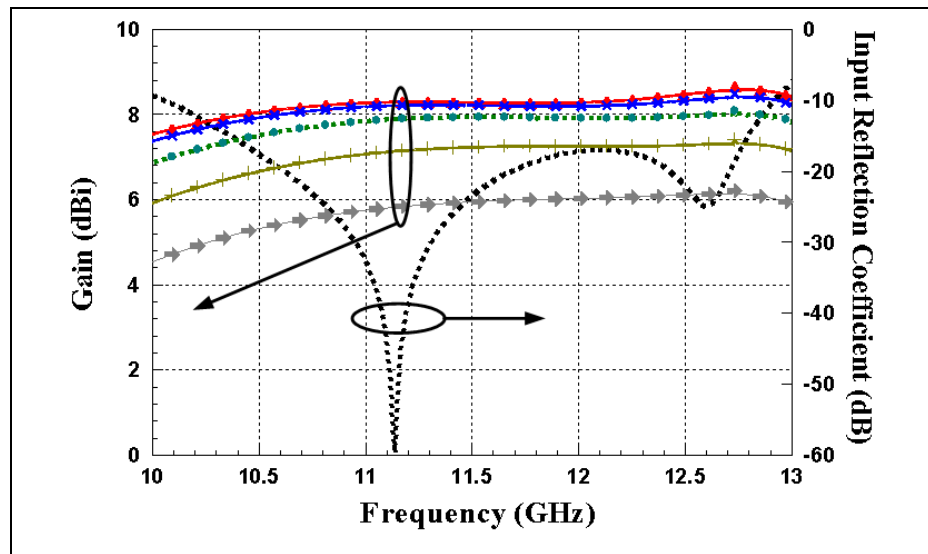


Figure 4.22. Single element input reflection coefficient and gain at 0° , 10° , 20° , 30° , and 40° . (\blacktriangle $\theta = 0^\circ$, \times $\theta = 10^\circ$, \bullet $\theta = 20^\circ$, $+$ $\theta = 30^\circ$, \rightarrow $\theta = 40^\circ$)

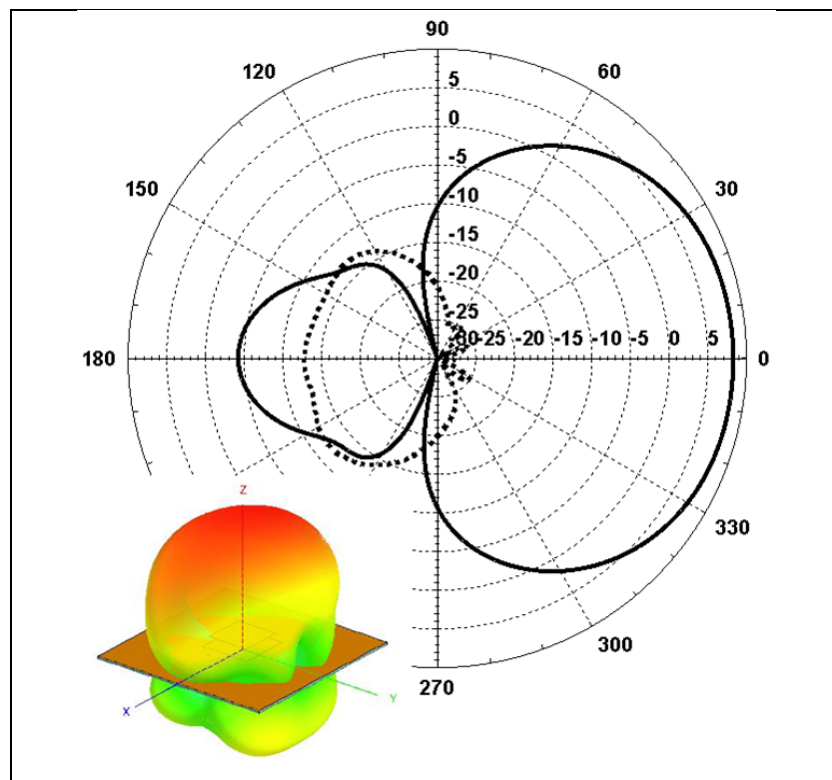


Figure 4.23. Single element antenna gain pattern at 12 GHz.

(— Co- Pol, - - - Cross - Pol)

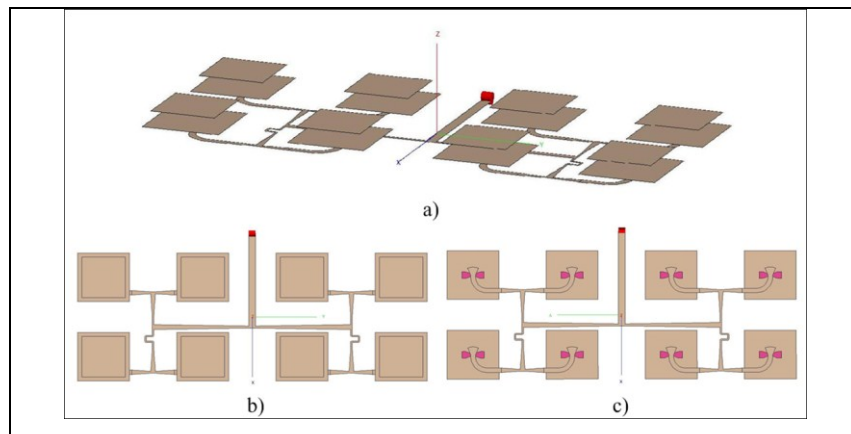


Figure 4.24. 2x4 Eight-element antenna array, a) 3D view (slot plane removed), b) looking from top (slot plane removed), c) looking from bottom (slots are shown in red).

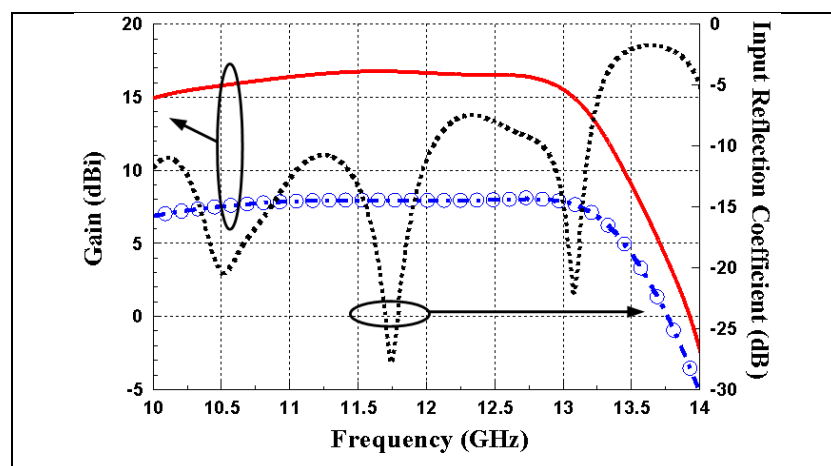


Figure 4.25. Single and eight-element antenna gain at $\theta = 20^\circ$ and input reflection coefficient of array. ($\text{---}\circ\text{---}\circ\text{---}$ Single element antenna gain, --- 8 element antenna gain)

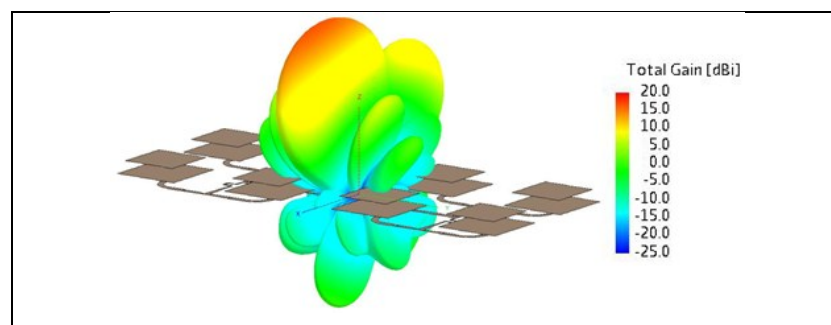


Figure 4.26. 3D gain pattern at 12 GHz.

The array antenna is realized and the prototype is shown in Figure 4.27. Measured array performance is displayed in Figure 2.8. The prototype antenna has an impedance match from 9.3 to 12.94 GHz. It attains maximum gain of 17.5 dBi and minimum gain of 16.7 dBi throughout the Ku band downlink frequencies. Measured gain is about 0.8 dB better than simulated gain due to finite array construction where the antenna is more directional with finite ground plane. Impedance match bandwidth, especially at lower frequencies, is also better than simulated result because copper loss associated with the feed network, which was not taken into account in simulations, improves match at the expense of reduced gain as shown in Figure 4.28.

Measured gain patterns at 10.8, 11.8, and 12.3 GHz are shown in Figure 4.27. HPBW is 38° which is consistent with its simulated value. The side-lobe level is about 7.5 dB relative to the peak at 10.8 and 11.8 GHz, but 5 dB at 12.3 GHz. As the elements in the array are increased, side-lobe level will be decreased.

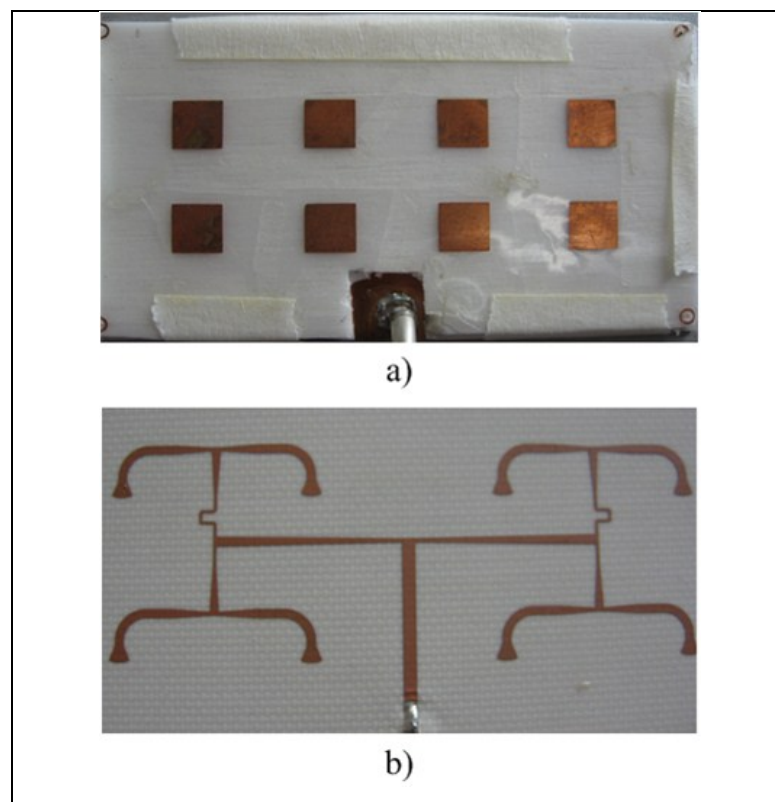


Figure 4.27. Array antenna prototype, a) top (patch) side, b) bottom (feed line) side.

Based on the results the element antenna given in Figure 4.21 is suitable for array design. However, in the following section the design will be continued using the element antenna shown in Figure 4.13.

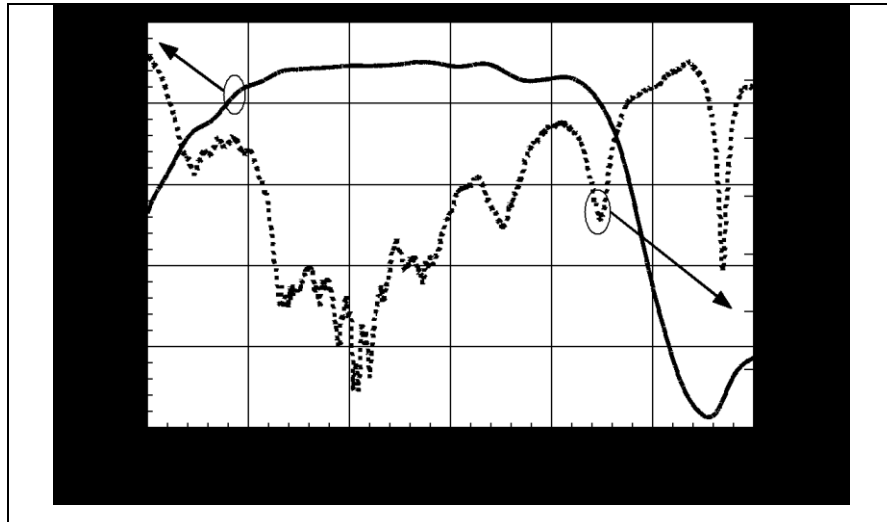


Figure 4.28. Measured antenna array gain at $\theta = 20^\circ$ and its return loss.

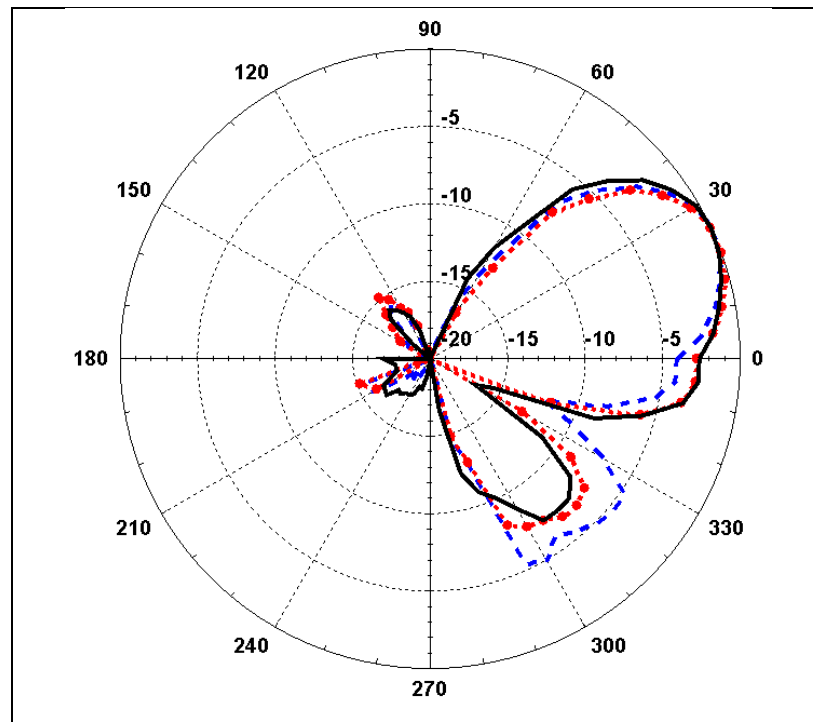


Figure 4.29. Measured array gain pattern at 10.8, 11.8 and 12.3 GHz.

(— Gain @10.8 GHz, - - - Gain @ 11.8 GHz, - - - Gain @ 12.3 GHz)

4.7.2. X/Ku band sub array antenna

Using the same methods in Section 4.7.1. a similar array design for an X/Ku band antenna array is constructed. An antenna array using 5 mm offset feed is formed using 16 (4x4) elements. As the element antenna already has 20° tilt, microstrip corporate feed network with proper phasing and tapered T junctions are formed to obtain 20° array tilt. The antenna is shown in Figure 4.30. Patch elements were etched on DuPont AP9232R polyimide thin film ($\epsilon_r=3.4$, $\tan\delta= 0.002$) and Rohacell HF31 foam ($\epsilon_r=1.046$, $\tan\delta=0.0017$) was used as air dielectric. Feedline substrate was Rogers RO3003 ($\epsilon_r=3$ and $\tan\delta=0.0013$) with 0.5 mm thickness. Fabricated antenna is shown in Figure 4.31.

In the array design, radiating edges are separated by 14 mm to minimize inter element coupling. While the separation is larger than the maximum allowed for grating lobes, low element gain at grating lobe directions lessen this affect in the antenna pattern. Measured and simulated array antenna gain at 20° with elements 5mm offset feed are shown in Figure 4.32. We also included the simulated gain of broadside array at 0° with elements center fed aperture (no offset). Comparison of tilted array gain with pre-tilted antenna elements to conventional broadside array reveals that both antennas agree well up to 11.5 GHz. However, there is approximately 44 mm height advantage of the array with pre-tilted elements. If broadside looking elements were used with properly phased feed network to tilt the beam to 20°, there would be reduction in gain due to decrease in element antenna gain at 20°. With or without mechanical tilt, it is clear that pre-tilted element antenna array is superior to broadside looking array for off-axis scan angles greater than $\pm 10^\circ$. Maximum gain of offset slot fed array at 8.75 - 12.25 GHz band is 20.6 dBi, which is 1.9 dB lower than the expected value from array theory due to loss in the microstrip feed network.

Measured and simulated input impedance match of the proposed array antenna is shown in figure 4.33. Although simulated result exhibits impedance match over a larger frequency band, realized antenna had 9.2 dB match up to 12.6 GHz, measured impedance bandwidth is nearly 44%. The radiation pattern measured at 11.5 GHz is shown in Figure 4.34. The discrepancy between simulations and measurements for backside radiation is due to measurement setup where rotation axis of the measurement system serves as a ground to

shield backside reception. Because of this, measured beamwidth also differ slightly than their simulated counterparts. Beam squint as frequency changed was also observed, but its effect was not considerable as measured gain at $\theta = 20^\circ$ was acceptable and agreed well with simulations. Measured side lobe level was 12.5 dB, whereas measured $HPBW_\theta$ and $HPBW_\phi$ were 13.5° and 12° , respectively. Overall, simulations and measurements of the array antenna corroborate well.

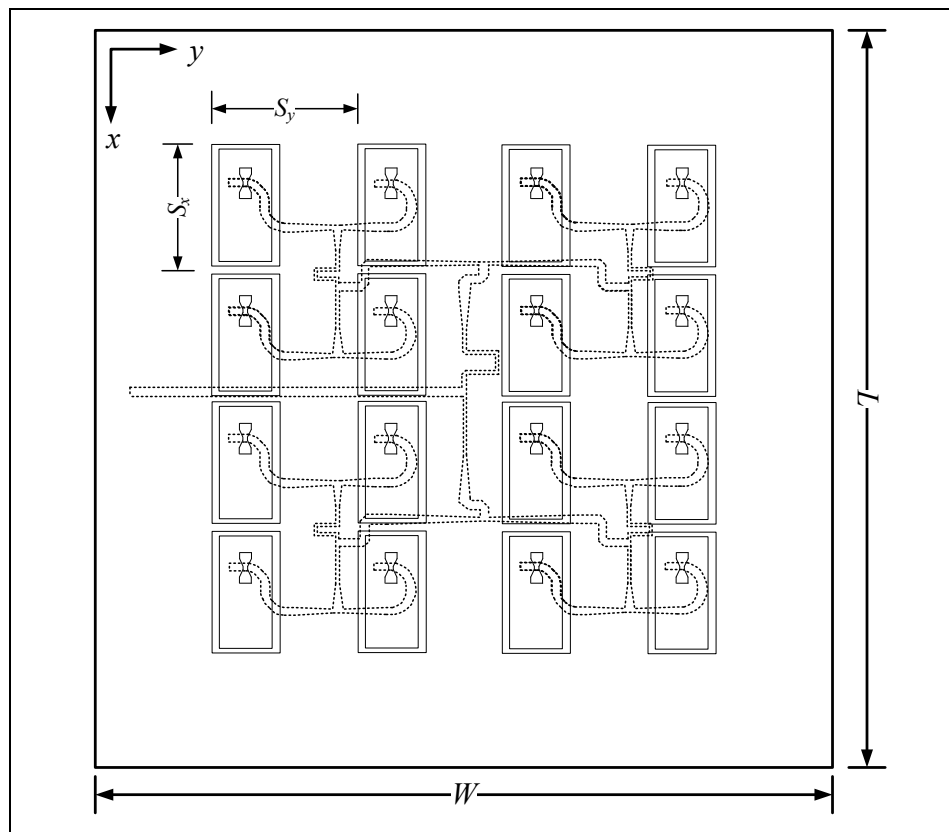


Figure 4.30. 16-element fixed beam array with feed network ($W \times L \times H = 128 \times 128 \times 3.5$, $S_x = 22$, $S_y = 25$, $L_{RP} = 11.5$, $L_{PP} = 9$, $W_{RP} = 20.5$, $W_{PP} = 19.5$, $W_1 = 2$, $W_2 = 0.5$, $L_1 = 5.2$, $h_1 = 1$, $h_2 = 2$, all in mm).

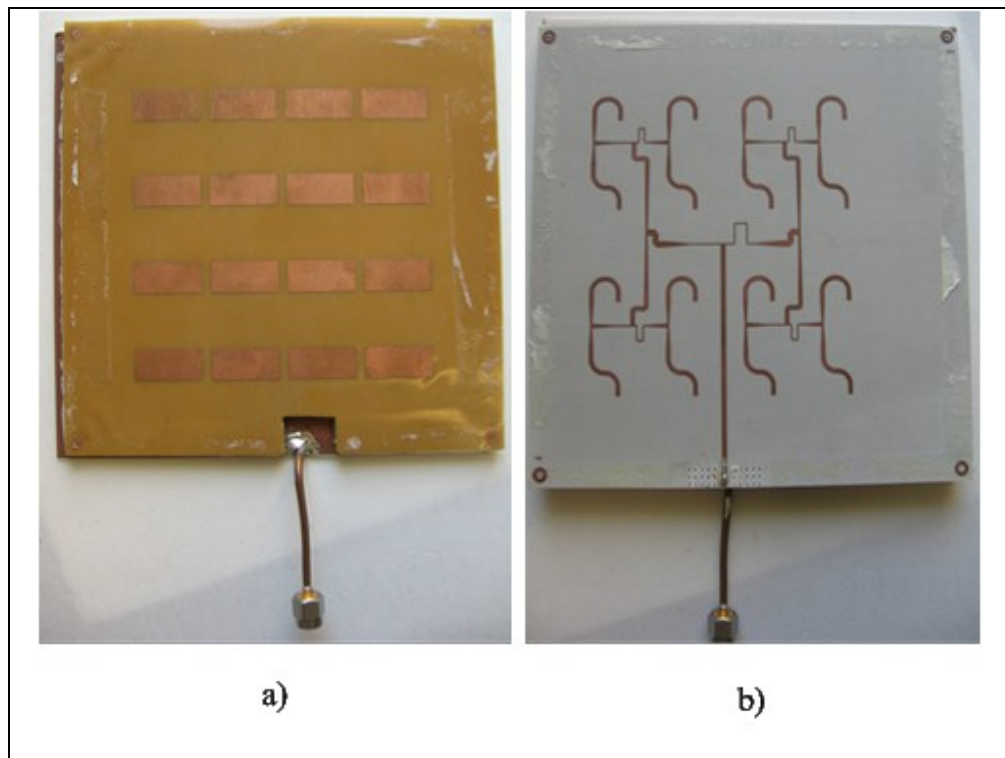


Figure 4.31. Fabricated 4x4 array, a) top view, b) bottom view.

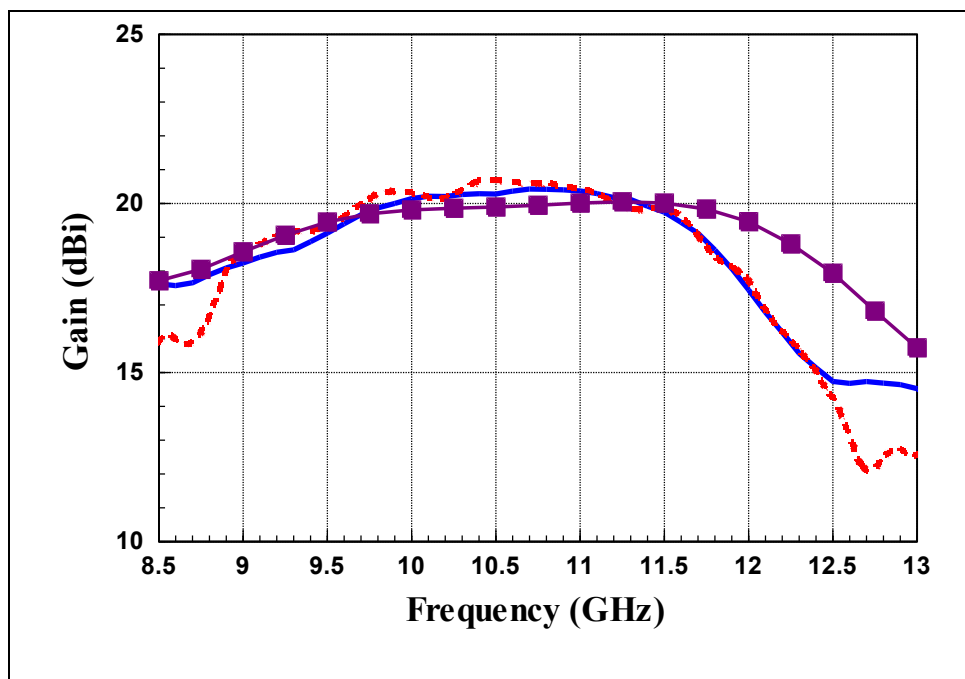


Figure 4.32. Gain of 4x4 array (—■—■— Simulated gain of broadside 4x4 array at $\theta = 0^\circ$, — Simulated Gain with 5 mm offset at $\theta = 20^\circ$, - - - Measured Gain with 5 mm offset at $\theta = 20^\circ$).

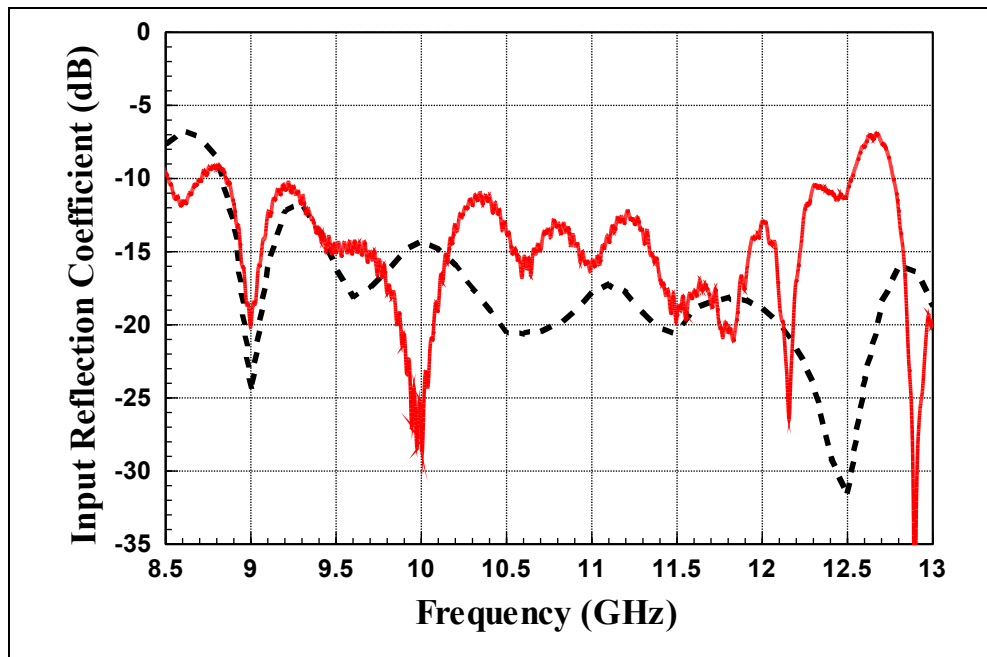


Figure 4.33. Input impedance match of proposed array

(- - - Simulated $|\Gamma|$ — Measured $|\Gamma|$).

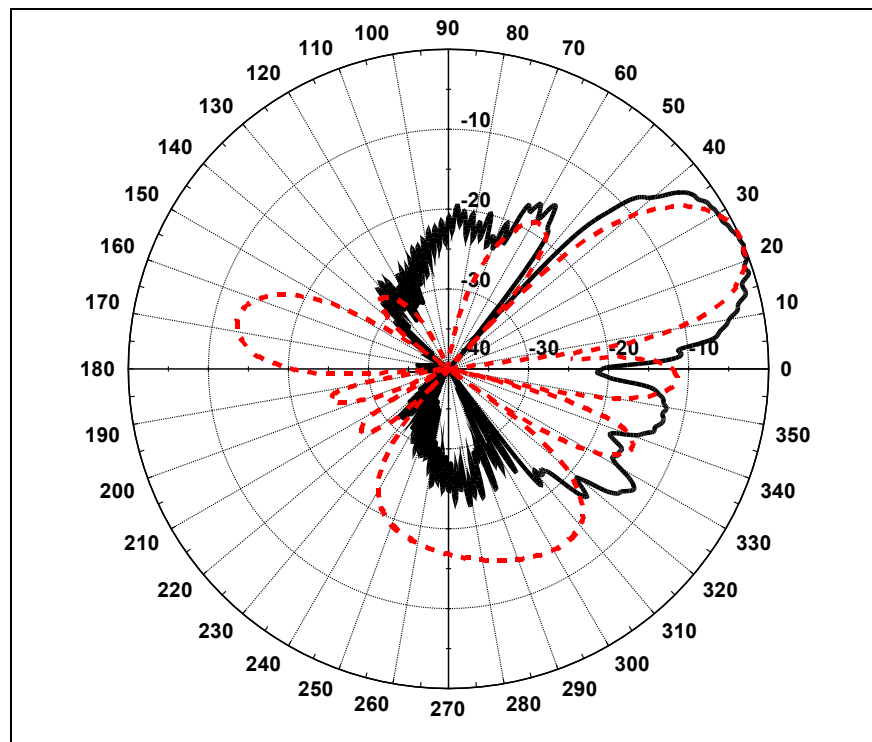


Figure 4.34 Normalized gain pattern @ 11.5 GHz (- - - Simulated, — Measured).

5. SIMULATION AND EXPERIMENTAL RESULTS

This section details of the design of a complete array capable for reception of Ku band DBS signals. As mentioned in Chapter 2, an estimate of 256 elements per polarization was made. The element antenna design in Section 4 (Figure 4.7) will be used while constructing the array. The main objective of this section is to build up an antenna array of 256 elements which has a radiation pattern tilt at 20° in the elevation axis. Synthesis of a rectangular array with tilted beam will be discussed and the design of a hybrid microstrip – waveguide feed network will be given.

5.1. ARRAY SYNTHESIS

There are multiple methods and formations possible to develop an antenna array capable to satisfy the specifications given in the second section. But the most important specification was the maximum dimensions and weight which was given according to the needs of the industry. The system diameter must not exceed 75 cm, the height must be less than 7 cm and the weight must be less than 5 kg. The antenna will have two panels, one for each polarization. Based on these facts the array should cover an area with lengths less than 73cm x 20 cm. Using array theory it is possible to synthesis an array 256 elements inside the given dimensions. Figure 5.1 shows the layout of a two dimensional array.

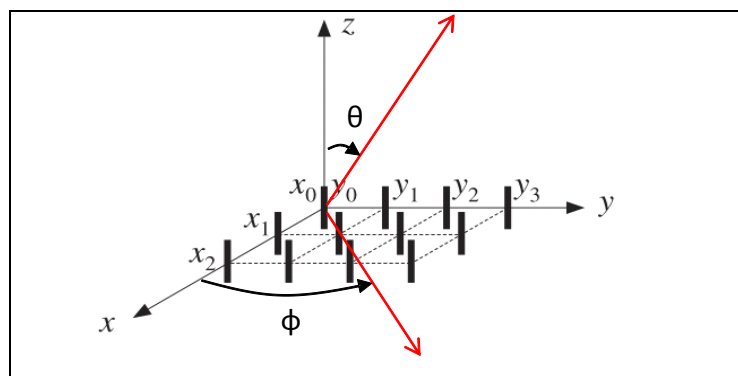


Figure 5.1. Two dimensional array

Let us say that, n and m are the number of elements in the x and y directions, respectively. The interelement spacing in the x and y directions are d_x and d_y , respectively. $x_{s_{n,m}}$ and $y_{s_{n,m}}$ are the positions of the source antennas on the (x,y) coordinate system. θ_0 and ϕ_0 are the angles pointing the main beam direction of the antenna pattern. The current distribution of each element being $I_{a,b}$, the array factor of such an array can be written as follows:

$$AF(\theta, \phi) = \sum_{b=1}^m \sum_{a=1}^n I_{a,b} \cdot e^{j\left\{\beta \left[x_{s_{n,m}} (\sin \theta \cos \phi - \sin \theta_0 \cos \phi_0) + y_{s_{n,m}} (\sin \theta \sin \phi - \sin \theta_0 \sin \phi_0) \right] \right\}} \quad (5.1)$$

The array antenna in this application should have the highest gain possible. Since it is a receive only structure, side lobe levels are not that important. Although HPBW in both elevation and azimuth axis's are very important for the design due to the physical limits given in the specifications. A tradeoff between azimuthal HPBW and gain has been made. For maximum gain elements in the azimuth axis have been placed 0.82λ apart (for high gain). On the other hand elements in the elevation axis have been placed 0.73λ apart. Spacing in the elevation axis was set in that magnitude so that the phasing of each row would have an electrical phase shift of 90° for a beam pointing at the desired beam angle ($\theta_0 = 20^\circ$, $\phi_0 = 0^\circ$). The array factor given in equation 5.1 would become:

$$AF(\theta, \phi) = \sum_{b=1}^{32} \sum_{a=1}^8 A_{a,b} \cdot e^{j\left\{2\pi \left[0.82(b-1.5)(\sin \theta \cos \phi - \sin(20^\circ)) + 0.73(a-4.5)(\sin \theta \sin \phi) \right] \right\} + \vartheta_{a,b}} \quad (5.2)$$

where, $A_{a,b}$ is the magnitude of current at each element (which is 1, for uniform excitation) and $\vartheta_{a,b}$ is the electrical phasing of each element (90° between each row, uniform in the azimuth axis). Figure 5.2 shows the synthesized array of 8 rows and 32 columns. Figure shows the elevation pattern of the synthesized array 256 elements.

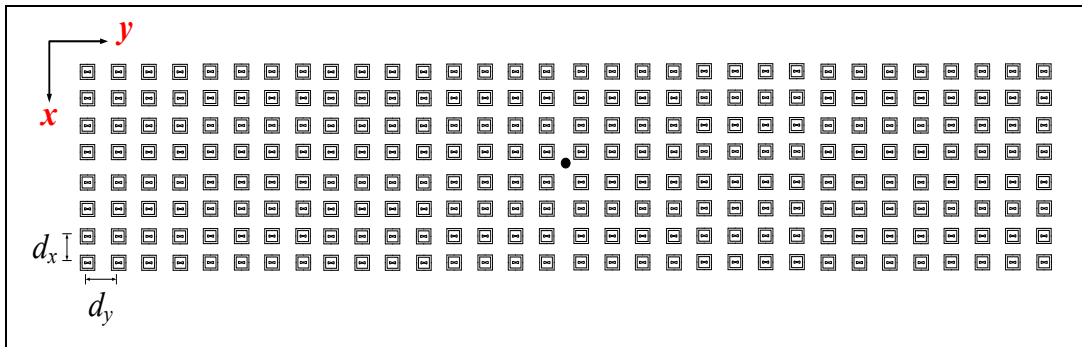


Figure 5.2. Formation of 256 element (8x32) antenna array
 ($d_x = 0.73\lambda$, $d_y = 0.82\lambda$, the black dot represents the origin of the x-y axis)

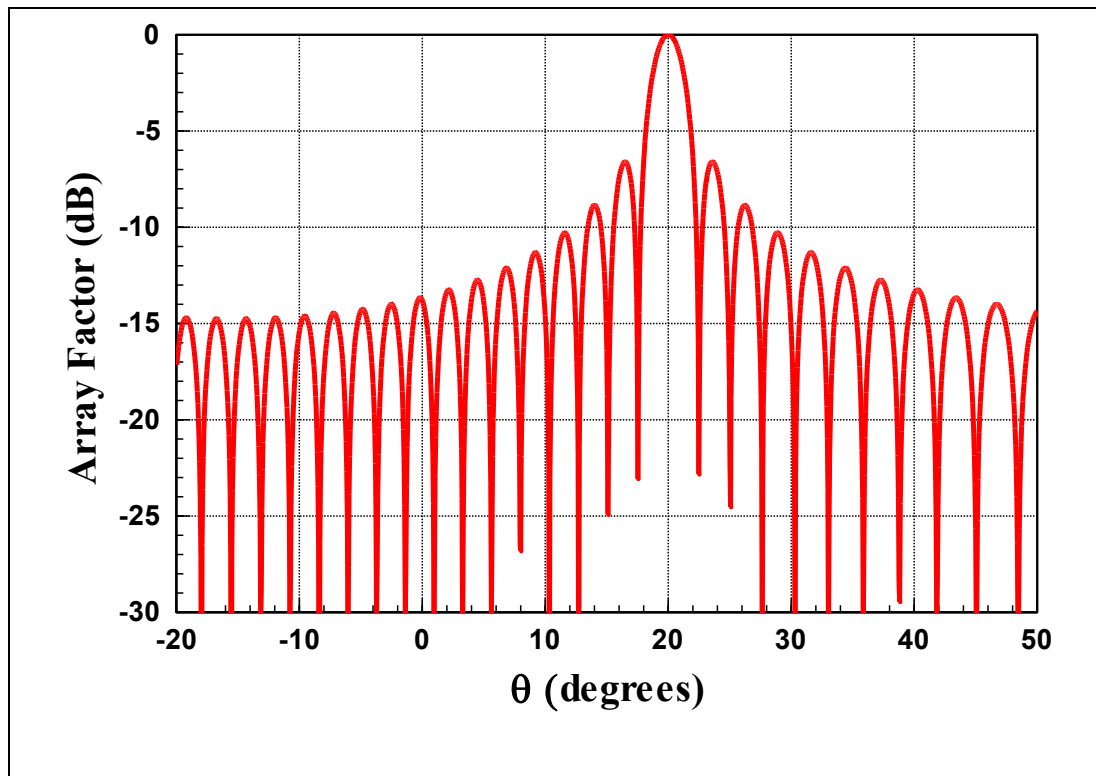


Figure 5.3. Array factor elevation pattern of synthesized array.

5.2. HYBRID MICROSTRIP AND WAVEGUIDE FEED NETWORK

Loss in the feed network is most severe in large arrays as dielectric and ohmic losses grow rigorously at high frequencies. Radiation and surface wave excitation losses of the array feed network must also be considered. Due to long microstrip lines, it is almost prohibitive to have large corporate microstrip feed network to combine 256 elements. To overcome feed network loss, series feed, parallel feed, series-parallel feed, all waveguide feed and waveguide-microstrip hybrid feed were proposed in the past. Waveguide-only feed, i.e. each antenna element is fed into the waveguide, is not attractive due to cost and weight of the die-cast structure. Series, parallel and their combinations exhibit poor bandwidth performance and work well for narrowband systems. Most suitable choice would be hybrid microstrip and waveguide feed system, but the size of the corporate feed for the subarray must be carefully determined. Dominant mode metallic hollow waveguide has very small loss along its walls. Most critical design would be microstrip-to-waveguide transition since waveguide is not directly underneath the feedline but rather 6 mm below, on the other side of the reflecting ground. Thus, a special transition structure must be carefully designed. In the following sub sections; the design of a low loss microstrip-to-waveguide transition, a detailed analysis on microstrip line and waveguide losses will be discussed and finally the optimization of the feed network will be shown.

The well-known reasons for losses in microstrip lines is listed as follows:

- Conductor losses
- Dielectric losses
- Radiation losses
- Surface wave losses.

Due to the fields within two guided-wave media, the microstrip does not support a pure TEM wave. When the longitudinal components of the fields for the dominant mode of a microstrip line are much smaller than the transverse components, the quasi-TEM approximation is applicable to facilitate design. Equations given below can be found in almost every book about Antennas and Microwave Theory. Although the accuracy of these equations are not that liable for the Ku band, but it gives a very good idea for the decision

of the subarray feed network size. Table 5.1. gives the electrical properties of the dielectric material.

Table 5.1. Electrical properties of Nelco NX9300

| | |
|--------------------------------------|------------------|
| Dielectric constant (ϵ_r) | 3 |
| Loss tangent ($\tan\delta$) | 0.0023 |
| Thickness (h) | 0.5 mm |
| Copper thickness (t) | 35 μm |

The frequency for which the effects of dispersion can be neglected can be calculated from (for h given in mm, f_{dis} is in GHz):

$$f_{dis} = 0.03 \sqrt{\frac{Z_0}{h\sqrt{\epsilon_r - 1}}} \quad (5.3)$$

Using the electrical properties given in table 5, f_{dis} is calculated to be nearly 8 GHz. For a Ku band application the dispersion effects cannot be neglected. The effects of dispersion mostly affect the effective dielectric constant. Calculations can be modified to include these effects with varying frequency.

Let W be the width of the feedline and t the copper thickness, the effective feedline width dielectric thickness ratio can be calculated as:

$$\frac{W_{eff}}{h} = \frac{W}{h} + \frac{t}{\pi h} \left(1 + \ln \frac{2h}{t} \right) \quad \text{for } W/h \geq 1/2\pi \quad (5.4)$$

$$\frac{W_{eff}}{h} = \frac{W}{h} + \frac{t}{\pi h} \left(1 + \ln \frac{4\pi W}{t} \right) \quad \text{for } W/h \leq 1/2\pi \quad (5.5)$$

Effective dielectric constant can be calculated as:

$$\varepsilon_{eff} = \frac{\varepsilon_r + 1}{2} + \frac{\varepsilon_r - 1}{2} \left(1 + 12 \frac{h}{W_{eff}} \right)^{-1/2} \quad \text{for } W_{eff}/h \geq 1 \quad (5.6)$$

$$\varepsilon_{eff} = \frac{\varepsilon_r + 1}{2} + \frac{\varepsilon_r - 1}{2} \left[\left(1 + 12 \frac{h}{W_{eff}} \right)^{-1/2} + 0.04 \left(1 - \frac{W_{eff}}{h} \right)^2 \right] \quad \text{for } W_{eff}/h \leq 1 \quad (5.7)$$

Effects of frequency variations on ε_{eff} :

$$\varepsilon_{eff}(f) = \frac{\varepsilon_r - \varepsilon_{eff}}{1 + (0.6 + 0.009Z_0) \left(\frac{8f\pi h}{Z_0} \right)^2} \quad (5.8)$$

Characteristic impedance:

$$Z_0 = \frac{60}{\sqrt{\varepsilon_{eff}(f)}} \ln \left(8 \frac{h}{W_{eff}} + 0.25 \frac{W_{eff}}{h} \right) \quad \text{for } W_{eff}/h \leq 1 \quad (5.9)$$

$$Z_0 = \frac{120\pi / \sqrt{\varepsilon_{eff}(f)}}{\frac{W_{eff}}{h} + 1.393 + 0.667 \ln \left(\frac{W_{eff}}{h} + 1.444 \right)} \quad \text{for } W_{eff}/h \geq 1 \quad (5.10)$$

Wavelength:

$$\lambda = \frac{\lambda_0}{\sqrt{\varepsilon_{eff}(f)}} \left[\frac{\varepsilon_{eff}(f)}{1 + 0.63(\varepsilon_{eff}(f) - 1) \left(\frac{W_{eff}}{h} \right)^{0.1255}} \right]^{1/2} \quad \text{for } W_{eff}/h \geq 0.6 \quad (5.11)$$

$$\lambda = \frac{\lambda_0}{\sqrt{\varepsilon_{eff}(f)}} \left[\frac{\varepsilon_{eff}(f)}{1 + 0.6(\varepsilon_{eff}(f) - 1) \left(\frac{W_{eff}}{h} \right)^{0.0297}} \right]^{1/2} \quad \text{for } \frac{W_{eff}}{h} \leq 0.6 \quad (5.12)$$

From these equations one can easily calculate that the width W , for 50 Ω line at the Ku band mid frequency, to be 1.055 mm. The total loss in a feedline can be calculated from the sum of the attenuation constants for α_c (conductor loss), α_d (dielectric loss), α_{surf} (surface loss) and α_{rad} (radiation loss). Since we are practically trying to calculate the losses of a microstrip feed network for an antenna array, the length of the feedline will be greater than 5λ . For this reason the effects of radiation and surface wave losses can be neglected since their effects are small compared to conductor and dielectric losses.

Conductor losses can be calculated by:

$$\alpha_c = 20 \log e^{\frac{R_s}{Z_0 W_{eff}}} \quad (dB/m) \quad (5.13)$$

where R_s :

$$R_s = \sqrt{\frac{\pi f \mu_0}{\sigma_c}} \quad (5.14)$$

Dielectric losses can be calculated by:

$$\alpha_d = 20 \log e^{A_d} \quad (dB/m) \quad (5.15)$$

where A_d is:

$$A_d = \frac{2\pi}{\lambda} \frac{\varepsilon_r (\varepsilon_{eff}(f) - 1) \tan \delta}{(\varepsilon_r - 1) \sqrt{\varepsilon_{eff}(f)}} \quad (5.16)$$

The transition geometry that involves copper disk and dielectric loaded pin for wideband match and low-loss. The geometry of the transition is illustrated in Figure 5.4. The transition is modeled in CST Microwave Studio where waveguide walls are assumed aluminum and probe was modeled as copper to account for all ohmic losses in the model. Simulated results for insertion loss and transmission loss are shown in Figure 5.5. Prototype of the metal disk loaded transition is made and measurements were performed on a straight section of the waveguide. Measured loss for this transition was found as 0.78 ± 0.02 dB in the design frequency band. Match was under 15 dB for the proposed transition.

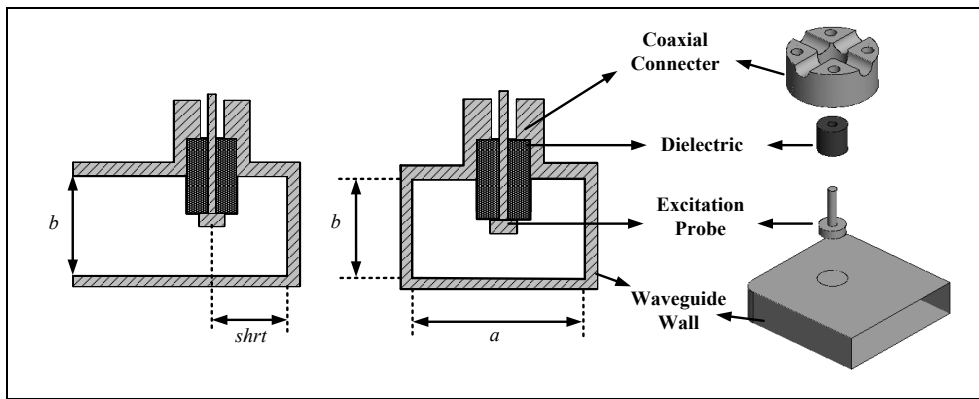


Figure 5.4. Microstrip-to-waveguide transition ($a = 18.85$ mm, $b = 4.75$ mm, $shrt = 7.2$ mm).

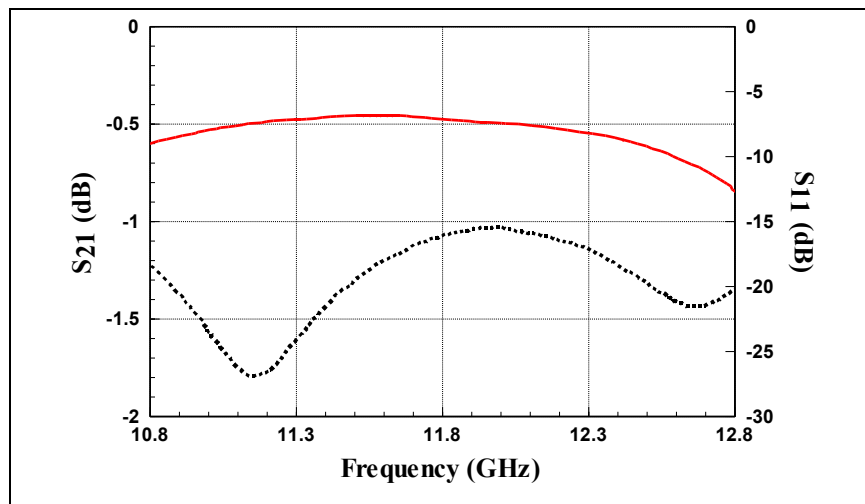


Figure 5.5. Simulated transmission loss and impedance match of microstrip to waveguide transition (— $|S_{21}|$, - - $|S_{11}|$).

Loss in the waveguide combiner must also be determined to quantify total loss in the hybrid system. *H*-type waveguide combiner was designed as opposed to an *E*-type combiner. Main motivation behind this choice was to reduce the overall height of the WR75 waveguide as electric field lines are parallel to longitudinal axis of the guide. In addition, output ports are in phase with each other and no phase compensation is needed as opposed to *E*-plane combiner. Manufacturing of this waveguide type is also simpler as one of the longer sections of the waveguide can be made flat and the rest of the waveguide can be machined from die cast. Summary of all losses are presented in Table 5.2. Once these are known, the size and the form of the subarrays and waveguide sections can be designed.

Table 5.2. Summary of losses

| Component | Value |
|------------------------------------|-------------|
| Microstrip line | 0.072 dB/cm |
| Microstrip T-junction | 0.11 dB |
| Microstrip-to-waveguide transition | 0.78 dB |
| Waveguide T-junction | 0.12 dB |

An optimization problem for minimum feed network loss can be formulated and solved for subarray size. Layout of a general array is illustrated in Figure 5.6. Number of elements in *x*- and *y*-directions is denoted as N and M , respectively. Let N_S and M_S represent number of elements in the subarray.

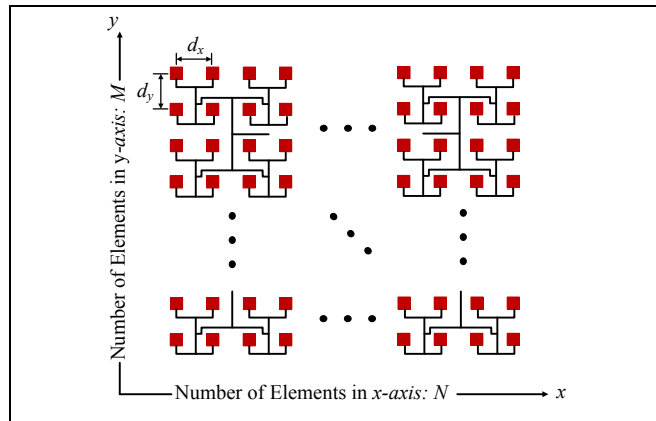


Figure 5.6. Layout of the feed network.

The number of levels for single output can be expressed as:

$$\log_2 NM = \log_2 N_S M_S + \left(\log_2 \frac{N}{N_S} + \log_2 \frac{M}{M_S} \right) \quad (5.17)$$

where, $\log_2 N_S M_S$ and $(\log_2 N/N_S + \log_2 M/M_S)$ represent number of levels in the subarray and in the waveguide, respectively. Loss in the hybrid combiner can be stated as:

$$\left(\log_2 \frac{N}{N_S} + \log_2 \frac{M}{M_S} \right) L_{T,WG} + L_{TRANS} = L_1 \quad (5.18)$$

where, $L_{T,WG}$ and L_{TRANS} denote waveguide T-junction loss and microstrip to waveguide transition loss. Although there are $NM/N_S M_S$ many transitions in the waveguide, only one transition is effective in the calculation of corporate feed network loss. Loss due to microstrip line can be expressed as,

$$\left(\frac{d_x + d_y}{2} + \left(\frac{N_S}{2} - 1 \right) d_x + \left(\frac{M_S}{2} - 1 \right) d_y \right) L_{MS} + (\log_2 N_S + \log_2 M_S) L_{T,MS} = L_2 \quad (5.19)$$

where, d_x, d_y represent inter element spacing in x and y directions, respectively, $L_{T,MS}$ and L_{MS} denote microstrip T-junction loss and microstrip line loss, respectively. Microstrip line loss includes ohmic and dielectric losses and it is calculated for 50Ω straight line section.

Then, total loss becomes,

$$L_{tot} = L_1 + L_2 \quad (5.20)$$

Furthermore, for corporate feed N, M, N_S and M_S must be multiples of 2, i.e. $N = 2^n, M = 2^m, N_S = 2^{n_s},$ and $M_S = 2^{m_s}$. Total loss can be restated as:

$$(n - n_S + m - m_S)L_{T,WG} + (n_S + m_S)L_{T,MS} + L_{TRANS} + (2^{n_S-1}d_x + 2^{m_S-1}d_y + l)L_{MS} = L_{tot} \quad (5.21)$$

where, l represents $-(d_x + d_y)/2$.

Optimization function for minimization of loss for subarray size n_S and m_S can be formulated as follows:

$$\begin{aligned} & \text{minimize } L_{tot}(n_S, m_S) \quad \forall n_S, m_S \in Z^+ \\ & \text{subject to} \\ & \quad 1 \leq n_S \leq \min(n, m) \\ & \quad 1 \leq m_S \leq \min(n, m) \\ & \quad w(n_S, m_S) \leq 3 \text{ kg} \end{aligned} \quad (5.22)$$

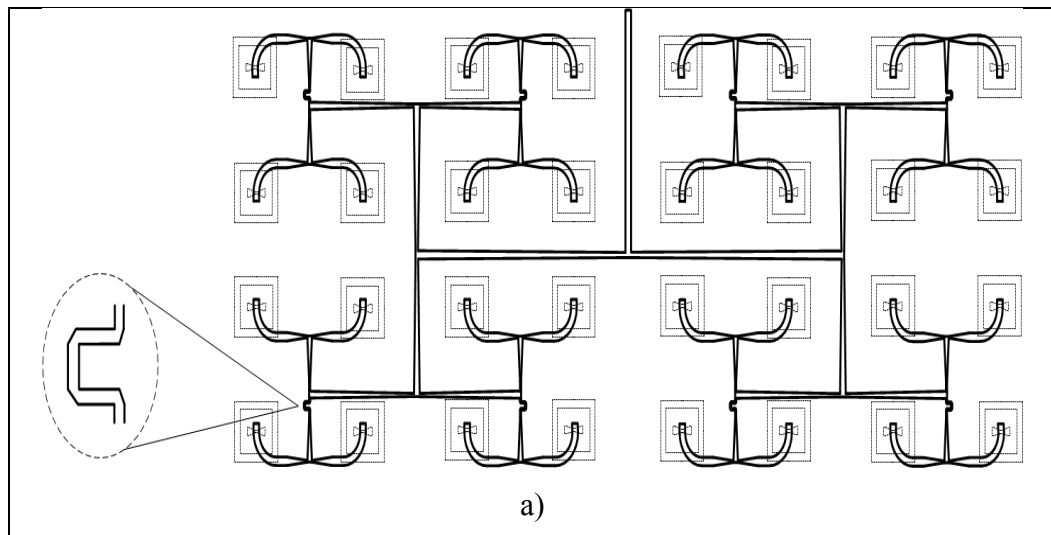
where, $w(n_S, m_S)$ represent the weight of the waveguide combiner, and subarray size cannot be larger than the full array size in either direction. The weight of the antenna is mostly due to waveguide feed network. For different combiner structures starting from 4:1 to 64:1, waveguide feed networks are designed in CST and modeled in SolidWorks (CAD program for mechanical design). Assuming aluminum alloy 6068 for die cast machining, weights of waveguide combiners are calculated, and it is observed that for only 8:1 or less combiner structure the weight criterion is satisfied. For example, 16:1 waveguide combiner, i.e. the elements in the subarray is 16, weighs 4.3 kg. Thus, the constraint on weight is replaced with $(n_S + m_S) \geq 5$. Since a total of 256 elements ($n + m = 8$) is used in the full array, we need at least 32 elements in x -direction to obtain 3° HPBW in azimuth. Hence, n and m are set to 5 and 3, respectively (i.e. 8, 32 element arrays). The optimization problem for subarray size (n_S, m_S) can now be solved. Using constrained nonlinear optimization toolbox of Matlab, (n_S, m_S) was found (3,2) as the optimal solution with 2.16 dB total loss. Realized loss is expected to be lower than this value as microstrip and waveguide T-junctions were overestimated.

The size of the subarray is set to 4 by 8 (32 elements total) and the subarrays are combined as 8:1 in the waveguide. We also observed that if we were able to use an alternative

material such as electro-form plated dielectric material, it was possible to reduce weight which would enable a larger combiner that had less total loss.

5.3. DESIGN OF A 4 x 8 (32 ELEMENT) SUBARRAY

Array antenna is divided into 8 subarrays for each polarization. Within each subarray, corporate feed network is used. Although corporate feed network is lossier than parallel feed network, it has much wider impedance bandwidth due to tapered lines and tapered T-junctions. AWR Microwave Office was used in the design of subarray feed network. First, each antenna input was defined as a port and S-parameters of 33-port network (32 for antennas and 1 for output port) was optimized for uniform power distribution, bandwidth, match and minimum port to port coupling. Then, simulated input impedance values of 32 antenna elements was placed as terminating loads in the feed network and the layout was retuned for best match at the combined output. For a fixed elevation tilt at 20° , vertical and horizontal subarrays are illustrated in Figure 5.7. Anti-phase feeding between upper and lower parts of the vertical polarization subarray is used to reduce microstrip line lengths for required phasing between the rows of the array. Same technique was not possible to implement in the horizontal polarization subarray due to perpendicular orientation of coupling slots to underneath feedlines. Element spacing along longer axis (azimuth tilt direction) and along shorter axis (elevation tilt direction) of the subarray is 0.82λ and 0.73λ , respectively.



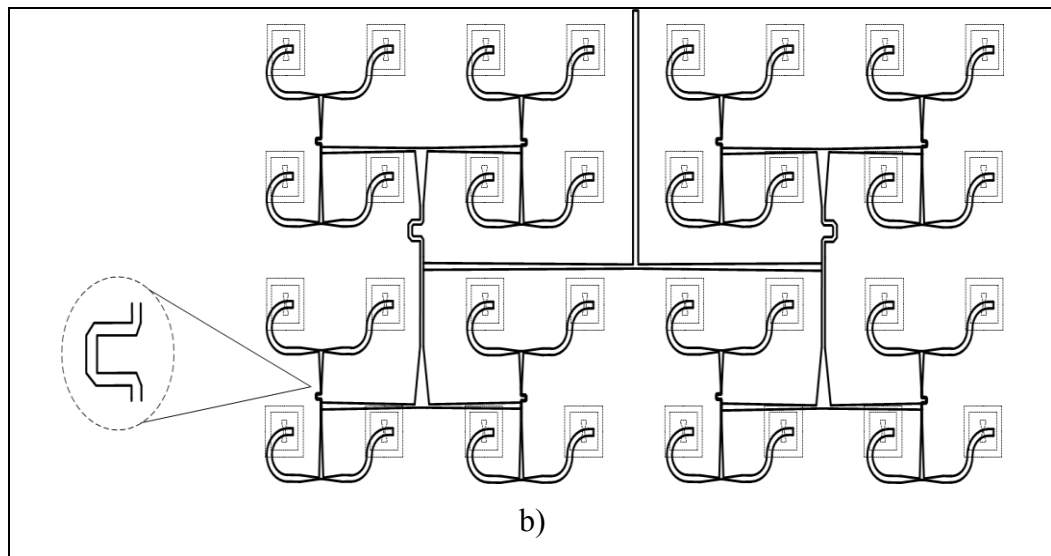


Figure 5.7. Subarray configuration for a) vertical polarization, b) horizontal polarization.

Subarrays for vertical and horizontal polarizations are built and the prototypes are shown in Figure 5.8. Simulation and measurement results for input impedance match and gain at $\theta = 20^\circ$ are shown in Figure 5.9. Simulations were carried out using FEKO, a commercial 3D electromagnetic field solver based on Method of Moments. Fast Multipole Method of the solver was invoked to speed up computations. Measured and simulated radiation patterns of subarrays at 11.9 GHz are shown in Figure 5.10. Assuming 22.13° mechanical tilt from zenith, subarray antenna provides the desired tilt at $\theta = 42^\circ$.

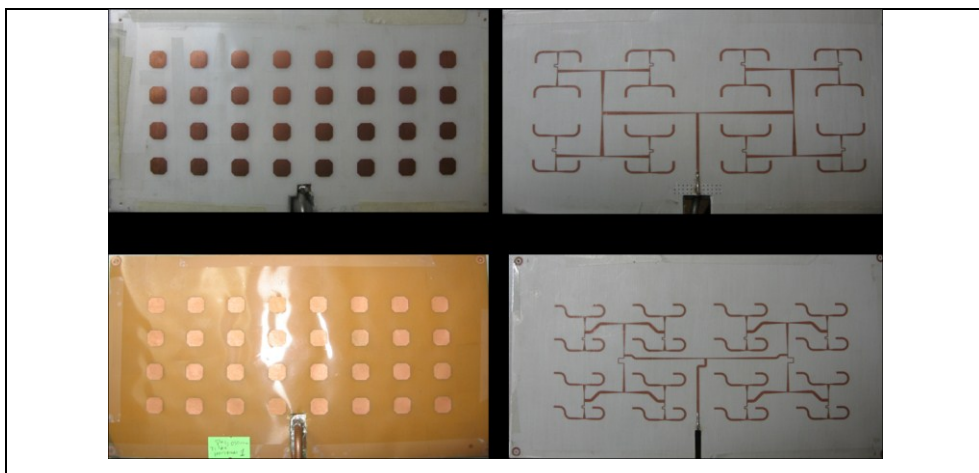


Figure 5.8. Prototypes of subarrays (top row vertical, bottom row horizontal polarization).

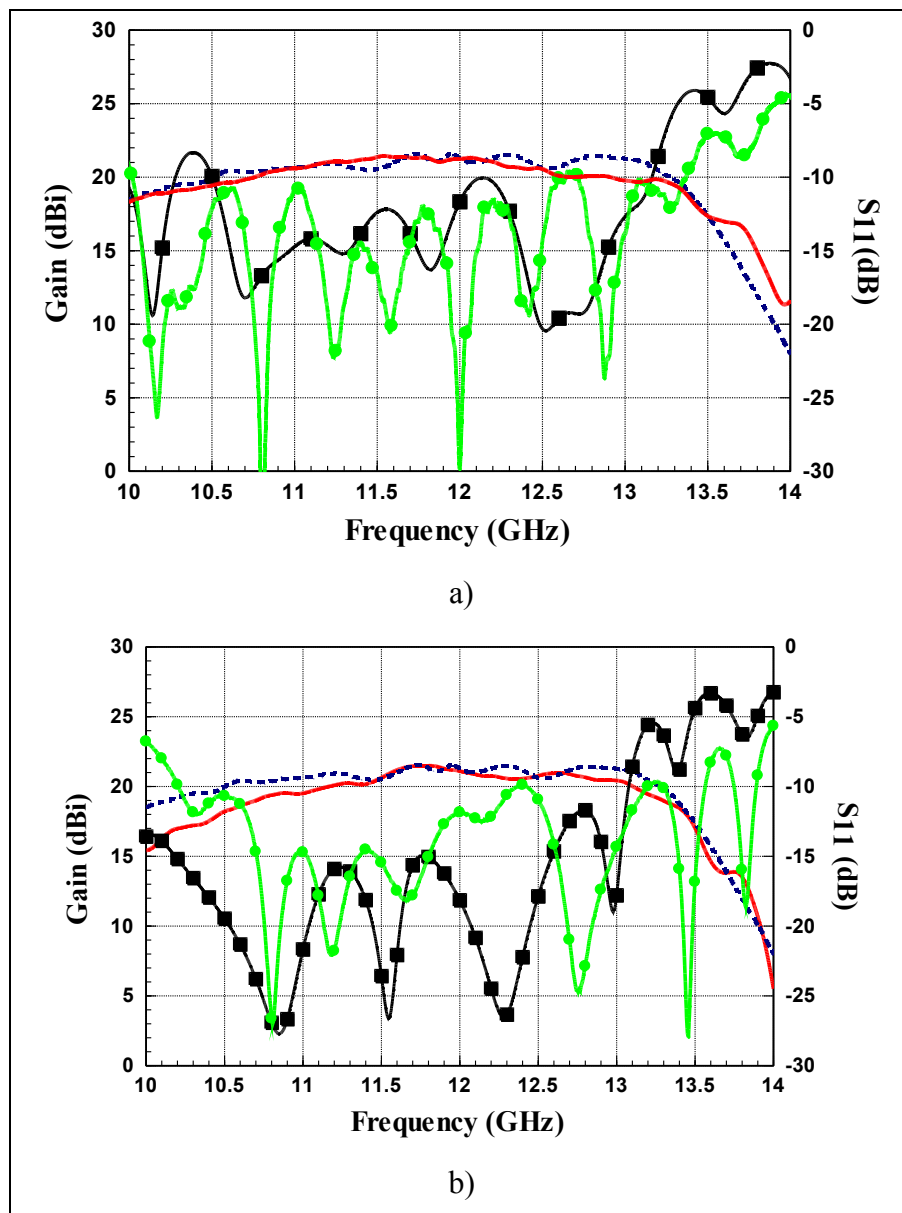


Figure 5.9. Input reflection coefficient and gain of 32 element subarray, a) vertical polarization, b) horizontal polarization.

(— Measured Gain, - - Simulated Gain, ●●● Measured S_{11} , ■■■ Simulated S_{11}).

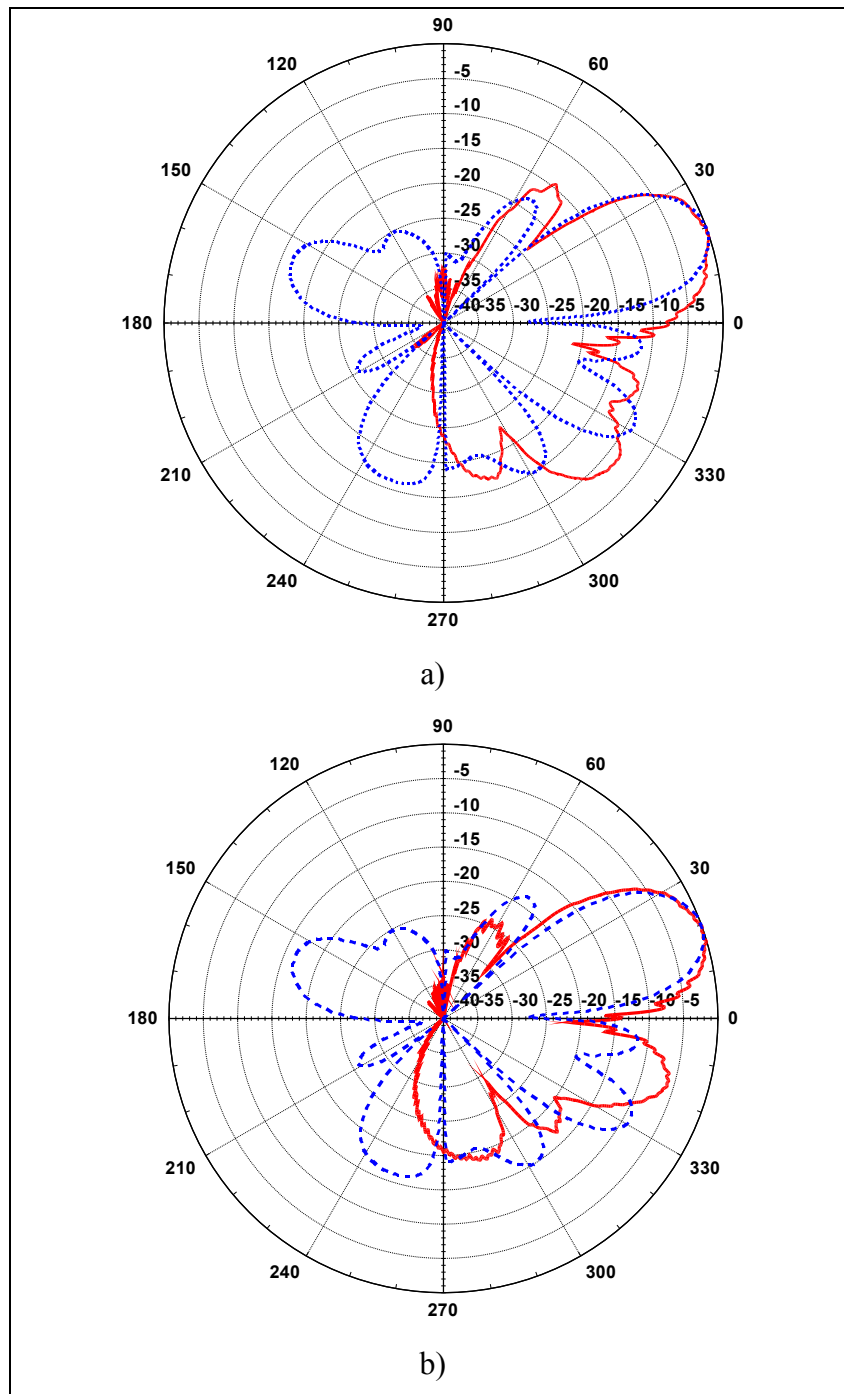


Figure 5.10 Radiation pattern of 32 element subarray at 11.9 GHz. a) vertical polarization, b) horizontal polarization. (— Measured, - - - Simulated).

5.4. DESIGN OF 8-TO-1 WAVEGUIDE POWER COMBINER

The optimum value for the waveguide combiner was calculated to be an 8-to-1 combiner, with reduced height. Figure 5.11 shows a sketch drawing of the waveguide combiner.

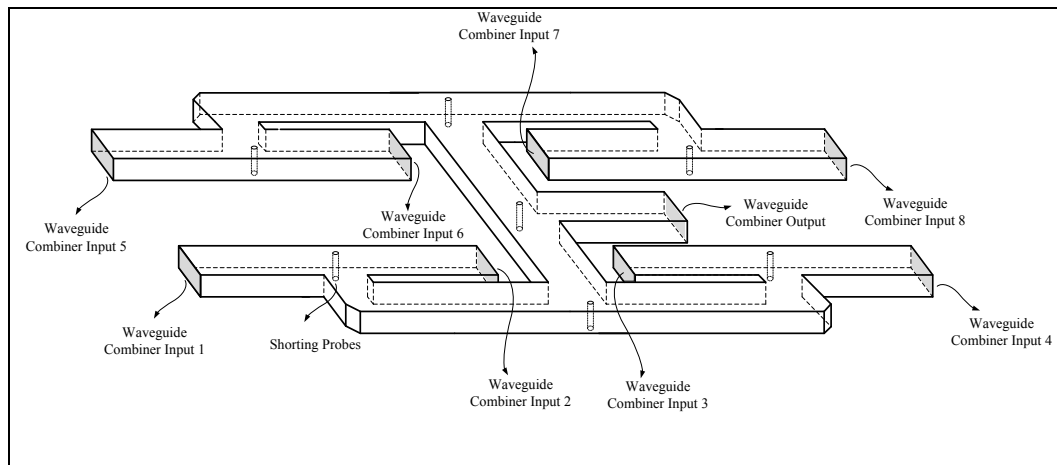


Figure 5.11. 8-to-1 Power combiner.

The design was made with WASP-NET, a commercial solver specialized in waveguide element design. Most of the losses and the power division take place in the bends and T-junctions. Figure 5.12 shows a closer view of the waveguide junctions and bends. Since the reproduction of a waveguide combiner prototype was too expensive, the same design was re-simulated with CST and FEKO in order to be sure if the design would work properly.

Optimized results are given in Figure 5.13 and 5.14. The structure has a very good impedance match which is less than 15 dB at port 1. Figure 5.14 shows the transition characteristic at all ports, simulations estimate the worst case loss 0.5 dB. Figure 5.15 shows the realized power combiner.

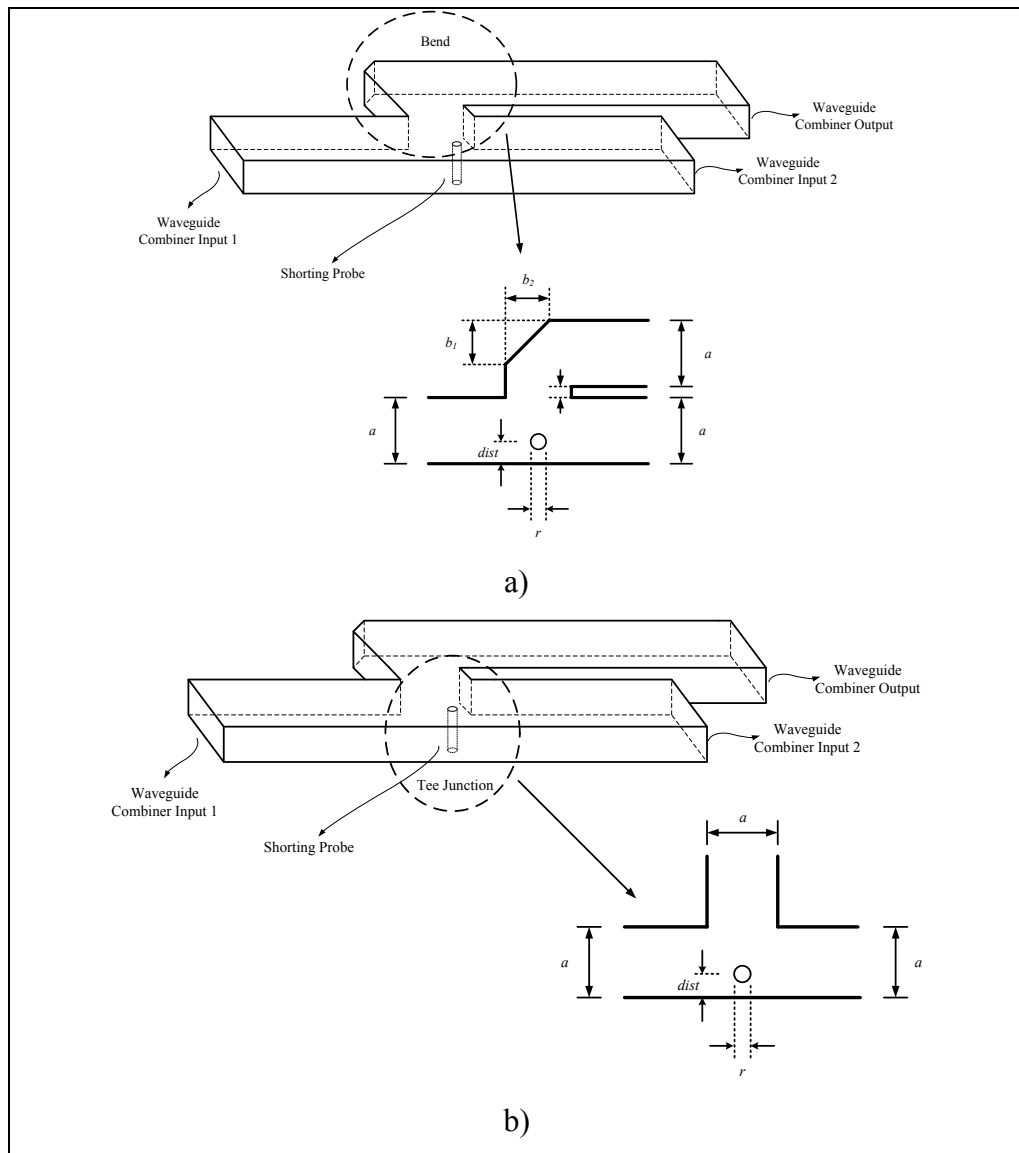


Figure 5.12. Waveguide bends and junctions. a) Bend b) T-Junction

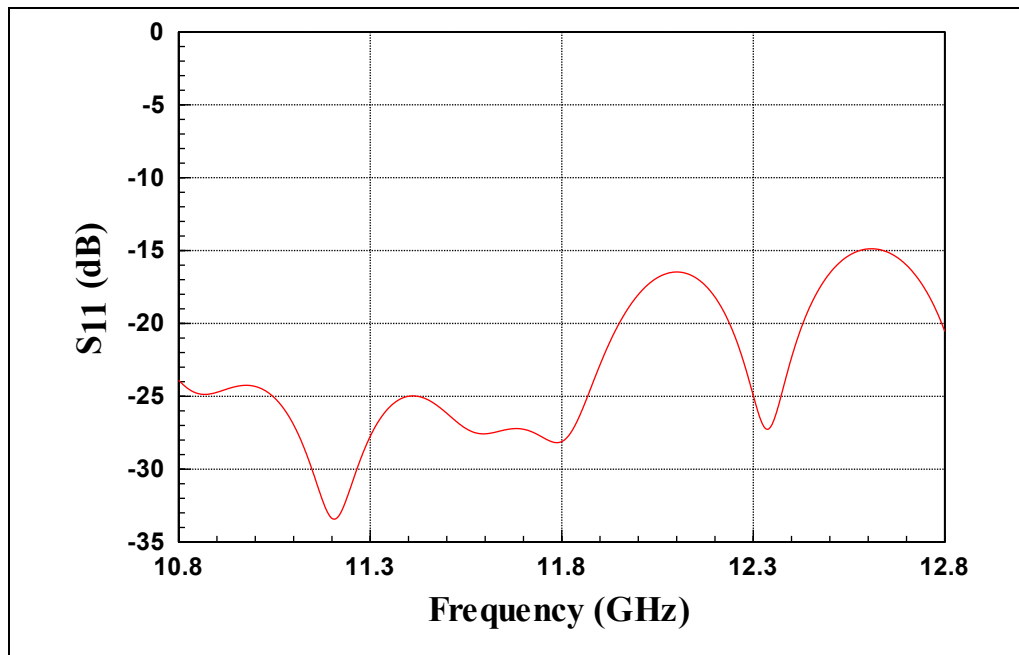


Figure 5.13. Simulated input reflection coefficient of 8-to-1 power combiner

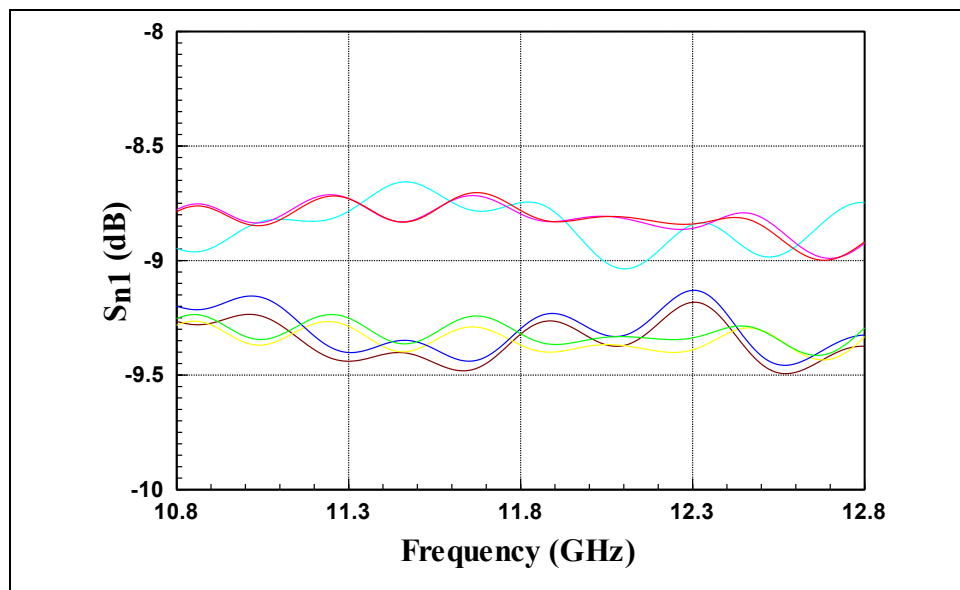


Figure 5.14. Simulated transmission coefficients of 8-to-1 power combiner.

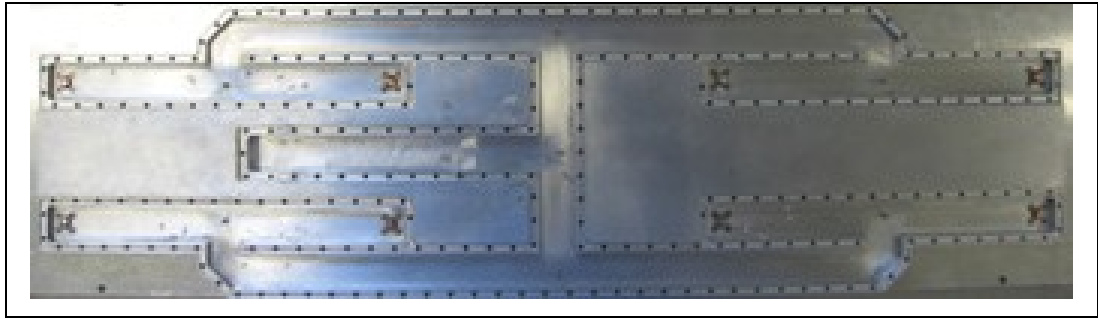


Figure 5.15. Realized power combiner.

5.5. DESIGN EXAMPLE OF A 64 ELEMENT BROADSIDE ANTENNA ARRAY WITH HYBRID FEED NETWORK

During the design alternative design were also made for either different purposes, such as the X/Ku band antenna and antenna array given in Section 4.6.2, or for validation of the concepts. This section introduces a 64 element Ku band broadside antenna array with hybrid feed network. The antenna used as the base element is the same element given in Section 4.3. The design also shows a different microstrip-to-waveguide transition with a dielectric loaded pin and a 2-to-1 waveguide combiner.

The 64 element array is built up by two 32 element subarrays similar to ones given in the previous section, but does not have any phasing in order to make the antenna a broadside array. Figure 5.16 depicts the 32 element subarray.

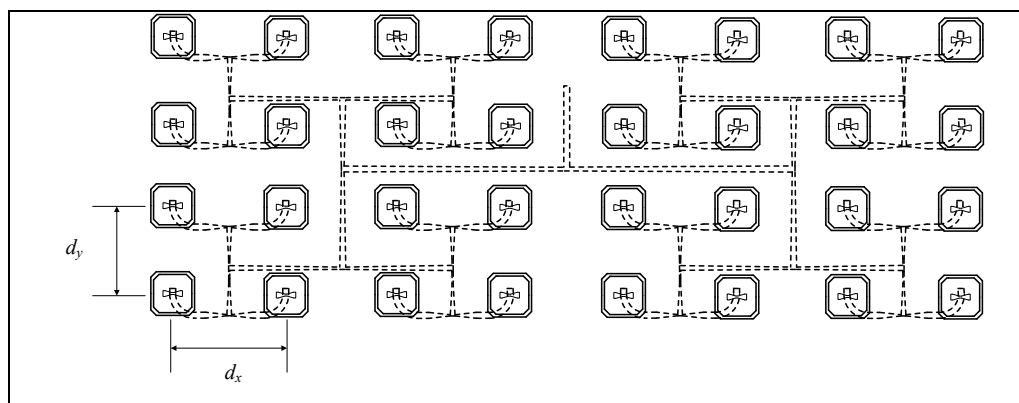


Figure 5.16. 32 element subarray with microstrip feed network.

The antenna is designed for single polarization only and vertical polarization is chosen for the implementation. However, dual polarization can also be designed using a different panel for the horizontal polarization. T-junction equal power dividers were optimized for impedance match, power division, and phase balance using AWR Microwave Office. Simulated antenna impedance of each element in the subarray is used as the terminating impedance on the feed network design. Simulations of the antenna were performed using FEKO, 3D electromagnetics field solver based on Method of Moments. Simulated and measured gain and input impedance match of the subarray are shown in Figure 5.14. Measured match is better than 10 dB throughout the Ku band downlink band and in-band worst broadside gain is 21.2 dBi. Maximum discrepancy between simulated and measured gain is about 0.8 dB, which is fairly acceptable considering that the feed connector was not taken into account in the simulations.

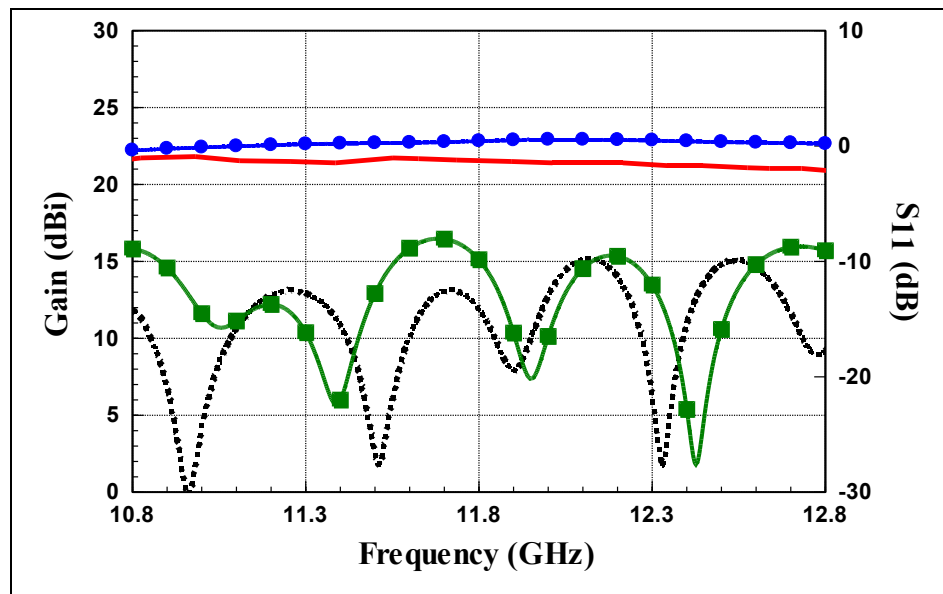


Figure 5.17. Subarray gain and input match (— Measured Gain, — Simulated Gain, Measured S₁₁, - - - Simulated S₁₁)

Normalized antenna patterns for the subarray are shown in Figure 5.18. Half-power beamwidth (HPBW) in azimuth and elevation are 8° and 15°, respectively. Noises on the measurements are related to measurement setup and they were not corrected or smoothed out.

These two subarrays were combined by a 2-to-1 power combiner similar to one given in the previous section. The 2:1 waveguide combiner is shown in Figure 5.19. H-type waveguide combiner as opposed to an E-type combiner was used. With H-type combiner, electric field lines are parallel to longitudinal axis of the guide and the height of the waveguide can be reduced by half. T-junction bents and shorting post were carefully designed for wideband impedance match. Simulation of the waveguide combiner for surface currents is shown in Figure 5.20.

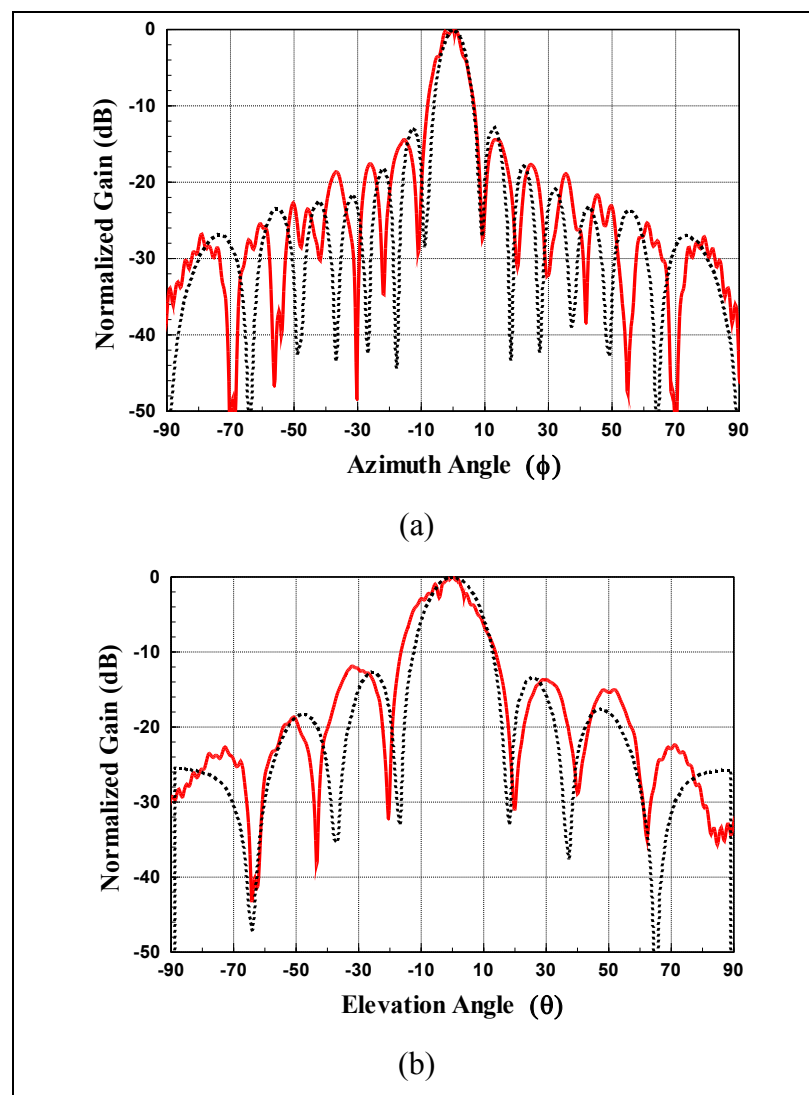


Figure 5.18. Normalized gain patterns of subarray a) azimuth b) elevation (— Measured, Simulated).

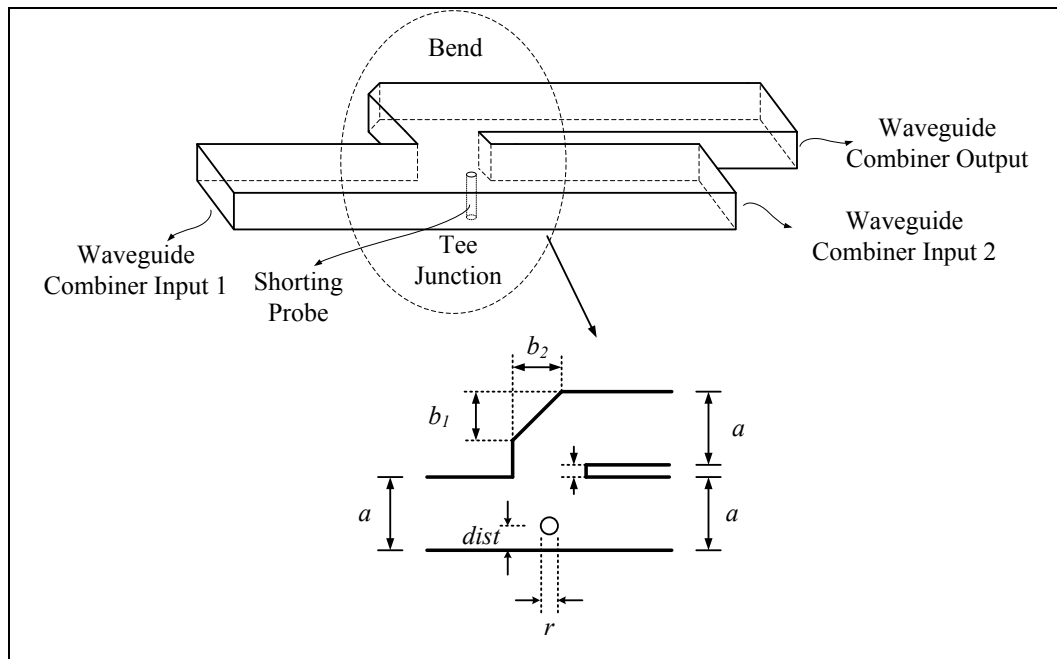


Figure 5.19. Waveguide combiner ($a = 18.85$ mm, $b = 4.75$ mm, $shrt = 7.2$ mm).

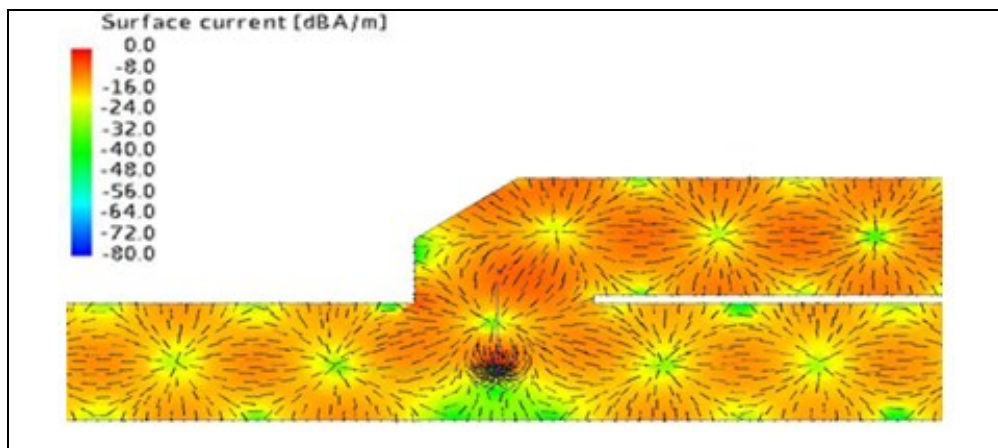


Figure 5.20. Simulation of surface currents for waveguide combiner.

Microstrip-to-waveguide junction is a crucial part of the design as its loss can be detrimental on array performance. Dielectric loaded probe transition is designed and verified using CST Microwave studio. Rexolite 1422 ($\epsilon_r=2.53$, $\tan\delta=0.0001$) was used as the dielectric material. The configuration of the transition is displayed in Figure 5.21. To assess the transition and the waveguide loss, prototypes of the waveguide combiner and transitions were made. Waveguide combiner was micromachined from aluminum alloy cast and shown in Figure 5.22. Also, a Wilkinson power divider using microstrip lines was

made. The outputs of Wilkinson power divider were connected to the microstrip-to-waveguide transitions and the output of the waveguide is connected to a coaxial probe using the same transition as shown in Figure 5.23. To eliminate the loss incurred by the Wilkinson power divider and output coaxial cable, an identical Wilkinson divider followed by the same type combiner was also made. That way, single input and single output measurement of the two Wilkinson dividers/combiners could be made. Measured transition and waveguide loss is shown in Figure 5.24. The impedance match looking from output is also shown in Figure 5.24.

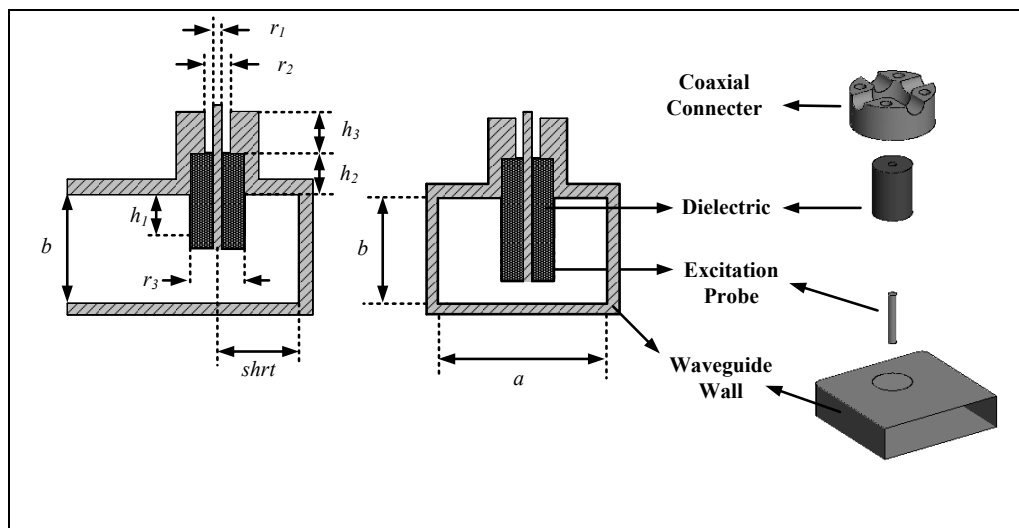


Figure 5.21. Microstrip to waveguide transition
($a = 18.85$ mm, $b = 4.75$ mm, $shrt = 7.2$ mm).

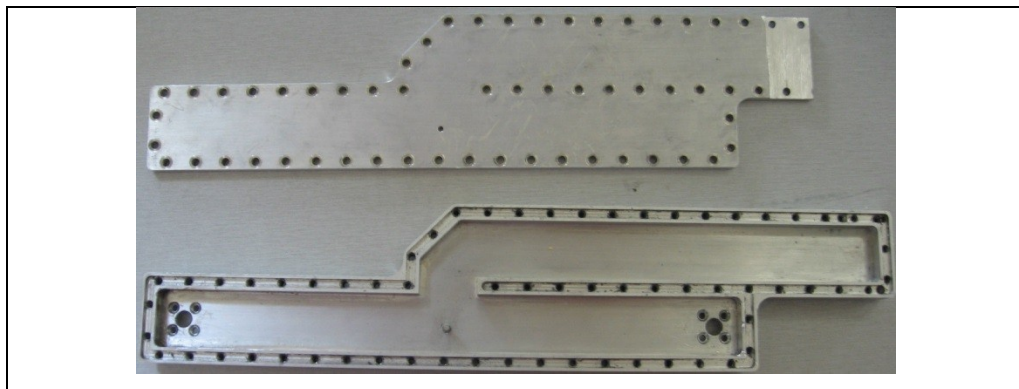


Figure 5.22. Waveguide combiner prototype.

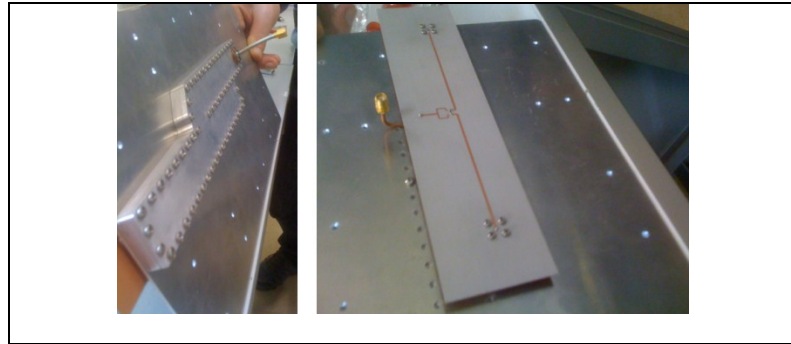


Figure 5.23. Wilkinson power divider on the inputs of waveguide combiner.

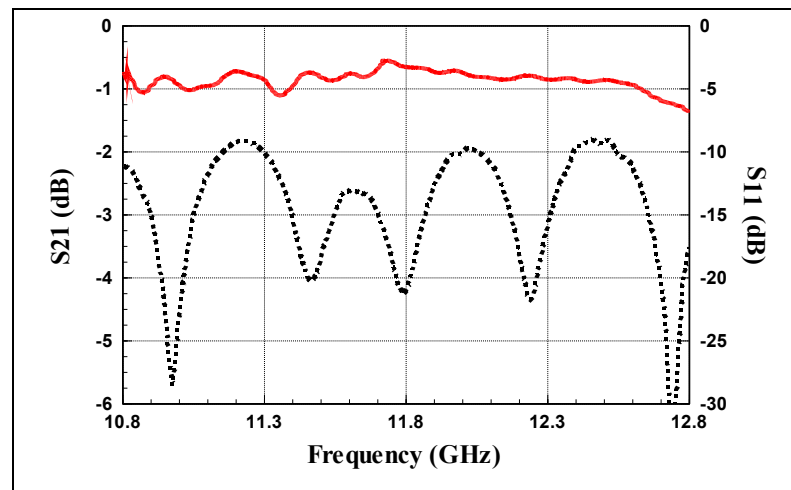


Figure 5.24. Measured transition and waveguide loss.

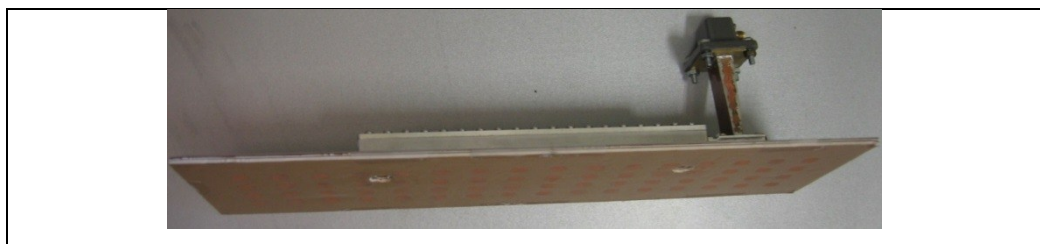


Figure 5.25. Prototype of the array ($L=176$ mm, $W=86$ mm).

Two subarrays combined with waveguide feed network constitute 64-element array antenna. The array prototype is shown in Figure 5.25. The output port is transitioned to WR75 waveguide port for low-noise block (LNB) connection for measurements and satellite reception tests.

Gain and input match of the array are shown in Figure 5.26. Simulated and measured gain agrees well except towards the end of downlink band which was mainly due to microstrip-to-waveguide transition loss. Measured broadside gain of the antenna is between 24.8 and 26.5 dBi and its measured input match is below 9.5 dB. Measured gain patterns (at 11.9 GHz) along azimuth and elevation axis are shown in Figure 5.27. $HPBW_{\theta}$ and $HPBW_{\phi}$ are 14° and 4.5° , respectively. The antenna achieves mostly above 61% aperture efficiency up to 12.2 GHz and 71% aperture efficiency at 11.1 GHz.

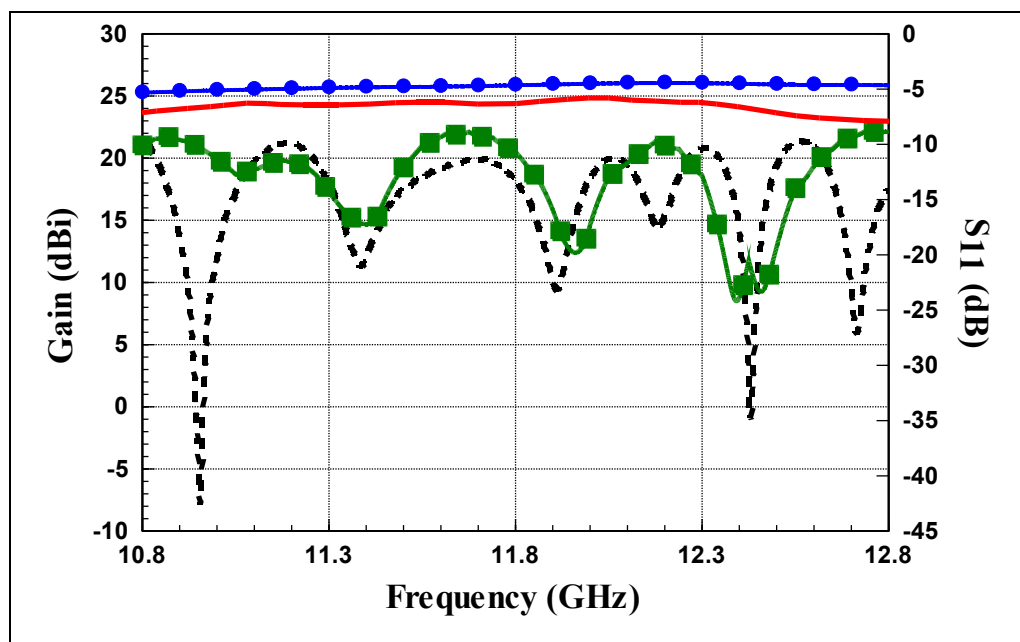


Figure 5.26. Array gain and input match (— Measured Gain, —•— Simulated Gain, - - - Measured Input Reflection Coefficient, —■— Simulated Input Reflection Coefficient).

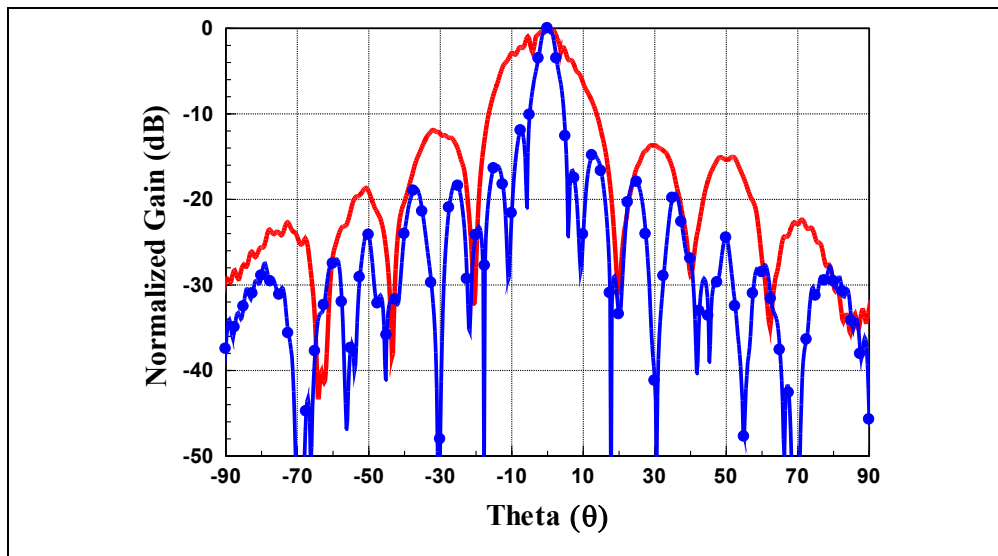


Figure 5.27. Measured gain patterns of the full array (— Elevation, —●— Azimuth).

The antenna was tested for reception quality using a DBS receiver targeted for Turksat 2A and 3A at 42° E. This particular transponder operates over entire Ku band downlink and has; 32 MHz IF bandwidth. The IF loop-out of the receiver, was connected to the spectrum analyzer (Rohde & Schwarz FSH-8). Figure 5.29 shows the received signal. The transponders on this satellite were clearly visible and good quality reception was possible for several channels. CNR at those particular channels were measured as 5.4 to 6.2 dB. If the diameter of the array is allowed to increase to 24 cm, two panels can be used to increase CNR to nominal values of usual reception. Although tracking and motion control are not discussed, these are relatively easy as azimuth HPBW is very close to that of a typical 40 cm diameter dish antenna. Hence, no phase shifters are required as mechanical tilt and rotation in azimuth can be controlled with high precision under dynamic driving conditions.

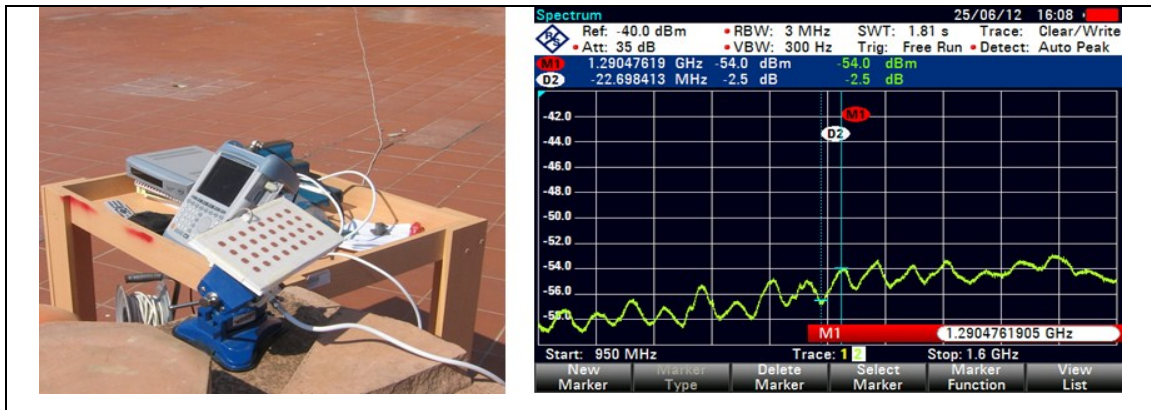


Figure 5.28. CNR measurement using DBS receiver and spectrum analyzer.
(with 32 element antenna array).

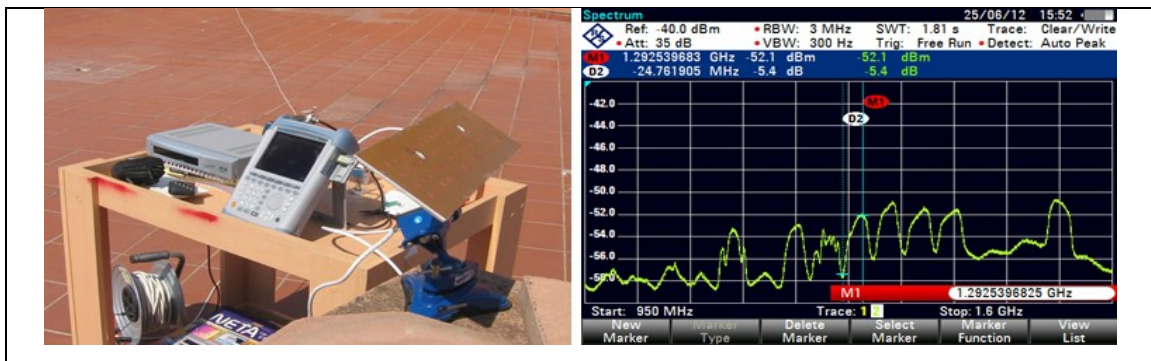


Figure 5.29. CNR measurement using DBS receiver and spectrum analyzer.
(with 64 element antenna array).

6. COMPLETE ARRAY REALIZATION AND FIELD TESTS

The prototype antenna with all subarrays is built and the prototype is displayed in Figure 6.1. The performance of the planar array must be compared to that of a dish antenna. Therefore, an existing commercial antenna which comprises a parabolic surface with corrugated circular feed horn is also modeled for basis of comparison and this antenna is called "Reference antenna", which was introduced in the third section. Reference antenna exhibits similar performance to that of a 40 cm diameter dish antenna except it has lower profile. Simulation of the full array with waveguide feed network was not possible due to large number of unknowns in the model. Instead, planar array and waveguide feed network were simulated separately for their S-parameters, and results were combined to get the final array performance. Measurements and simulations of planar array for input impedance match and gain at 20° tilt are displayed in Figure 6.2 and Figure 6.3. Gain simulations of Reference antenna and planar array closely resemble to each other but measured gain is lower than simulated one due to waveguide-to-coax adaptor used in the measurements and non-ideal simulation setup as mentioned above. Nevertheless, measured gain at desired tilt angle is above 28.4 dBi over entire target frequency band. Planar array gain is 1.2 dB lower than the expected value from array theory. The radiation patterns of planar array at 20° tilt angle for azimuth and zenith cuts are shown in figure 6.4 and figure 6.5. Measured $HPBW_{\theta}$ and $HPBW_{\phi}$ are measured to be 8° and 2.5°, respectively. If the antenna was designed for broadside reception, its gain would have been definitely higher. The aperture efficiency of the planar array is between 57 - 67% over the target frequency band.

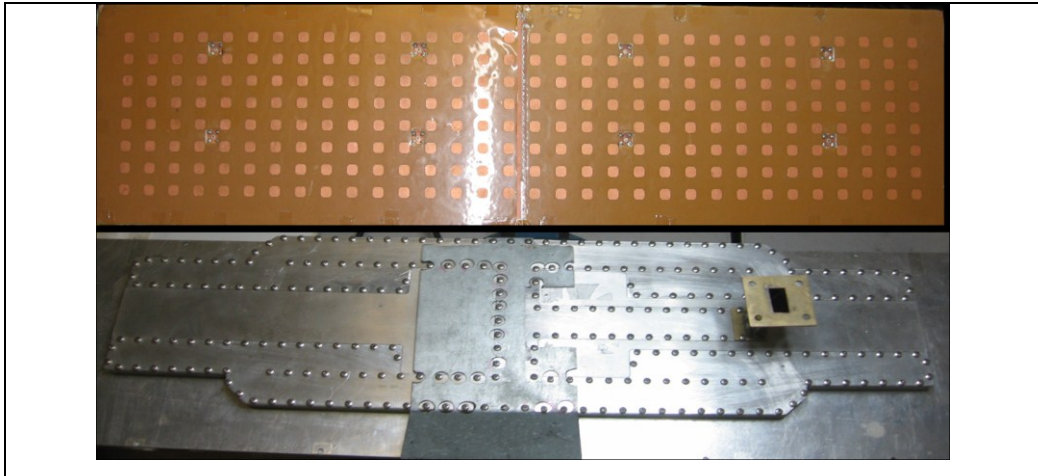


Figure 6.1. Prototype of vertical polarization 256 element array (dimensions: 70.73 cm x 18.23 cm x 2.43 cm, the height of the waveguide adapter is excluded from dimension).

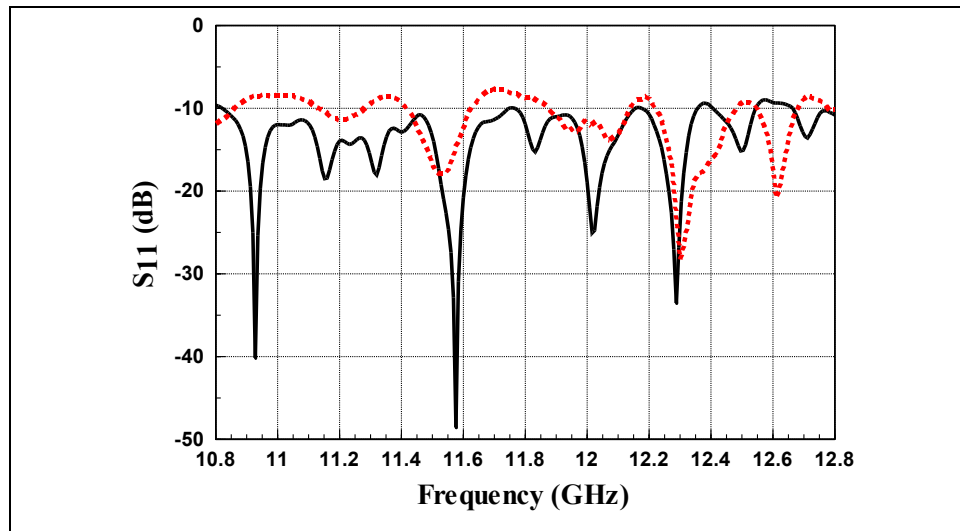


Figure 6.2. S_{11} of array antenna. (— Measured, - - Simulated).

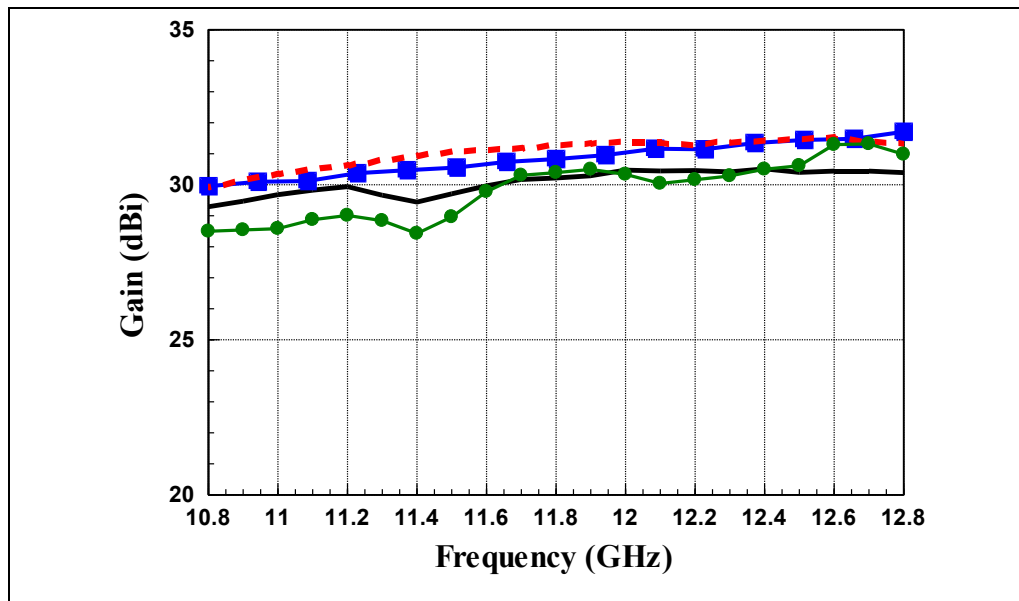


Figure 6.3. Gain of array antenna ($\theta = 20^\circ$ cut). (— Measured Vertical Polarization, - - - Measured Horizontal Polarization, - - - Simulated 256 Element Array, - - - Simulated Reference).

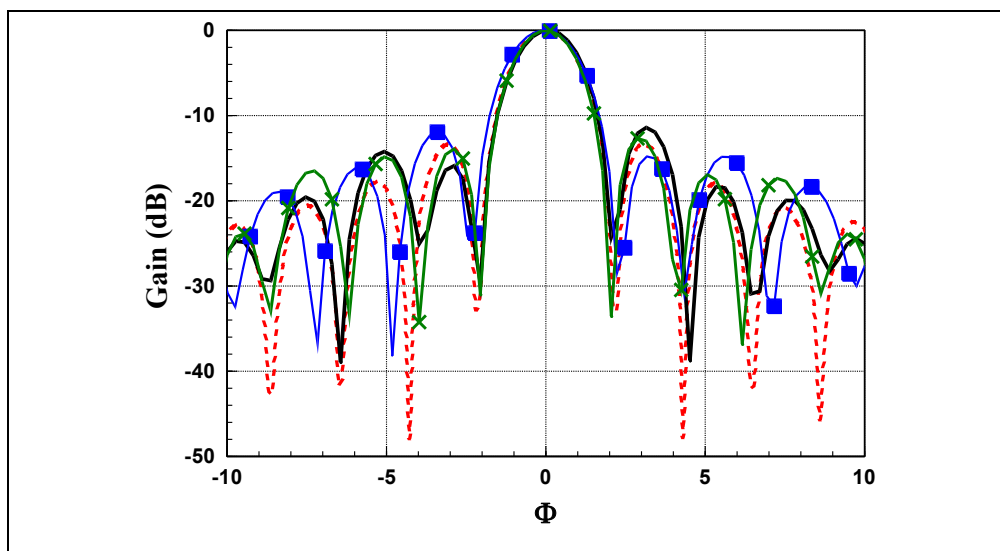


Figure 6.4. Radiation pattern of vertical polarized full array in azimuth plane ($\theta = 20^\circ$ cut) (— Measured @ 11.9 GHz, - - - Simulated @ 11.9 GHz, - - - Measured @ 10.8 GHz, - - - Measured @ 12.8 GHz).

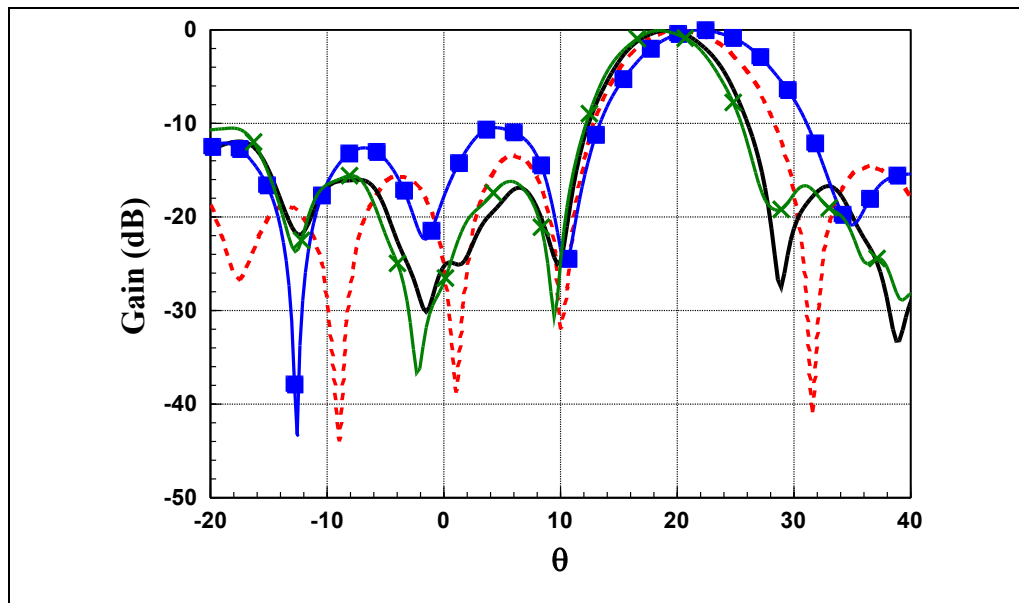


Figure 6.5 Radiation pattern of vertically polarized full array in θ -plane ($\phi=0$ cut) (— Measured @ 11.9 GHz, - - - Simulated @ 11.9 GHz, + + + + Measured @ 10.8 GHz, - x - x - x Measured @ 12.8 GHz)

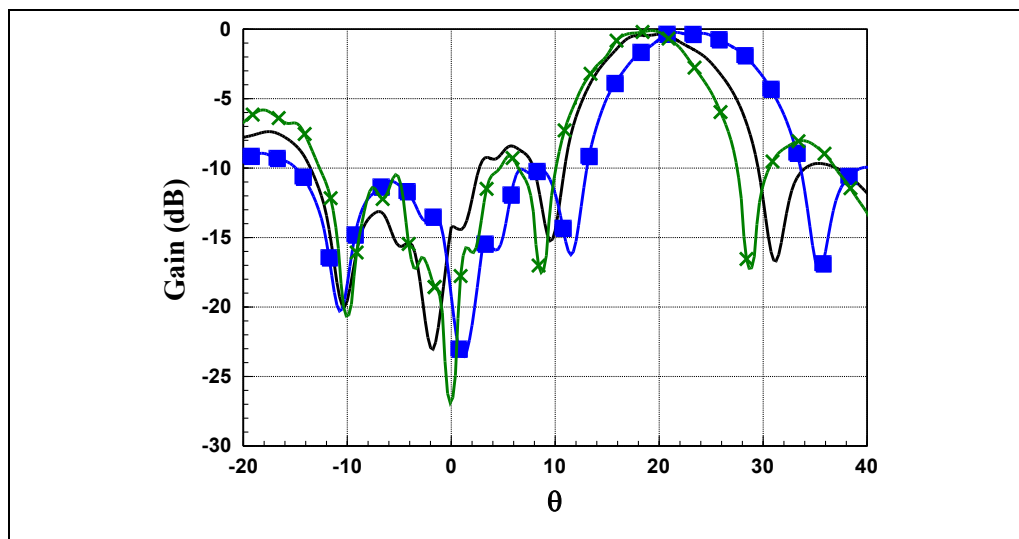


Figure 6.6 Radiation pattern of horizontally polarized full array in θ -plane ($\phi=0$ cut) (— Measured @ 11.9 GHz, + + + + Measured @ 10.8 GHz, - x - x - x Measured @ 12.8 GHz)

Full array is also tested for signal quality and satellite reception using an LNB and receiver. The IF loop output of the receiver is connected to spectrum analyzer (Rohde &

Schwarz FSH-8 GHz) and the signal from transponders were clearly visible with average CNR of 9.5 dB. Measurement result is shown in figure 6.7. Reception quality retrieved from the receiver digital outputs was above 65%, which is slightly lower than that of the Reference antenna (71%).

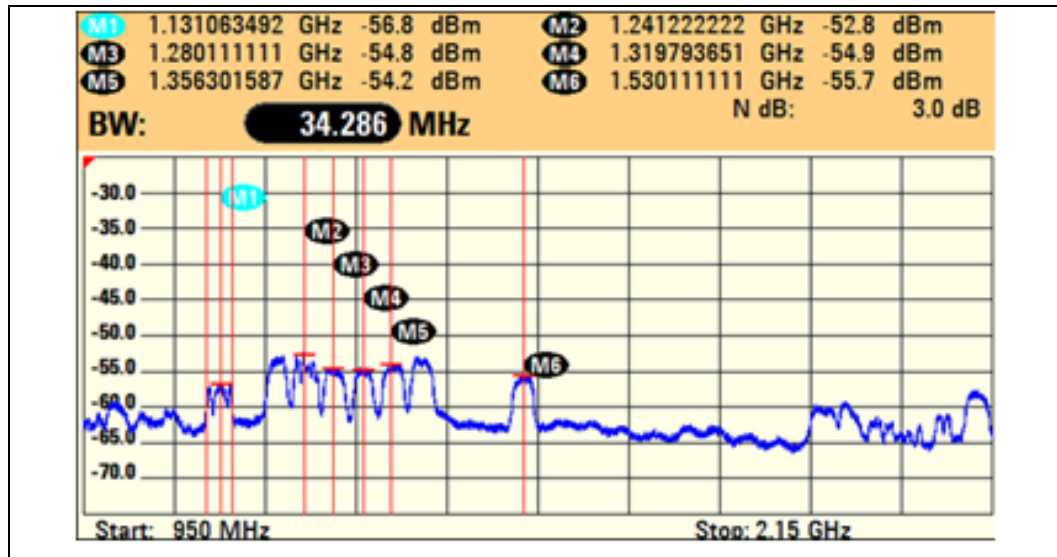


Figure 6.7 Spectrum analyzer measurement of DBS signal.

7. CONCLUSION

Wideband, high gain, low-profile Ku band array antennas for DBS reception are essential for vehicles. Past works only achieved limited bandwidth over the target transponder. In this study, we present the widest bandwidth ever reported in the open literature with high gain. To achieve broad band operation, special antenna structures were developed. One of these designs involved hour-glass type non-resonant aperture coupled antenna that achieved almost 50% bandwidth. Unlike previous studies, we optimized antenna configuration not only for bandwidth but also for antenna gain. We defined new figure-of-merits (FOMs) that included gain-bandwidth product and based on these FOM's the optimal antenna structure was arrived.

We took the element antenna design and created a full two dimensional array to meet the required gain and bandwidth requirements as well as HPBW and pattern tilt. Array feedline loss was formulated as an optimization function with constraints that were formulated from target specifications. We found the optimal subarray and array configuration based on this analysis. Although subarray configuration was utilized in many prior designs, none of the designs were able to specifically calculate the subarray size. In that respect, this study shed light on this critical design phase of antenna arrays.

To minimize feed line loss and to maximize aperture efficiency, hybrid waveguide and microstrip line feed network was designed. Although this idea was not new, the type of the waveguide combiner, microstrip to waveguide transition and reduced waveguide dimensions were unique in our design. The full array design was realized and the performance of the full array was fully measured and compared to an existing reflector type antenna. It was shown that proposed design performed as good as reflector type antenna with much reduced height and smaller profile.

REFERENCES

1. Mousav, P.; Fakharzadeh, M.; Jamali, S.H.; Narimani, K.; Hossu, M.; Bolandhemmat, H.; Rafi, G. and Safavi-Naeini, S.: "A Low-Cost Ultra Low Profile Phased Array System for Mobile Satellite Reception Using Zero-Knowledge Beamforming Algorithm," *IEEE Transactions on Antennas and Propagation*, Vol. 56, No. 12, December 2008.
2. Hirokawa, J.; Ando, M.; Goto, N.; Takahashi, N.; Ojima, T. and Uematsu, M.: "A single-layer slotted leaky waveguide array antenna for mobile reception of direct broadcast from satellite," *IEEE Transactions on Vehicular Technology*, vol. 35 No.4, pp. 749-755, November 1995.
3. Ito, Y.; Yamazaki, S.: "A mobile 12 GHz DBS television receiving system," *IEEE Trans. Broadcasting*, Vol. 35, Iss. 1, pp. 56 – 62, March 1989.
4. Watanabe, T.; Ogawa, M.; Nishikawa, K.; Harada, T.; Teramoto, E. and Morita, M.: "Mobile antenna system for direct broadcasting satellite," *Antennas and Propagation Society International Symposium*, Vol. 1, pp. 70 - 73, 21-26 July 1996.
5. Vaccaro, S.; Tiezzi, F.; Rúa, M. and De Oro, C.: "Ku-Band Low-Profile Rx-only and Tx-Rx antennas for Mobile Satellite Communications," *IEEE International Symposium on Phased Array Systems and Technology*, pp. 536 - 542, 2010.
6. Jeon, S.I.; Kim, Y.W. and Oh, D.G.: "A new active phased array antenna for mobile direct broadcasting satellite reception," *IEEE Transactions on Broadcasting*, Vol. 46, No. 1, pp. 34 - 40, March 2000.
7. Xiang, H.; Jiang, X.; Li, S.: "Design of a high gain low sidelobe microstrip antenna array at Ku-band," *WRI International Conference on Communications and Mobile Computing*, Vol. 1, pp. 29 - 32, 6-8 January 2009.

8. Azdegan, R.: "A Ku-band planar antenna array for mobile satellite TV reception with linear polarization," *IEEE Transactions on Antennas and Propagation*, Vol. 58, No. 6, pp. 2097 - 2101, June 2010.
9. Shahabadi, M.; Busuioc, D.; Borji, A. and Safavi-Naeini, S.: "Low-cost, high-efficiency quasi-planar array of waveguide-fed circularly polarized microstrip antennas," *IEEE Transactions on Antennas and Propagation*, Vol. 53, No. 6, pp. 2036 - 2043, June 2005.
10. Kraus, J. D. and Marhefka, R. J., *Antennas*, McGraw Hill Int., 3 Ed., 2001, pp. 24-25.
11. Bilgic, M. M. and Yegin, K.: "Wideband high-gain aperture coupled antenna for Ku Band phased array antenna systems," *Microwave and Optical Technology Letters*, Vol. 55, No. 6, June 2013.
12. McLean, J.: "A re-examination of the fundamental limits on the radiation Q of electrically small antennas," *IEEE Transactions on Antennas and Propagation*, Vol. 44, No. 5, May 1996.
13. Yaghjian, A. and Best, S.: "Impedance, bandwidth and Q of antennas," *IEEE Transactions on Antennas and Propagation*, Vol. 53, No. 4, pp. 1298 - 1324, April 2005.
14. Pozar, D.: "Microstrip antenna aperture-coupled to a microstrip line," *Electronics Letters*, Vol. 21, No. 2, pp. 49 - 50, January 1985.
15. Kumar, G. and Ray, K. P.: *Broadband Microstrip Patch Antennas*, Chapter 4, Artech House, 2003, p. 151-169.
16. James, J. R. and Hall, P. S., *Handbook of Microstrip Antennas*, IET, 1989.

17. Targonski, S.; Waterhouse, R. and Pozar, D.: "Wideband aperture coupled stacked patch antenna using thick substrates," *Electronics Letters*, Vol. 32, No. 21, pp. 1941 - 1942, October 1996.
18. Pozar, D. and Targonski, S.: "Improved coupling for aperture-coupled microstrip antennas," *Electronics Letters*, Vol. 27, No. 13, pp. 1129 - 1131, June 1991.
19. Serra, A.; Nepa, P.; Manara, G.; Tribellini, G. and Cioci, S.: "A Wide-Band Dual-Polarized Stacked Patch Antenna," *IEEE Antennas and Wireless Propagation Letters*, Vol. 6, pp. 141-143, 2007.
20. Rostan, F.; Gottwald, G. and Heidrich, E.: "Wideband aperture-coupled microstrip patch array for satellite TV reception," *Eight International Conference on Antennas and Propagation*, Vol. 1, pp. 190-193, 1993.
21. W. Choi, Y. H. Cho, C. Pyo, and J. Choi, "A high-gain microstrip patch array antenna using a superstrate layer," *ETRI Journal*, vol. 25, no. 5, pp. 407-411, October 2003.
22. A. Pirhadi, H. Bahrami, and J. Nasri, "Wideband high directive aperture coupled microstrip antenna design by using a FSS superstrate layer," *IEEE Trans. Antennas Propagat.*, vol. 60, no. 4, April 2012.
23. W. Choi, J. M. Kim, J. H. Bae and C. Pyo, "High gain and broadband microstrip array antenna using combined structure of corporate and series feeding," *Proc. IEEE Antennas Propagat. Soc. Int. Sym.*, vol.3, pp. 2484 – 2487, June 2004.
24. J. Lee, C. Ahn, and K. Chang, "Broadband circularly polarized aperture-coupled microstrip antenna with dual-offset feedlines," *Proc. IEEE Int. Sym. Antennas Propagat.*, pp. 1127–1130, July 2011.
25. Jackson, D. and Alexopoulos, N.: "Simple approximate formulas for input resistance, bandwidth, and efficiency of a resonant rectangular patch," *IEEE Transactions on Antennas and Propagation*, Vol. 39, No. 3, pp. 407-410, 1991.

26. Gera, A.: "The radiation resistance of a microstrip element," *IEEE Transactions on Antennas and Propagation*, Vol. 38, no. 4, pp. 568-570, 1990.
27. Das, B. and Joshi, K.: "Impedance of a radiating slot in the ground plane of a microstrip line," *IEEE Transactions on Antennas and Propagation*, Vol. 30, No. 5, pp. 922- 926, 1982.
28. Pues, H. and Van de Capelle, A.: "Accurate transmission-line model for the rectangular microstrip antenna," *IEE Proceedings Microwaves Antennas and Propagation*, Vol. 131, No. 6, pp. 334 – 340, December 1984.
29. Edimo, M.; Mahdjoubi, K.; Sharaiha, A. and Terret, T.: "Simple circuit model for coax-fed stacked microstrip patch antenna," *IEE Proceedings Microwaves Antennas and Propagation*, Vol. 145, No. 3, pp. 268 – 272, 1998.
30. Himdi, M.; Daniel, J. P. and Terret, C.: "Transmission line analysis of aperture-coupled microstrip antenna," *Electronics Letters*, Vol. 25, No. 18, pp. 1229 – 1230, 1989.
31. Coulibaly, Y.; Denidni, T.A. and Boutayeb, H.: "Broadband microstrip fed dielectric resonator antenna for X-band applications," *IEEE Antennas Wireless Propagat. Lett.*, Vol. 7, pp. 341 – 345, 2008.
32. Neves, E.S.; X Elmarissi, E.S. and Dreher, A.: "Design of a broad-band low cross-polarized X-band antenna array for SAR applications," *IEEE APS International Symposium*, Vol. 3, pp 2460 – 2463, June 2004.
33. Klefenz, F. and Dreher, A.: "Aperture coupled stacked microstrip patch antenna with dual polarization and low back radiation for X-band SAR applications," *IEEE Radio and Wireless Conf. RAWCON*, pp. 179 – 182, 2000.
34. Keller, S.D. and Weiss, S.: "Microstrip patch antenna array for a scalable X-band radar system," *IEEE APS International Symposium*, pp. 1–4, July 2010.

35. Infante, L.; De Luca, A. and Teglia, M.: "Low-profile ultra-wide band antenna array element suitable for wide scan angle and modular subarray architecture," *IEEE Int. Symp. on Phased Array Systems and Technology*, pp. 157-163, Oct. 2010.
36. Livingston, S. and Lee, J. J.: "Evolution of wide band array designs," *IEEE International Symposium on Antennas and Propagation (APSURSI)*, pp. 1957-1960, Jul. 2011.
37. Rajo-Iglesias, E.; Villaseca-Sanchez, G.; Martin-Pascual, C.: "Input impedance behavior in offset stacked patches," *IEEE Antennas Wireless Propagat.Lett.*, Vol.1, No.1, pp.28-30, 2002.
38. E. Rajo-Iglesias, J.L. Vázquez-Roy, L. Inclán-Sánchez, D. Segovia-Vargas, V. González-Posadas, C. Martín-Pascual, "Offset stacked patches behavior in an array," *MOTL*, Vol. 40, pp. 262-265, 2004.